SEPTEMBER 2020 Ph.D. in Mechanical Engineering GÜLAĞA TAŞ

REPUBLIC OF TURKEY

GAZİANTEP UNIVERSITY

GRADUATE SCHOOL OF NATURAL & APPLIED SCIENCES

PRECISION FORGING OF ASYMMETRIC SPUR GEAR

Ph.D. THESIS

IN

MECHANICAL ENGINEERING

BY

GÜLAĞA TAŞ

SEPTEMBER 2020

PRECISION FORGING OF ASYMMETRIC SPUR GEAR

Ph.D. Thesis

in

Mechanical Engineering

Gaziantep University

Supervisor

Prof. Dr. Ömer EYERCİOĞLU

by

Gülağa TAŞ

September 2020

REPUBLIC OF TURKEY
GAZİANTEP UNIVERSITY
GRADUATE SCHOOL OF NATURAL & APPLIED SCIENCES
MECHANICAL ENGINEERING

Name of the Thesis : Precision Forging of Asymmetric Spur Gear

Name of the Student : Gülağa TAŞ

Exam Date : 17.09.2020

Approval of the Graduate School of Natural and Applied Sciences

Prof. Dr. A. Necmeddin YAZICI
Director

I certify that this thesis satisfies all the requirements as a thesis for the degree of Doctor of Philosophy.

Prof. Dr. Melda ÇARPINLIOĞLU
Head of Department

This is to certify that we have read this thesis and that in our consensus opinion it is fully adequate, in scope and quality, as a thesis for the degree of Doctor of Philosophy.

Prof. Dr. Ömer EYERCİOĞLU
Supervisor

Examining Committee Members:	Signature
Prof. Dr. A. Kadir EKŞİ	…………………..
Prof. Dr. Oğuzhan YILMAZ	…………………..
Prof. Dr. N. Fazıl YILMAZ	…………………..
Prof. Dr. Ömer EYERCİOĞLU	…………………..
Assoc. Prof. Dr. A. Tolga BOZDANA	…………………..

I hereby declare that all information in this document has been obtained and presented in accordance with academic rules and ethical conduct. I also declare that, as required by these rules and conduct, I have fully cited and referenced all material and results that are not original to this work.

Gülağa TAŞ

ABSTRACT

PRECISION FORGING OF ASYMMETRIC SPUR GEAR

TAŞ, Gülağa
Ph.D. in Mechanical Engineering
Supervisor: Prof. Dr. Ömer EYERCİOĞLU
September 2020
151 Pages

The use of asymmetric gear tooth profile can be considered as a creative and innovative solution for many power transmission applications where gear wheels often rotate in only one direction. However, the production of the asymmetric gear profile by the conventional thread cutting method is dependent on the cutting tool design and the machining process. Recent studies in this area have shown that asymmetric profiles designed independently from the cutting tool are more efficient. In precision gear forging, on the other hand, the final tooth profile is determined by the die geometry, and therefore the limitations of the cutting tool can be eliminated totally. The precision forging of asymmetric spur gear was studied in this thesis and the design criteria for the asymmetric spur gear die were presented. For this purpose, upper bound energy analyses (UBEA) and finite elements (FE) simulations of the gear forging process were carried out to determine the forging load and die stresses. The gear tooth profile modifications of the die required for the dimensional accuracy of the forged gear were evaluated. The UBEA and FEA results were compared with the experimental studies. The study shows that precision forging is a feasible method for the manufacturing of asymmetric spur gears and the method eliminates the limitations of the tooth profile of gear cutting or generation methods. However, the design of the forging die is critical in the success of the process. The design criteria presented in the study can be used successfully.

Key Words: Asymmetric Gear, Precision Forging, Finite Element, Upper Bound, Die Design, Gear Tooth Profile, Gear Manufacture.

ÖZET

ASİMETRİK DÜZ DİŞLİLERİN HASSAS DÖVMECİLİĞİ

TAŞ, Gülağa
Doktora Tezi, Makina Mühendisliği
Danışman: Prof. Dr. Ömer EYERCİOĞLU
Eylül 2020
151 Sayfa

Asimetrik dişli diş profilinin kullanımı, dişli çarkların genellikle yalnızca bir yönde döndüğü birçok güç aktarımı uygulaması için yaratıcı ve yenilikçi bir çözüm olarak düşünülebilir. Bununla birlikte, asimetrik dişli profilinin geleneksel diş kesme yöntemiyle üretilmesi, kesici takım tasarımına ve işleme sürecine bağlıdır. Bu alandaki son çalışmalar, kesici takımdan bağımsız olarak tasarlanan asimetrik profillerin daha verimli olduğunu göstermiştir. Hassas dişli dövmede ise son diş profili kalıp geometrisi ile belirlenir ve böylelikle kesici takımın sınırlamaları tamamen ortadan kaldırılabilir. Bu tezde asimetrik düz dişlinin hassas dövmesi incelenmiş ve asimetrik düz dişli kalıbı için tasarım kriterleri sunulmuştur. Bu amaçla, dövme yükü ve kalıp gerilmelerini belirlemek için dişli dövme işleminin üst sınır enerji analizleri (ÜSEA) ve sonlu elemanlar (FE) simülasyonları gerçekleştirilmiştir. Dövme dişlinin boyutsal doğruluğu için gereken kalıbın dişli diş profili modifikasyonları değerlendirildi. ÜSEA ve FEA sonuçları deneysel çalışmalarla karşılaştırıldı. Çalışma, hassas dövmenin asimetrik düz dişlilerin üretimi için uygun bir yöntem olduğunu ve yöntemin dişli kesme veya üretim yöntemlerinin diş profilindeki sınırlamaları ortadan kaldırdığını göstermektedir. Bununla birlikte, dövme kalıbının tasarımı, işlemin başarısında kritik öneme sahiptir. Çalışmada sunulan tasarım kriterleri başarıyla kullanılabilir.

Anahtar Kelimeler: Asimetrik Dişli, Hassas Dövme, Sonlu Eleman, Üst Sınır, Kalıp Tasarımı, Dişli Diş Profili, Dişli İmalatı

''Dedicated to my parents and family''

ACKNOWLEDGEMENTS

I would like to express my deepest respect and most sincere gratitude to my supervisor Prof. Dr. Ömer EYERCİOĞLU for his guidance and encouragement at all stages of my work. I will always be grateful for his valuable advice and insight, supervision, and encouragement to me during this research.

I am also very grateful to Prof. Dr. Necip Fazıl YILMAZ, Prof. Dr. Oğuzhan YILMAZ and Assist. Prof. Dr. Kürşad GÖV for their valuable supports and advises.

I extend my sincere thanks to Mehmet ALADAĞ and Adem AKSOY, and for continuous motivation and support. I am also very grateful to the staff of the Mechanical Engineering Department Workshop and Laboratories of Gaziantep University for their help.

I would like to express my love and gratitude to my mother, father, wife, daughters, brother and sisters for their support.

I would like to thank The Scientific and Technological Research Council of Turkey (TUBİTAK Grand No: MAG-217M063) and BAPYB (Grand No: MF. YLT.19.03) of Gaziantep University for their financial supports.

TABLE OF CONTENTS

LIST OF TABLES

Page

LIST OF FIGURES

Page

LIST OF SYMBOLS

A	Punch/workpiece contact area
a	Pitch diameter of asymmetric spur gear die
b	Inner diameter of shrink ring
C	Concentration of the media
c	Outer diameter of shrink ring
$\mathbf{D_a}$	Tip diameter of asymmetric spur gear
$\mathbf{D_f}$	Root diameter of asymmetric spur gear
$\mathbf{D_o}$	Pitch diameter of asymmetric spur gear
E	Elastic Modulus
$\mathbf{E_d}$	Elastic Modulus of Die
$\dot{E}_f$	Frictional power dissipation
$\dot{E}_p$	Internal power of deformation
$\dot{E}_S$	Shear power dissipated at the surface of velocity discontinuity
$\dot{E}_T$	Total energy rate
G	Spark gap
$\mathbf{H_a}$	Addendum of the rack tooth
$\mathbf{h_t}$	Height of asymmetric spur gear tooth
h	Instantaneous height of the billet being deformed
K	Tooth asymmetry factor
$\mathbf{K_1}$	Yield strength ratio of the shrink ring and gear die material
$\mathbf{L_m}$	Length of the abrasive media
$\mathbf{L_W}$	Length of the workpiece
m	Module of the gear
N	Teeth number of the gear
$\mathbf{N_a}$	Particle number per area
$\mathbf{N_S}$	Number of the particle that pass in one cycle

$\mathbf{P_i}$	Applied internal pressure inside of the asymmetric spur gear die
$\mathbf{P_o}$	External pressure
$\mathbf{P_p}$	Interference pressure between gear die and shrink ring
$\mathbf{P_{av}}$	Punch load
p	Circular pitch of the gear
$\mathbf{p'}$	Ratio of internal pressure to yield stress
$\mathbf{R}$	Radius from the center of the base circle to the considered point
$\mathbf{R_B}$	Radius of the base circle
$\mathbf{R_C}$	Length of the unwrapped yarn
$\mathbf{R_P}$	Pitch circle radius
$\mathbf{R}_o$	Initial radius of bore
$\mathbf{R}_s$	Radius after shrink fit
$\mathbf{R_{BC}}$	Base circle of the coast-side
$\mathbf{R_{BD}}$	Base circles of the drive -side
$\mathbf{R_{ac}}$	Tooth tip radius for coast side
$\mathbf{R_{ad}}$	Tooth tip radius for drive side
$\mathbf{S_A}$	Virtual tooth tip land thickness
$\mathbf{S_{Ar}}$	Real tooth tip land thickness
$\mathbf{S_a}$	Arc length between point a and Y axis
$\mathbf{S_b}$	Arc length between point b and Y axis
$\mathbf{S}_y$	Yield strength
$\mathbf{S}_{y(die)}$	Yield strength of die
$\mathbf{S}_{y(ring)}$	Yield strength of ring
$\mathbf{U_a}$	Change in dimension when the punch load is removed
$\mathbf{U_c}$	Thermal product contraction
$\mathbf{U_e}$	Change in dimension of forged workpiece during the ejection
$\mathbf{U_r}$	Radial displacement
$\mathbf{U}_s$	Reduction of bore radius due to the shrink fit
$\mathbf{U_t}$	Thermal Die Expansion
$\mathbf{U_{ri}}$	Radial velocity of the i region
$\mathbf{U_{tp}}$	Radial expansion of die due to pre-heat temperature
$\mathbf{U_{ts}}$	Radial expansion of die due to radial temperature gradient
$\mathbf{U_{\theta i}}$	Circumferential velocity of the i region

$\mathbf{U_{AFM}}$	Change of the die dimension caused by AFM
$\mathbf{u}$	Velocity of the punch
v	Poisson's ratio
v_d	Poisson's ratio of die
v_w	Poisson's ratio of workpiece
$\mathbf{W}$	Total material which is removed after n cycle
$\mathbf{W_a}$	Amount of material removed by an abrasive particle
$\mathbf{W_t}$	Amount of the material that removed in one cycle
$\mathbf{z}$	Radial interference value of shrink fit
ϕ_D	Pressure angle of the drive side
ϕ_C	Pressure angle of the coast side
ρ	Density of the die material
σ_r	Radial stress
σ_θ	Tangential stress
ε_θ	Tangential strain
ε_r	Radial strain
$\dot{\varepsilon}$	Strain rate
φ	Angle between the radial velocity vector and the normal direction to the die surface at the fillet (rad)
λ	Thermal expansion of the material

LIST OF ABBREVIATIONS

AGMA	American Gear Manufacturers Association
AFM	Abrasive Flow Machining
CNC	Computer Numerical Control
DIN	German Institute for Standardization
FE	Finite Element
FEM	Finite Element Method
ISO	International Organization for Standardization
JIS	Japanese Industrial Standards
UBEA	Upper Bound Energy Analysis
WEDM	Wire Electro-discharge Machine

CHAPTER 1

INTRODUCTION

1.1 Asymmetric Gears

Gears are the most common mechanical power transmission elements that are used to changing speed, transferring torque and force, and change the direction of motion. They have been used for over four thousand years. The gear technology has developed and expanded during this century with the requirements of modern technology. Nowadays, the industry is focused on the reduction in weight to reduce energy consumption and carbon footprint. Therefore, during the design of the gears minimizing gear weight while maintaining the necessary balance of tooth bending strength, pitting resistance, and scuffing resistance is gaining high priority. The use of asymmetric gears instead of standard gears is considered an innovative approach to this area. Asymmetric gear is the gear that has different pressure angle for drive and coast side. A comparison of tooth profile for asymmetric and symmetric gear can be seen in Figure 1.1.

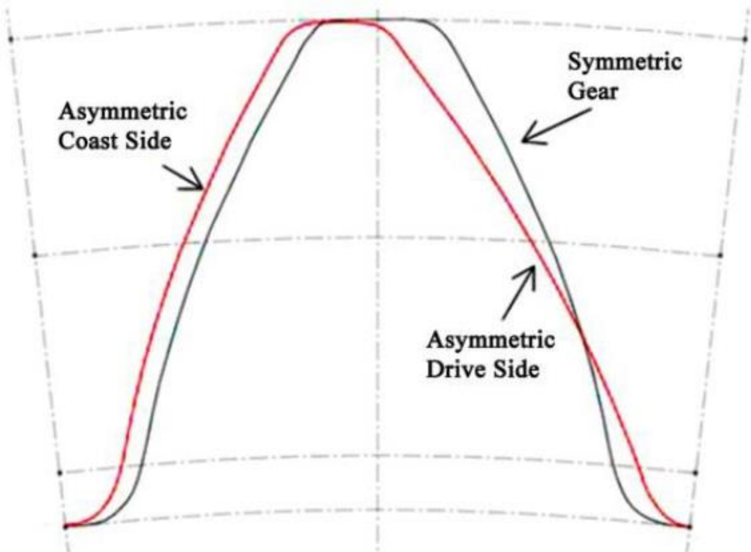

Figure 1.1 Comparison of tooth profile of asymmetric and symmetric gear

The use of asymmetric gear tooth profile can be considered as a creative and innovative solution for many power transmission applications such as cars, commercial vehicles, ships, lifting gear, generators, turboprop and helicopter gearboxes and gear pumps. In these applications, gear wheels often rotate in only one direction throughout their entire service lives, so that the tooth load on one flank is considerably higher than on the opposite one. Asymmetric tooth profiles make it possible to simultaneously increase the contact ratio and operating pressure angle beyond those limits achievable with conventional symmetric gears.

1.2 Asymmetric Gear Manufacturing and Precision Gear Forging

In gear manufacturing, a variety of processes can be used, however, they can be classified into two basic methods: generating processes and forming processes. The type, material, size, and quality of the gear affect the choice of a particular manufacturing process and the processes may vary for roughing or finishing of the gear. Some of the gear manufacturing processes are not feasible or have limitations in asymmetric spur gear manufacturing. The asymmetric gears that are using in the industrial applications are manufacturing by using the conventional thread cutting methods as shown in Table 1.1 [1].

Table 1.1 Asymmetric spur and helical gear machining processes [1]

Type of Process	Type of Tooling	
Form machining	Cutting	Form disk cutter, broach, etc.
	Grinding	Grinding wheel
Generating machining	Cutting	Hob, shaper cutter, rack cutter, shaver cutter
	Grinding	Grinding wheel
Contour machining	CNC milling	Cylinder or ball mill cutter
	Wire cut EDM[a]	Wire
	Laser cutting	Laser beam
	Water Jet cutting	Water or water and abrasive media mixture stream

[a] EDM: electric discharge machining.

The gear manufacturing by forming methods like die casting, injection molding, extrusion, rolling, powder metallurgy processing and near-net forging, etc. have gained popularity in the last decades. The forming methods providing a high benefit-cost ratio for mass production of gear drives and progress of these technologies allowed a significant increase in their accuracy [1]. However, the selection of the forming methods is dependent on the gear materials and considerable efforts are required in the tooling and process design to facilitate the processes.

However, the production of the asymmetric gear profile by the conventional thread cutting method is dependent on the cutting tool design and the machining process. Due to the profile geometry of the asymmetric gears, the production with the conventional thread cutting method limits the design of the profile. Recent studies in this area have shown that asymmetric profiles designed independently from the cutting tool are more efficient [2].

In precision gear forging, on the other hand, the final tooth profile is determined by the die geometry and therefore the limitations of the cutting tool can be eliminated totally. The cutting process of the gear die is wire electrical discharge machining (WEDM) and it presents a flexible design opportunity for gear tooth profile design. In the production of asymmetric gears, the use of precision forging technology may enable the production limitations stemming from the profile to be removed and the gears with high strength to be produced efficiently.

Gear fabrication with precision forging has started with relatively easy bevel gears and has been successfully applied in recent years to spur and helical gears. There are many studies that show the superiority of gears manufactured with precision forging in terms of strength and cost [3-5]. However, these studies have been carried out for symmetrical gears. The precision forging method enables the manufacturing of complex profiles and therefore the flexibility of the gear profile to be produced would be advantageous in the use of precision forging in asymmetric gear manufacturing. However, there is a need to improve forging die and process design so that precision forging technology can be applied to asymmetric gears. The design and manufacture of the die with the desired precision will directly affect the quality of the gear to be produced. In addition, due to the high forging load resulting from precision forging, die strength and service life are important parameters, so the design of material flow, die components, and forging parameters (temperature, deformation speed, lubrication, etc.) arise as problems to be overcome. For asymmetric teeth, there is not yet a study in the literature on this subject.

1.3 The Purpose and the Research Program of the Study

The aim of this study is to investigate the precision gear forging method for the manufacture of asymmetric spur gears. The main goals of the study can be briefly summarized as follows:

- Investigation of the feasibility of asymmetrical spur gears with near-net shape with precision forging,
- Development of a mathematical model that will create the tooth profile of the asymmetric gear forging die, depending on the final gear profile.
- Development of an upper bound analysis model for prediction of the forging load,
- Determining material flow, forging load and mold stresses by performing finite element analysis,
- Performing verification studies with experimental forging processes,
- Determination of design criteria for asymmetric spur gear forging dies.

For the production of asymmetrical gears with precision forging, the forging die was first be designed. For this purpose, using the finite element method, the material flow was modeled, the forging load and the die stresses were determined. For the calculation of the forging load, an upper bound analysis model was developed and the software was prepared to reduce the time for calculation. Numerical analyzes were carried out taking into consideration the material and the profile of the preform, the forging temperature and the lubrication conditions and the die geometry (tooth profile), the material and the components (inner die, outer ring, lower and upper punches, etc.) of the die was designed accordingly. The tooth profile with the required modifications and the toolpath was generated by the developed software. The designed die components were manufactured using wire erosion and CNC lathe-machining. Abrasive Flow Machining (AFM) was applied to increase the surface quality of the dies. Forging experiments were carried out using lead. The experimental and the finite element results were compared and the boundary conditions were verified accordingly.

Using the obtained experimental and numerical analysis results, die and process design criteria of asymmetric precision gear forging method were presented. The flowchart of the research program is given in Figure 1.2.

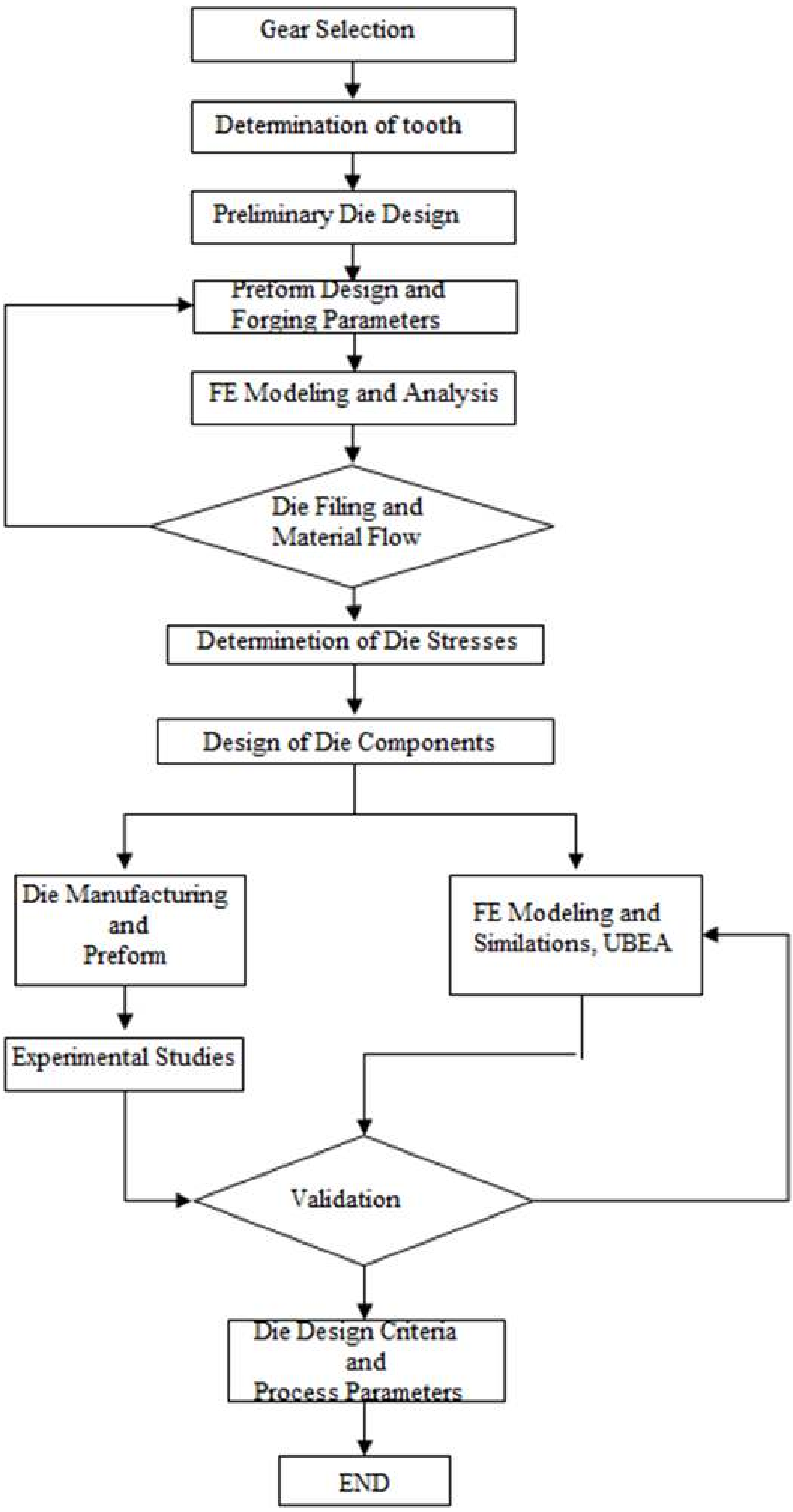

Figure 1.2 The flowchart of the research program

1.4 Organization of the Thesis

This section is for how the chapters are organized in the thesis. The contents of the chapters are given briefly.

Chapter 2 contains a literature survey. Especially the literature survey focused on the studies performed in the last two decades. In the literature, studies were given under heading asymmetric gear design and stress analysis, asymmetric gear manufacturing, and precision gear forging.

In Chapter 3, the asymmetric tooth profile generation and tooth profile optimizations were explained based on the direct gear design method. In addition, the selection of a prototype of asymmetric gear for this study is explained.

The finite element simulation models for warm-, hot-, and lead-forging processes of the asymmetric gear precision forging were discussed in Chapter 4.

Upper- Bound energy analysis (UBEA) of the asymmetric gear forging was explained in Chapter 5. Also, the development of software used in the calculation of upper-bound analysis was explained.

The die design procedure of the precision forging of the asymmetric gear was described in Chapter 6.

In Chapter 7 experimental setup, materials, measurements and procedure were explained.

The results of Upper-Bound energy analysis, FE simulations, and experimental studies were compared with each other and discussed in Chapter 8.

In Chapter 9, conclusions that are deduced from the study were explained and future works that can be done were recommended for the researchers that study in this area.

CHAPTER 2

LITERATURE SURVEY

2.1 Introduction

Asymmetric gears are able to transport more power and torque between the parallel and nonparallel shafts than symmetric gears that have the same size as asymmetric gears especially in the one-directional motion. Thus researchers have had an increasing interest in the studies about the asymmetric gears.

In this chapter, the results of literature survey on asymmetric gears are presented under the headings mainly as; asymmetric gear design and stress analysis, asymmetric gear manufacturing, precision gear forging, and precision gear forging of asymmetric gear

2.2 Asymmetric Gear Design and Stress Analysis

Deepak and Kumar [6] designed an asymmetric gear pair using standard gear formula and Lewis Buckingham Equation. Asymmetric gear pair was modeled in Creo parametric 2.0 of PTC then the asymmetric gears were fabricated by using a 3D printer. Also, two shafts had been manufactured in order to assemble gear pair, and then the parts were assembled. In this way, an asymmetric gear drive was obtained in a fully operational condition.

Kapelevich and Shekhtman [7] studied the optimization of tooth root which is generated with protuberance hob because the tooth root load capacity is a major contributor to gear load transmission performance. They showed that optimization of the tooth root fillet with protuberance hob reduces the root tensile stresses by about%10 with respect to tooth root fillet generated by the full tip radius profile protuberance hob.

Mo et al. [8] established an asymmetric gear model considering the influence of friction and shear stress on root bending stress. They created a 2D model of symmetric gear (20^0-20^0) and a model of asymmetric gear (20^0-35^0). They claimed that root bending stresses increase with the increase of pressure angle under friction effect.

Shuai et al. [9] studied a two-stage asymmetric helical gear star drive system in order to analyze the influence of eccentricity error, load, and input speed on the load sharing performance. To make this study a virtual prototype model based on ADAMS was created and analysis of the dynamic meshing force of gears, the load sharing coefficient of each star gear was calculated and the results compared with MATLAB solution results. They showed that by changing the pressure angle of the drive side, the load sharing coefficient of the system fluctuates and the working condition of the asymmetric gear is more stable than the symmetric gear.

Thomas et al. [10] studied to determine time-varying mesh stiffness for normal contact ratio asymmetric spur gear tooth by using FEM. Then the time-varying mesh stiffness which is determined had been used to predict dynamic load under non-extended contact conditions by using two different speeds values. After that, the power loss was analytically computed under dynamic and quasi-static load conditions according to two different friction conditions Elastohydrodynamic lubrication (EHL) and Dowson and Higginson). They showed that both friction conditions predict a lower value for higher speeds and EHL predicts lower values than the Dowson and Higginson. Also, it was shown that power loss is relatively higher when the speed approaches the resonance speed.

In the paper presented by Prabhu Sekar [11] a method was proposed to improve load-carrying capacity in bending and contact, as well as to improve wear resistance, in order to increase gear efficiency by asymmetric tooth. In the study, fillet and contact stresses, wear resistance, frictional power losses, load sharing by tooth pair and mechanical efficiencies were investigated, multi-pair contact model was simulated in ANSYS and comparative assessment of symmetric and asymmetric gear was done. It was shown that load sharing increases in the double pair region. A normal contact ratio asymmetric spur gear can be designed according to load sharing in this case point C is to be treated as a critical loading point for maximum fillet strength and point B is to be treated as a critical point of loading for maximum contact strength (see in Figure 2.1). Also, they showed that in the case of symmetric gears, bending strength improves with increasing pressure angle up to 25 degrees, the best bending stress improving is obtained in the asymmetric gears when the pressure angle of the drive side and coast side is 37.5 and 20 degrees respectively. Furthermore, because of the increasing moment arm, the maximum fillet stress and contact pressure reduce significantly due to an increase in the pinion teeth number.

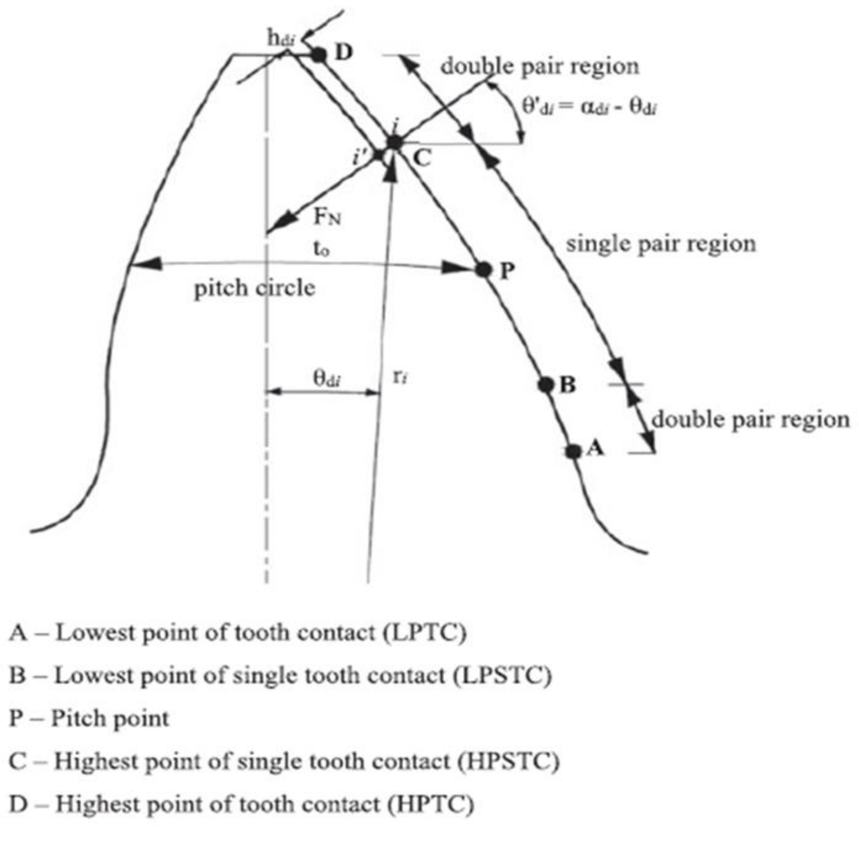

Figure 2.1 Asymmetric tooth loading points and regions.[11]

Abhang and Dekhane [12] determined the design parameters of asymmetric gear after that they created the asymmetric gear model by using CATIA, then the asymmetric gear was produced by 3D printing method. Finally, finite element analysis and experimental studies were performed. The results showed that FEM results and experimental results are suitable for each other. They concluded that bending load capacity increases and bending stress decreases by increasing pressure angle on the drive side of the gear.

Benny et al. [13] tried to predict the bending stresses of asymmetric gears based on the analytical approach. They suggested a new coordinate system and methods (Search Method 1 and Search Method 2) for analytically predict of bending stresses in normal contact ratio asymmetric spur gears. Furthermore, they performed FE simulations in Hyperworks and compared the results of the newly suggested method and ISO-6336-3 standard with each other. They found that FE results and newly suggested Search method 1 are in good agreement with each other than the ISO-3663-3 standard results. Also, they stated that Search Method 1 is more accurate than the Search Method 2. In addition, it was demonstrated that by keeping coast side pressure angle fixed gear tooth proportion, maximum tensile bending stress, and radius where it occurs decrease whit asymmetry factor. Finally, they showed that increasing tooth number and asymmetry factor effect bending moment due to the eccentricity of the radial component of gear tooth load.

Vaghela and Prajapati [14] presented an approach to reduce bending stress at the tooth root fillet therefore, to increase load-carrying capacity. To achieve this purpose Bezier curve was used at the tooth root of asymmetric gear and FEM simulations were performed in ANSYS. They showed that by using the Bezier curve in root profile optimization, Von-Mises stresses which are occur at the tooth root reduce by 16.68 %.

Demet and Ersoyoğlu [15] designed and manufactured asymmetric spur gears using circular fillet method in the tooth root region and investigated fatigue life of the gears due to fatigue damages caused by cyclic loading and effects of material hardness (48 HRC and 38 HRC). To investigate the fatigue performance of the gears, a new single-tooth bending fatigue test apparatus was developed. Also, Low-cycle and High-cycle loading tests were performed to determine the fatigue performance of the asymmetric spur gears. The single tooth bending fatigue test results showed that because of the material hardness increases the residual stresses on the material surface increase, gears with 48 HRC have lower fatigue strength than that of the gears with 38 HRC. In addition, it was found that in the 48 HRC gears, breaks occur on the coast side surface of the gears due to high residual stresses on the surface and in the 38 HRC gears breaks occur in the inner surface of the tooth.

Yılmaz et al. [16] derived a mathematical equation of pinion cutter then by using coordinate transformation the points of internal gear were obtained. The internal gear was built in CATIA as a 3D model. Several case studies were performed in ANSYS to see how pressure angle and tip radius effect bending stresses. It was proved that by the results, the bending strength of the asymmetric internal gear is higher than the symmetric gear.

Chen et al. [17] derived a mathematical model based on coordinate transformation and mathematical relations to obtain an imaginary asymmetric rack cutter with a parabolic profile. Then a relationship was set up between rack cutter and gear pair. After that, a family of imaginary rack cutter surfaces was obtained. By using a homogeneous coordinate transformation matrix, the coordinate system of the rack cutter was transferred to a gear pair coordinate system. A pinion and a gear were generated. Then tooth contact analysis was performed to determine the influences of kinematic errors and the asymmetric tooth profile due to assumed assembly errors. The study shows that kinematics errors are sensitive to misaligned angles but insensitive to center distance error. Also, it was shown that by increasing rotation angles the contact area gradually moves to the tooth flank, the contact area becomes smaller and teeth disengaged.

Marimuthu and Muthuveerappan [18] presented a finite element study on maximum fillet and contact stresses of asymmetric spur gear which was designed by using the direct design method based on the load-sharing ratio. An Ansys parametric design code was developed in order to find the load sharing ratio, maximum fillet, and contact stresses. It had been concluded that a smaller contact ratio and a higher pressure angle at the loading side of the asymmetric gear must be preferred to enhance load-carrying capacity.

Masuyama and Miyazaki [19] investigated torque transmission capacity of asymmetric gears with respect to different pressure angles. Deflection and bending stress of the tooth were calculated by using the finite element method by taking into account the load-sharing ratio. Additionally, Hertzian contact stress was calculated with respect to contact pressure. They showed that bending stresses and Hertzian contact stresses decrease by increasing pressure angle so the larger the pressure angle the more the torque transmission capacity.

Marimuthu and Muthuveerappan [20] carried out a parametric study for high contact ratio spur asymmetric gears depending on load sharing method in order to arbitrate non-dimensional fillet and contact stresses. Also in the study, symmetric and asymmetric gears which are designed by using direct gear design were used and the results of both gears were compared with the conventional high contact ratio spur gears. In addition to these, the effect of gear parameters such as gear ratio, addendum pressure angle, the backup ratio of non-dimensional stresses is analyzed in detail. They showed that the non-dimensional fillet and contact stresses in the asymmetric gear which is designed with a direct gear design method are less than the symmetric one. Also, they showed that the non-dimensional fillet and contact stresses in the symmetric gear which is designed with direct gear design method are less than the symmetric gears which are designed conventionally. Additionally, it was shown that by increasing gear ratio and teeth number a reduction in non-dimensional contact stresses was obtained.

Dharashivkar et al. [21] studied to evaluate bending stresses at the root of the asymmetric tooth by using the 3D photoelasticity method. To achieve this aim, ISO/TC-60 was used to calculate bending stresses theoretically, 3D model of the gear was drawn in CATIA V5 R15, finite element simulations were done in ANSYS and 3D photoelasticity method was used to evaluate stresses experimentally. Also, they performed finite element simulations for symmetric and asymmetric gears to observe bending stress changes due to asymmetry. They derived from their study that the 3D photoelasticity method is the best method to evaluate bending stresses. FEM results and theoretical results are almost the same. Based on bending stresses at the tooth root, the strength of the asymmetric gear is higher than the strength of the symmetric gear. A very small change at the critical thicknesses of the tooth has a great effect on its bending strength.

In the paper which was presented by Cazan and Plesu [22] on one hand a mathematical approach was suggested for fatigue strength of gear, on the other hand, this mathematical approach was applied to a particular system regarding a better fillet geometry of symmetric and asymmetric gears.

Xiao-he et al. [23] studied on characteristics of asymmetric gears. Based on meshing properties, they proposed an involute slope modification method considering the effects of static transmission errors. They studied involute slope modification by changing parameters. Furthermore, for modified and unmodified asymmetric spur gears mesh stiffness and synthetic mesh stiffness were analyzed. They revealed that appropriate modification can help to obtain better involute profile to decrease instant changes of stiffness curves. Also, it was concluded that with proposed modification, harmonics' amplitudes can be impaired; enabling to diminish stiffness excitation and this can be a guide for researchers who study noises and vibrations of gears.

Prabhu Sekar and Muthuveerappan [24] adapted a standard ISO B methodology to estimate tooth form factor and the stress correction factor of the asymmetric gear. Also, a comparative finite element studies were carried out for a set of different drive side and cost side pressure angle to determine tooth form factor and critical root fillet parameters. They concluded from the study that maximum fillet stresses which are developed in the asymmetric gear are lower than the symmetric one. In addition to this, they proved that the tooth fillet stresses are lower when the higher pressure angle was used for the drive side. Also, it was shown that the tooth fillet stresses decrease with increasing drive side pressure angle and vice versa for the coast side.

Kargin [25] reviewed the literature data about the involute transmission with asymmetric tooth profiles. In light of the already knowledge, prospects for use of asymmetric involute profiles were considered. It was assessed that by the author, the use of asymmetric involute gears in a three-component gear mechanism will have significant changes in the future.

Deng et al. [26] proposed a design method for the geometric shape and modification of asymmetric spur gears. In the proposed method geometric shape was obtained by way of rack cutter which has different pressure angles and fillet radius in the driving and cost sides so the gear has different pressure angles and fillet radius in the drive and coast side. Also in the modification design of the gear firstly the geometry of the rack cutter was modified then the modified gear was obtained. Then the gear was drawn by using computer-aided design software. FE simulations were done in order to analyze the meshing process, transmission errors, and load sharing ratio for the modified and unmodified asymmetric gears. They concluded from the results of the study that the proposed design method was feasible and gear with better transmission properties can be obtained.

Banica and Ravai-Nagy [27] investigated the dynamic behavior of asymmetric gear by replacing it into a place of symmetric gear. They studied how does effect the tooth flank error dynamic behavior of the gear and how does the configuration of the gears influence the dynamic behavior of asymmetric gear comparing with symmetric gear. They showed that great deviations affect the real active length of flank and this is not desirable. Also, it was concluded that dynamic and static bending stresses in the symmetric gear are greater than the asymmetric gear at a range of 27,3-31,5%.

Olguner and Filiz [28] studied the design of spur gear with asymmetric teeth in the external gear pump. They generated a model for asymmetric gears and instantaneous flow rate equations were derived by the authors. In the study, a computer program was developed by the researchers. Different seventeen gear pair which have different drive side pressure angle and coast side pressure angle and profile shift coefficient was tested. The effect of these parameters on the flow rate, flow rate fluctuations, tooth contact, and bending stresses was investigated. They showed that it is possible to decrease root bending and contact stresses by 20 % by increasing the drive side pressure angle, also increasing the drive side pressure angle increases flow rate, and decreases flowrate fluctuation without increasing gear size and center distance. Besides this, it was shown that increasing the profile shift coefficient decreases tooth root bending stresses, tooth contact stresses, and flow rate fluctuation while increases the mean flow rate slightly. But increasing the profile shift coefficient is not efficient than the increasing drive side pressure angle.

In the paper presented by Prabhu Sekar and Muthuveerappan [29] load sharing ratio and corresponding load sharing ratio depended on maximum fillet stresses with respect to non-dimensional stress number were estimated for conventionally designed symmetric and direct designed symmetric helical gears. The study also covers direct designed asymmetric helical gears in terms of these parameters. It was proved that the maximum root fillet stresses in the asymmetric helical gear are always less than that of the symmetric helical gear. Non-dimensional stress number drastically decreases when the gear ratio increases.

Marimuthu and Muthuveerappan [30] dealt with an accurate estimation of optimum profile shifts for normal and high contact ratio asymmetric spur gears based on gear and pinion tooth fillet strength for a load which is at the critical loading point considering load sharing of pinion and gear. In the study, gears were designed by the direct design method. Also, they developed area of existence for high contact ratio asymmetric gears.

Kapelevich [31] presented an analytical approach for gear mesh characteristics such as contact ratio, operating pressure angle, gear mesh efficiency as functions of the pitch factors, specific sliding velocities. The study also contains the area of existence of involute gear pairs for the given constant values of the pitch factors.

Marimuthu and Muthuveerappan [32] studied the effect of the direct design asymmetric high contact ratio spur gear based on tooth load sharing. They used a unique ANSYS parametric design language code for the study. For different drive side, contact ratios load sharing based on bending stress and contact stress were determined. They stated that the load sharing ratio based on contact stresses decreases due to load at the critical loading point according to the study.

Zhao et al. [33] derived the equations of teeth surface of double pressure angles asymmetric face-gear, according to the theory of gear geometry. Then by using ANSYS, the finite element model was created for a single tooth pair which contact each other. The results showed that when the number of elements in the finite element model increases, the maximum tooth contact pressure angle is bitten by bit moves to values calculated by Hertz theory and finally fully coincide. Also, it was deduced that increasing pressure angle at the drive side results in a reduction in the maximum tooth contact pressure and maximum tooth root tensile stresses, and reducing the coast side pressure angle may cause an increment of the maximum tooth root tensile stress. But the effect of reduction of coast side pressure angle on the tooth root tensile stress is less than the that of the increasing drive side pressure angle.

Marimuthu and Muthuveerappan [34] investigated the influence of pressure angle on drive and coast sides in asymmetric normal contact ratio gear which is designed conventionally, considering load sharing between the gear teeth pair. Multi-pair teeth contact model was created for finite element simulation in ANSYS in order to find the load sharing ratio and respective stresses. It was found that when the pressure angle of the drive side is 35 degrees if the drive side is loaded and when the pressure angle of the coast side is 25 degrees if the coast side is loaded, the maximum fillet stress is at its lowest value.

Deng and Cai [35] created an involute slope modification model of asymmetric spur gear, considering modification angle and modification coefficient ratio. They stated that the modification angle affects the maximum value of contact stresses and the modification coefficient ratio impresses the shape of the contact stress curve. Also, it was deduced that both parameters have an effect on the contact performance, suitable values of the parameters improve the transmission performance of the gear pair.

Karpat et al. [36] built a 2D tooth model for asymmetric gear by using finite element analysis. They derived formulas to estimate tooth stiffness with respect to the pressure angle of the drive side and teeth number. The results of the derived formulas were compared with well-known formulas in the literature and they showed that the newly derived tooth stiffness formula and developed FE models can be used in dynamic simulations and the result of both are precision compared with other formulas.

Ning and Li [37] analyzed the relationship between rack cutter parameters and the parameters of the gear profile, based on the rack cutter with an asymmetric tooth. 3D model of asymmetric helical gear was built. It was shown that asymmetric helical gears can be manufactured by traditional methods. Additionally, they deduced that the 3D model reflects the correct relationship between parameters and meshing formulas.

Liming and Guimin [38] analyzed the dynamic performance of asymmetric gear transmission systems by using MSC.ADAMS software. They compared results of asymmetric gear with symmetric gear and concluded that asymmetric gear transmission system is superior to symmetric gear transmission system according to vibration characteristics, during the transmission.

Sandooja and Jadhav [39] presented a mathematical model for asymmetric helical gear pairs. Load carrying capacity and gear performance of the gear were investigated in terms of mesh stiffness and noise during power transmission, by increasing gear drive side pressure angle. They showed that asymmetric helical gear design, reduce noise and sliding velocity, increase load carrying capacity, reduce weight, and under dynamic conditions maintain the life of the gear for a longer time.

Agrawal and Himte [40] carried out FE analyses by using ANSYS for symmetric gear, asymmetric gear, and asymmetric gear which has a relief circular hole at the vicinity of the root fillet region. They showed that maximum bending stress, in the symmetric gear is 432.698 N/mm^2, in the asymmetric gear is 420.916 N/mm^2 and in the asymmetric gear with a circular hole at root fillet region is 419.441 N/mm^2. They concluded that a suitable stress relief feature at the root fillet region decreases bending stress and the stress relief feature should be in the vicinity of the root fillet region.

Alipiev [41] suggested a new method which is called Realized Potential method for geometric design of asymmetric and symmetric involute meshing where the potential of the gear drive is equal to its contact ratio. By using gear drive potential as an input value, the geometry of the gears, rack cutters, and involute meshing was determined. He showed that Realized Potential Method is suitable for gears that have small teeth numbers.

Kargin [42] studied the analytical detection of the transition curves at the base of asymmetric gear teeth and this was done by using two-stage. In the first stage, it was determined by roulette constructions which associated with initial gear circumferences that roll over one another. A radial gap was constructed in the second stage and this facilitates manufacturing and reduces stress concentration at the tooth root of the gear.

In the paper presented by Li et al. [43] a calculation method was formulated to calculate contact stresses of helical gears with asymmetric teeth. In order to calculate instantaneous contact stresses at the contact line, computer software was developed. Results of asymmetric helical gear and symmetric gear were compared. They deduced from the results that contact stresses reduce significantly with the increasing pressure angle at the drive side of the helical gear.

In the paper which was presented by Liu and Fan [44] an asymmetric double circular gear was designed for large-scale high-pressure gear pumps. According to the results of the study, asymmetric double circular gears are suitable for large-scale high-pressure gear pumps which have advantages such as smooth flow, no pulse, and no tooth tipping. In addition to this, newly designed large-scale high-pressure gear pumps can meet the demands of high-pressure and large displacement.

Pedersen [45] studied to improve bending stress in spur gears using gears with asymmetric teeth and shape optimization which is made through rack cutter. Based on this idea, two types of rack cutters were proposed which can be seen in Figure 2.2. From the study, it was concluded that a great amount of improvements in bending stress can be achieved by using asymmetric gear and by changing rack cutter geometry which is directly affect the shape of gear tooth a bending stress reduction in the order of % 40 can be obtained.

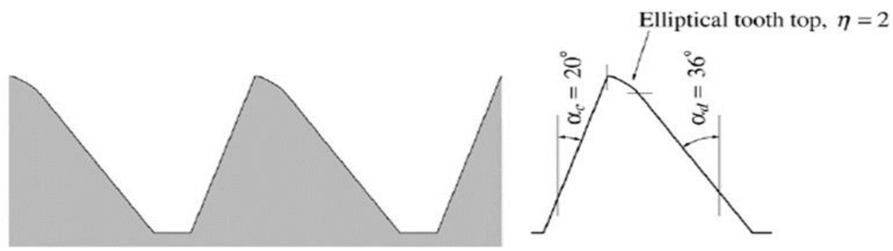

a) New standard asymmetric elliptic cuter AE1.

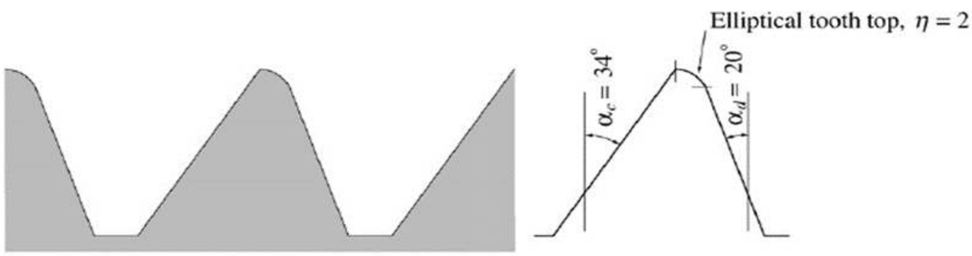

b) New standard asymmetric elliptic cuter AE2.

Figure 2.2 Type of proposed rack cutter. [45]

Kargin [46] had foreseen that involute gear transmissions with asymmetric tooth profiles can be divided into three levels according to the applicability, and methods of synthesis and manufacture. The properties of these three levels were studied and it was concluded that involute gear transmissions with asymmetric tooth profile can be divided into three-level. Also, it was shown that due to different properties of these three levels, they can be used for different purposes such as increasing longevity and reliably of transmission and smoothness of operation.

Costopoulos and Spitas [47] introduced an idea of one-sided involute asymmetric spur gear tooth, to rise load carrying capacity, increase the strength of non-involute curve and to associate meshing properties of driving involute of the gear. To investigate this idea, FE simulations were performed. The FE results showed that a reduction of pinion fillet bending stresses up to 28 % was obtained comparing with standard design gears and this can be interpreted as an increment of load-carrying capacity. Also, it was concluded from the study that, without changing the size or number of the teeth in the gearbox a reduction of bending stresses and improving pitting resistance can be obtained by using proposed asymmetric design in automobiles.

Kumar et al. [48] by using injection molding, produced an asymmetric gear made from unreinforced polypropylene material and has pressure angles of 34^0 and 20^0 at a drive and coast-side respectively and has 3 mm module. Also, a test rig was developed in order to analyze surface durability and kinematics characteristics of the asymmetric gear. It was shown that when the drive side pressure angle of the gear is higher than the coast side, the transmission efficiency of the gear pair is superior and also exhibits lower surface temperature.

Muni and Muthuveerappan [49] attempted to achieve the optimum design for asymmetric internal gear considering desired values of input parameters such as working center distance, top land thickness coefficient, asymmetric factor, the gear ratio, and contact ratio. They determined the optimum value of the addendum modification for a given asymmetry factor, using the mentioned parameters.

Spitas et al. [50] introduced an idea of a one-sided involute asymmetric spur gear tooth to rise load carrying capacity and increase the strength of the non-involute curve and to associate meshing properties of driving involute of the gear. Both profiles of the tooth were generated by a hob. FE simulations were performed and the results showed that a reduction of pinion fillet bending stresses up to 28 % was obtained comparing with standard design gears and this can be interpreted as an increment of load-carrying capacity. Also, it was concluded from the study that, without changing the size or number of the teeth in the gearbox a reduction of bending stresses and improving pitting resistance can be obtained by using proposed asymmetric design in automobiles.

Senthil Kumar et al. [51] developed non-standard rack cutters in order to generate pinion and gear with asymmetric involute surfaces and trochoidal filet. Several non-standard rack cutters were designed to analyze different combinations of the parameters that are pressure angle, speed ratio, profile shift, top land thickness ratio, and asymmetric factors. FE simulations were performed for symmetric gears, the results were compared with the results of ISO and AGMA codes to prove the results of the FE simulations. They showed that peaking which occurs in the symmetric gears at a high-pressure angle can be overcome by using asymmetric gear. Also, it was shown that asymmetric involute surfaces improve the fillet load capacity of the gears.

In another paper presented by Karpat et al. [52] the feasibility of using asymmetric gear in microelectromechanical systems was studied. They analyzed root stresses, applied the Weibull failure theory, and investigated the capacity of different asymmetric gear configurations. They demonstrated that maximum bending stresses increase with increasing tooth high parameters. In addition, it was shown that asymmetric gear tooth with 36 degrees of pressure angle on the drive side provides the best solutions.

Yang [53] studied on the asymmetric internal gears. Driving and driven gears with asymmetric spur and helical teeth were generated. He developed a mathematical model of meshing properties of the driving and driven gears. He investigated kinematic errors according to a mathematical model developed for meshing. The results of the study showed that the kinematical errors of the asymmetric helical internal gear are less than that of the asymmetric spur internal gear, kinematic errors are sensitive to misaligned angles but not to center distance assembly errors. In additionally it was shown that asymmetric helical internal gears are superior to asymmetric spur gear in terms of stresses and contact engagement.

Francesco and Marini [54] created a calculation method for the dimensioning of the asymmetric gear and to determine equivalent form factor and equivalent notch factor for asymmetric gear, which allows to designer to estimate root bending stress. They showed that gear designers may use ISO procedure in order to certify bending stresses in the case of asymmetric gear conveniently.

Muni et al. [55] suggested two procedures in order to optimize a given asymmetric gear designed with the direct design method. A set of asymmetric tooth profiles of pinion and gear were generated, considering a set of pressure angles of the pinion and gear for the required contact ratio. They made suggestions to improve bending strength capacity, by the way, changing parameters such as top land thickness coefficient, asymmetry factor, and teeth number.

Karpat et al. [56] studied asymmetric gears used in the micro-electro-mechanical system. A computer program was developed; the probability of failure of asymmetric gear was investigated considering pressure angle, tooth height, and contact ratio by using the Weibull failure theory. It was shown that asymmetric gear which has 36 degrees' pressure angle for the drive side is most useful for the design of the micro-electro-mechanical system.

Yang [57] developed a mathematical model for asymmetric helical gear. Based on the mathematical model, an assembly of pinion and gear with asymmetric teeth was developed. Undercutting conditions for asymmetric helical gear were investigated according to the proposed mathematical model and a 3D stress analysis was carried out in a simulation. It was shown that asymmetric helical gear is superior to asymmetric spur gear in terms of stresses.

Litvin et al. [58] designed a face gear with asymmetric tooth profile which is used in helicopter transmission and developed computer software in order to analyze the conventional and new types of geometry of asymmetric face gear. By using the finite element method, meshing and tooth contact analysis were carried out. In the study drive side pressure angle was selected higher than that of the coast side. It was shown that by using the asymmetric profile in face gear, more than 10 % reduction of bending and contact stresses were obtained.

Kapelevich [59] developed a basic geometric theory of asymmetric gears. Also, he determined formulas and equations, for asymmetric gears and generating rack-cutter parameters. In the study, it was shown that the geometry of asymmetric gears allows for an increased load capacity of the gear while reducing the dimension and weight of the gear and when the contact ratio and drive side pressure angle is increased.

2.3 Asymmetric Gear Manufacturing

Ravai and Lobontiu [60] studied on asymmetric gear cutting processes. They classified asymmetric gear manufacturing through cutting into two main groups; conventional technologies and unconventional technologies (Figure 2.3).

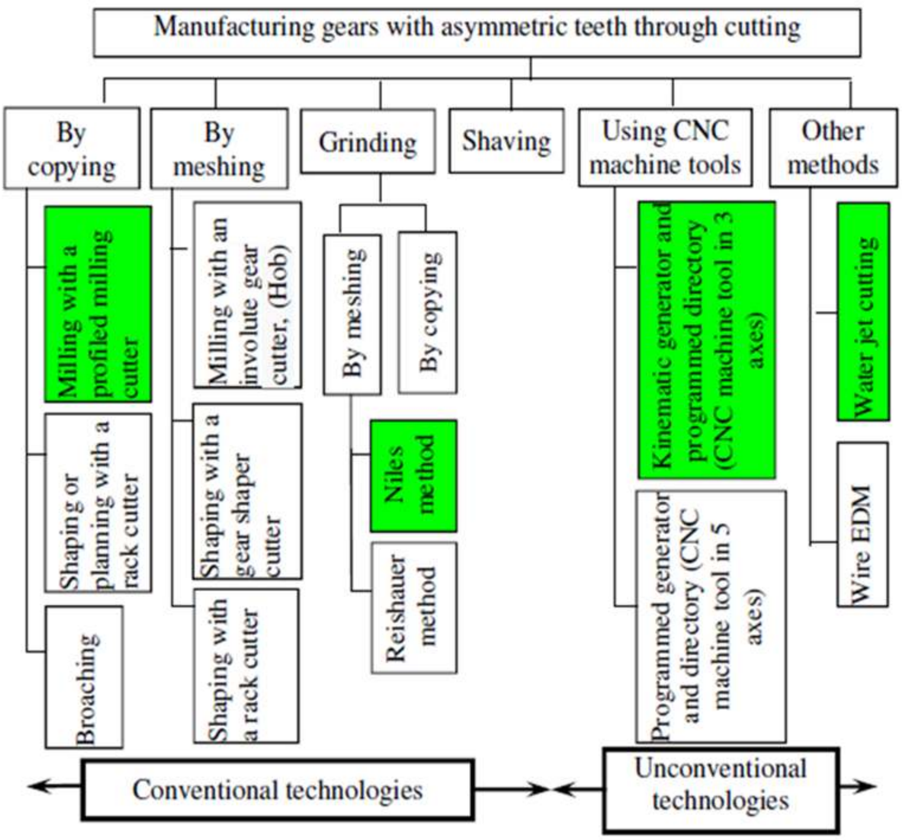

Figure 2.3 Classification of the manufacturing technologies used in the processing of the asymmetric gears. [60]

In another study by Ravai and Lobontiu [61] manufacturing a plastics (HD500) gear with asymmetric teeth (see Figure 2.4) by using the CNC machine was presented. Accuracy of the gear machined on CNC was compared with that of the gears produced by gear tooth side milling cutter or gear tooth end mill. They predicted that steel gears can be produced by a CNC machine.

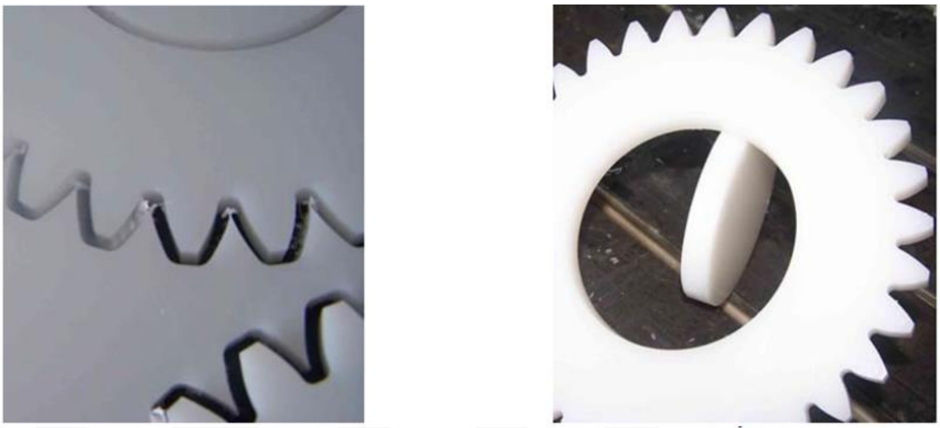

Figure 2.4 Gears with asymmetric teeth made on CNC controlled machine tool. [61]

2.4 Precision Gear Forging

Although there are many studies about the design and stress analysis of the asymmetric gear, and there are a few studies about asymmetric gear manufacturing, there is no study about the precision forging of asymmetric gears. However, in the literature, there is only a paper which is called "Study on Warm Forging Process of 45 Steel Asymmetric Gear" available but this is about the radial extrusion of asymmetric gear [62].

Dang et al. [63] performed three-dimensional rigid-plastic finite element simulations of the cold forging of helical gear using recurrent boundary conditions and compared FE results with experimental ones. They showed that the experimental load is smaller than that of the simulations, especially at the last stage and results of experiment and FEM simulations are in good agreement with each other in terms of profile surface. Thus they concluded that the proposed method of analysis can be effectively used in the cold forging of the helical gear.

Samołyk [64] performed FE simulations and experimental work for the cold orbital forging process of AlMgSi alloy bevel gear (see Figure 2.5). He concluded that planetary motion is recommended for the orbital forging of bevel gear and the degree of deformation and energy consumption increase if the spiral scheme is used.

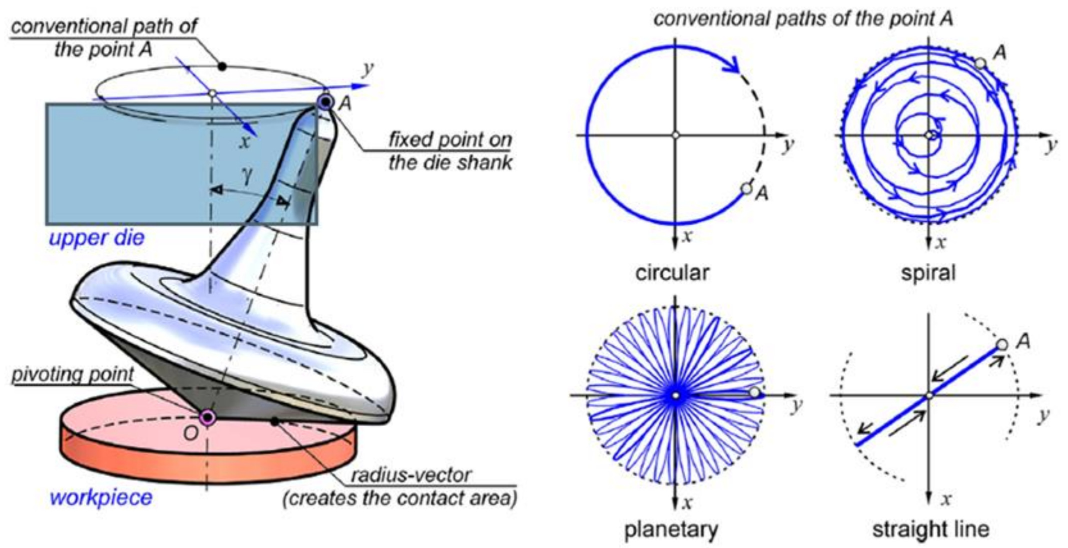

Figure 2.5 Schemes of upper die rocking motion for Marciniak's press. [64]

Feng et al. [65] calculated maximum forging load by using the finite element method (DEFORM-3D) and created an ANN (neural networks) model with the BP (backward propagation) learning algorithm. Using FEM data, they trained ANN model with the BP. It was shown that predicted force by ANN model with BP agrees with simulation results and predicted results satisfy the industrial requirement.

Feng et al. [66] investigated the effect of the billet geometry on the cold precision forging of the helical spur gear. By using DEFORM 3D, the forming load and uniformity of deformation were investigated. In the FE simulations, lead was selected as the workpiece material and simulations were performed for six different geometries by keeping other conditions the same for all simulations. The outer diameter of the billets is equal to the root diameter of the gear and other parameters of the billets can be seen in Figure 2.6. The results showed that forging load decreases with the increase of relief-hole -do-, the best uniformity is obtained when the relief-hole equal to 10 mm, effective strain distributions are very inhomogeneous in the axial and radial directions.

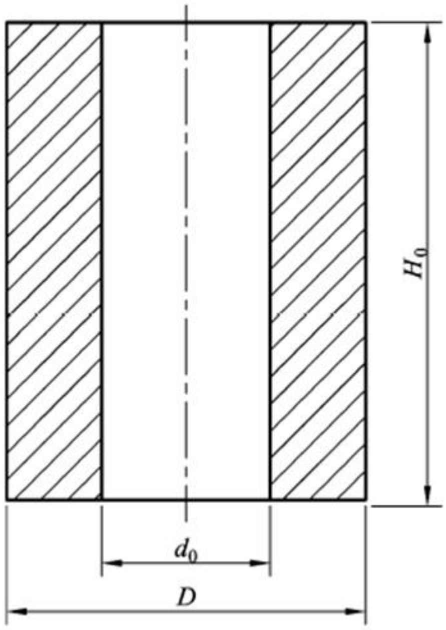

d_0/mm	0	5	10	15	20	25
H_0/mm	21.5	21.8	22.8	24.6	27.8	33.3

Figure 2.6 Dimension of the billets. [66]

Cai et al. [67] performed finite element simulations by using DEFORM-3D in order to analyze metal flow law and stress distribution of billet for a different type of vibration parameters during spur bevel gear forging. They concluded that deformation resistance of the gear in the vibration rotary bevel gear is lower than that of the conventional rotary forging and strain distribution is more uniform so the better forming quality is obtained. In additionally they concluded that when the higher amplitudes are used, smaller stresses, better forming quality and faster forming were obtained.

Deng et al. [68] created a finite element model of the cold rotary forging of a 20CrMnTi alloy spur bevel gear for the DEFORM-3D. Experimental studies were performed to validate the proposed FEM model. They concluded the workpiece can be divided into two regions; active deformation area and passive deformation area. The metal flow occurs primarily in the active deformation area.

Khalilpourazary et al. [69] performed simulations of the hot precision forging of straight bevel gear by using finite volume, computer-aided design and computer-aided engineering, and forging force and final shape of the gear were determined and compared the simulations results with the available experimental data in DIN standards. They concluded that the presented method can be used effectively to improve die strength, reduce material waste and to determine under-fill die cavities before the forging process begins.

Wei and Lin [70] presented a paper. In the paper, they proposed an optimization method based on the finite element method and the Taguchi method. They considered optimal objectives as maximum forging force and die filling quality and they investigated these objectives whit respect to process parameters such as deformation temperature, punch velocity and friction conditions affect. They showed that the deformation temperature and friction coefficient are the most affecting process parameters on the maximum forging force and die filling quality. Also, it was shown that experimental results run-in with that of the proposed optimization method.

In the paper presented by Zhao et al. [71] frictional coefficient, initial die hardness and rules of the wear were analyzed based on numerical simulations of the Steel Synchronizer Gear Ring Forging Process. They concluded that higher initial die hardness and good lubrication conditions provide the better die wearing resistance, and higher die temperature and longer forming time result in serious die wear. In addition, they showed that most of the die wear occurs between the two teeth.

Li [72] performed finite element simulations and experiments in order to analyze cold extrusion of inner ring gear by changing process parameters. It was shown that experimental results prove the finite element simulations.

Yang and Zhao [73] performed FE simulations by using DEFORM-3D in order to analyze the effects of floating die on the material flow and the tooth corner filling. Three different cases were simulated as seen in Figure 2.7. They showed that floating die has no significant effect on the load-stroke diagram, if the die is stationary, metal fills top region more rapidly, if the die moves with the speed of punch, metal fills bottom region rapidly and if the die moves with the speed equal to half speed of the punch, the metal flows similar to the upsetting process.

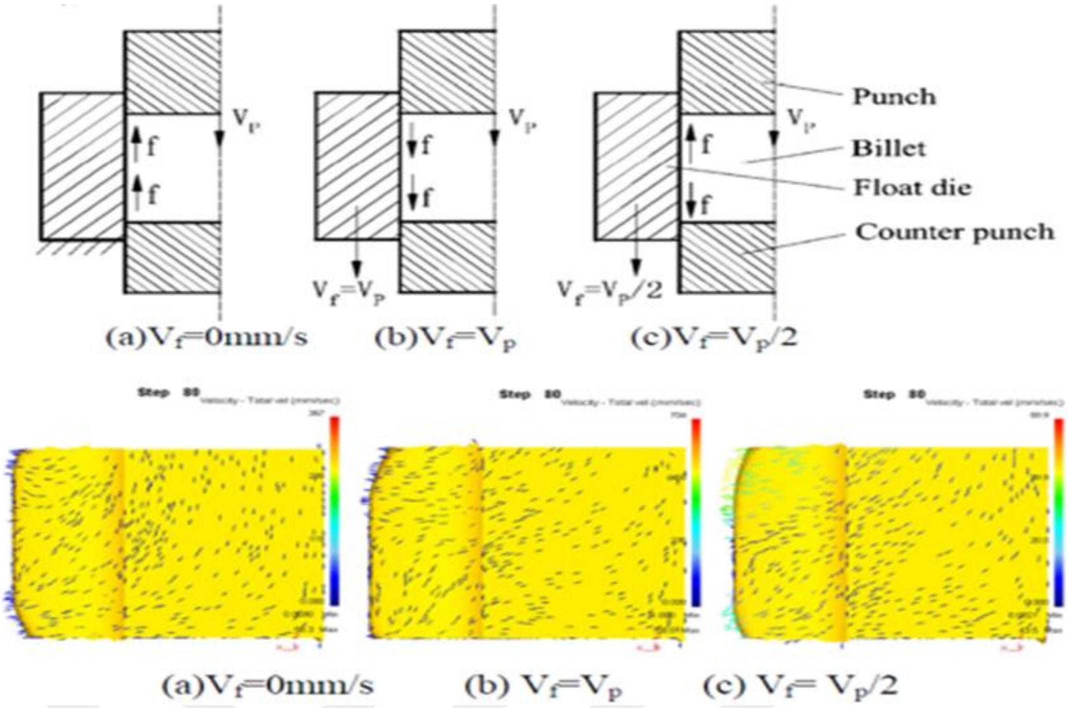

Figure 2.7 Three different case of floating die simulations. [73]

Chang and Kuo [74] experimentally investigated the effects of temperature and grain size on the closed die micro gear forging process. They developed a forging system equipped with heating devices and applied heat treatment in order to keep the grain size of the copper material between 4 and 46 µm. They prepared copper billets with coarse and fine grains for forging at different temperatures. It was shown that grain refinement and moderate increase of forming temperature improve material flow and this results in better filling of die cavities and uniform distribution of grains and hardness in the gear which is forged.

Hu et al. [75] put forward a novel specific gear forging technology based on a hypothesis of radial rigid-parallel-motive (RPM) flow mode. It is proved that the radial-rigid-motive (RPM) flow mode by performing numerical simulation and physical experiments. They showed that by using the novel specific gear forging technology, forging load decreases significantly, about 35 % compared with the conventional processes. Conventional flow mode and RPM flow mode can be seen in Figure 2.8.

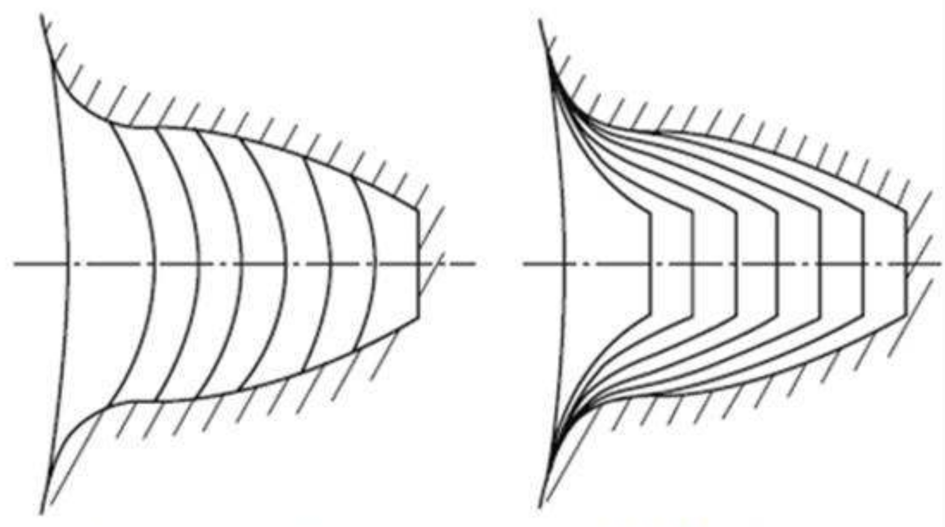

Figure 2.8 Metal flow rule of gear forging. [75]

Wang et al. [76] performed finite element simulations by using DEFORM-3D and an experimental study was done to prove simulations results for the forging process of starter motor ring gear. They obtained variation of metal flow, stress and strain. It was shown that experimental results and FEM results agree with each other.

Zhang et al. [77] conducted three-dimensional finite element simulations of the precision forging of bevel gear and investigated material flow, forging load levels and product geometry. Based on FEM simulations a die was designed. They showed that this procedure can shorten the die design and manufacturing period.

Ji et al. [78] designed two types die set for the bevel gear forging process. The first type die set has a back cone relief cavity and the second type die set has a small end relief cavity. Schematic of die set and relief cavities can be seen in Figure 2.9 and Figure 2.10. Die sets were used in finite element simulations and experimental studies. Then the results of FEM simulations compared with the results of experiments. They showed that the results of experiments and simulations are consistent in terms of forging load and clamping force. The die set with a small end relief cavity is superior to die set with a back cone relief cavity.

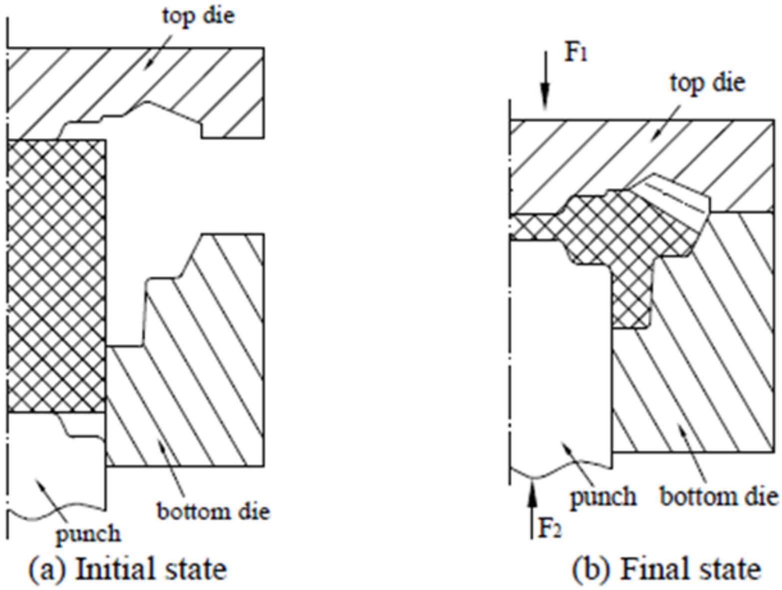

Figure 2.9 Schematic of the closed-die forging. [78]

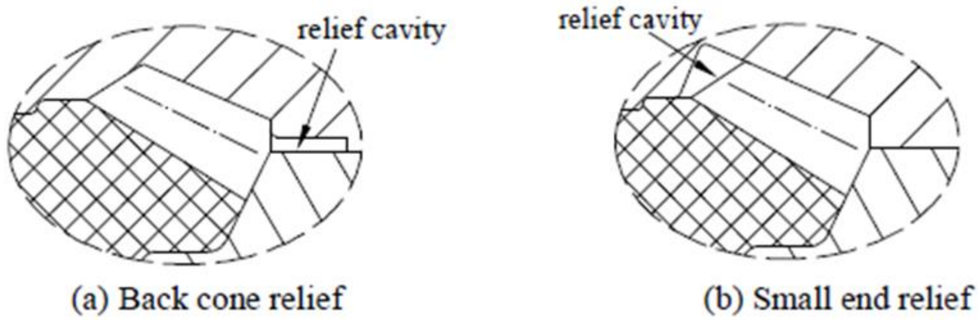

Figure 2.10 Schematic of relief cavities. [78]

Debin et al. [79] presented a novel hybrid process combining isothermal enclosed forging process with two kinds of piercing methods- double-ended piercing and central piercing method- to manufacture the micro-double gear. By using finite element simulations, filling quality and metal flow were investigated. Based on finite element simulations, experimental studies of the hybrid processes were performed and micro-double gear was produced with good surface quality by using the central piercing method. They showed that the hybrid process with the central piercing method is superior to the double-ended piercing method in terms of filling quality. Also, it was shown that the hybrid forging process has advantages of manufacturing efficiency, assembly precision and reproducibility compared with precision machining and directly forming.

Eyercioglu et al. [80] performed finite element simulations and experimental studies and proposed a set of the new formula by modifying cylindrical approach, for the shrink-fit design of precision forging spur gear dies. By comparing the result of FEM simulation, experimental studies and analytical solution, they concluded that newly proposed formulas can be safely used in the shrink-fit design of precision forging spur gear dies. Additionally, they stated that the highest value of P' - internal pressure divided by yield strength of the die material- must be 0,7. For values that are beyond this value, multiple ring assembly die should be considered as a solution.

Liu and Cui [81] by selecting magnesium alloy AZ31B as workpiece material, carried out finite element simulations and experiments for hot forging of spur bevel gear. Furthermore, to investigate the influence of preform shape, finite element simulations were performed by using commercial software MARC. The results of finite element simulations were compared with the results of the experimental studies in terms of the load-stroke diagram and it was shown that the results are consistent with each other.

Kim et al. [82] presented a paper that contains FE simulations, experimental studies and heat treatment of the forged helical gear. By using DEFORM-3D/HT, forming load, normal pressure, effective strain distributions on the workpiece, and stress distributions on forging dies were investigated. Results showed that computer-aided engineering can be used as an effective method to improve process design and allows to researcher to predict dimensional changes of the final product.

Chen and Jung [83] presented a robust design method based on the finite element method in order to optimize process parameters such as die wear, manufacturing tolerance, dimensional variation caused by temperature and the different friction conditions, etc. They performed a case study of hot gear forging processes based on a robust design method. The results proved the robust design method.

Irani and Taheri [84] investigated the effect of the temperature on the microstructure and hardness of the precision forged spur gear which is made from low carbon steel. They selected temperature range from 750 ^{0}C to 1050 ^{0}C to perform experimental studies. The results showed that 950 ^{0}C forging temperature is the optimum temperature for the homogeneous distribution of microstructure and hardness in forged spur gear.

Song and Im [85] carried out cold forging of a bevel gear using three-dimensional finite element simulations by selecting process parameters as press type, punch location, and billet diameter. In the study, the material flow and the load levels required for complete die filling were investigated. Based on the FE simulation results a die set was designed and bevel gear made of AISI1020 was cold-forged. By comparing FEM results and experimental results it was assessed that to increase die clamping force an additional clamping device was needed.

In the paper presented by Yang et al. [86] finite element analysis was performed to investigate the effects of yielding stress, strength coefficient and strain hardening exponent, on forging load and maximum effective stresses. Also, they performed adductive network synthesis to predict maximum effective stresses and forging load. They concluded that the results of FEM simulation and adductive are in good agreement with each other.

Sheu and Yu [87] designed die of cold orbital forging to produce a hollow ring gear. Different preform geometries were used to analyze deformation characteristics of the orbital forging. Also, they conducted finite element simulations to foresee the forging load. They concluded that forging load of cold orbital forging is one out of nine of the conventional forging process, the preform which is designed with smaller volume is better for both material flow and material saving, and the smaller the outer diameter of the preform the higher maximum effective strain and damage value occur.

Skunca et al. [88] analyze cold forging process of the bevel gear having straight tapered flanks. They performed experimental and FE simulations in MSC Marc Mentat 2005r2. They compare the FE results and experimental results with each other in terms of strain distribution and load-displacement diagrams. They obtained completely overlapping load-stroke diagram results of FEM with results of experiments, by changing the friction coefficient in simulations.

Zhang and Xie [89] analyzed three different forging processes and deformation behaviors of Zr41.25Ti13.75Ni10Cu12.5Be22.5 BMG fine spur gear by using FEM simulations and by doing experimental studies. In the first forging process a punch with mandrel was used to form billet and while punch with mandrel moves down to create the final shape of billet, the mandrel creating a hole at the center of the final product. In the second process, a punch without mandrel was used and punch moves down and squeezes the billet against the mandrel, a hole is being created by the mandrel at the center of the final product. In the third process, a punch with mandrel was used and firstly, punch moves down then mandrel moves down and creates a hole at the center of the final product. The results show that there are significant differences between the results of three processes in terms of load- time curves and material flow behaviors and the Third process is superior to other processes and FEM results were verified by comparing with experimental results.

Yang and Hsu [90] investigated maximum forging load and final face width by changing process parameters such as modules, number of teeth, based on finite element simulations. Simultaneously they applied abductive network analysis. They showed that the results of FEM simulations and abductive network analysis consistent with each other in terms of forging load and face width.

In another study of Yang and Hsu [91], a set of finite element simulations carried out by using DEFORM-3D to analyze the spur gear forging process. In the simulations, ring-type billets were used and process parameters such as friction factor, module, etc. were investigated. The results of the simulations were compared with the previous experimental results available in the literature. They showed that the maximum forging load increases when module, teeth number, and friction factor increase, and maximum forging load decreases when the inner diameter of billet increases.

Kang et al. [92] presented a numerical approach to the cold forging of a component of automobile starter motor assembly (sleeve cam) which is featured gear tooth outside and cam profile inside, using FEM combined with equivalent area mapping method. Since the sleeve cam is a non-axisymmetric part, it is considered as a simple circle with an appropriate radius, which has an equal area. FEM results and experimental results were compared and it was concluded that the presented numerical approach can be used to predict successfully the plastic deformation of the non-axisymmetric forged part.

Kutuk et al. [93] performed finite element simulations and analytical solutions based on thick-wall cylinders for shrink-fit die design of precision forging spur gear. FEM simulations and analytical calculations were done for both die with teeth and die without teeth (cylindrical die). They showed that while the results of the FEM simulations and analytical computation are well agreeing with each other for die without teeth in terms of maximum stresses, the results of FEM simulations are much higher than the results of analytical computation for gear die with teeth in terms of maximum stresses. Also, it was shown that by re-optimizing interference value, maximum stresses reduce considerably.

Hsu [94] presented a mathematical model using an upper bound method for the precision forging of spur gear forms and splines in order to analyze the plastic deformation behavior of billet in the die cavity. They compared their results with the results of other researcher's analytical and experimental studies. They concluded that the presented mathematical model offers a useful knowledge of die designing of precision forging process of spur gear form and spline.

Chitkara and Kim [95] performed a forging process for crown gears with trapezoidal and rectangular teeth. Tellurium lead was chosen as a billet material. Also, they studied the upper bound analysis of the gears. They showed that relative forging pressure for forging of the rectangular teeth is a bit greater than the relative forging pressure for forging of the trapezoidal teeth.

Lee et al. [96] simulated a bevel gear forging process by using three dimensional FEM. In the simulations, dies were selected as rigid and the workpiece was selected as plastic material. They applied the FE simulations for two types of bevel gear forging in order to obtain a defect-free forging process. Firstly, they designed a die set then modified this die set by adding a lower pin, and it was shown that a modified die set with an added lower pin allows better filling of the die cavity.

Kim and Chitkara [97] presented kinematically admissible velocity fields for forging of crowned gear and finite element simulations were carried out to determine the effects of preform on the dimensional accuracy of the forged gear. They showed that the preform shape based on upper bound analysis improves the dimensional accuracy of the gear.

2.5 Precision Gear Forging of Asymmetric Gear

Although there are many studies about the precision forging of the symmetrical tooth gears only one study is available on the precision forging of asymmetric gears. However, the paper titled "Study on Warm Forging Process of 45 Steel Asymmetric Gear" [62], it is an extrusion process. In the paper, Qi et al. [62] studied the warm extrusion process of asymmetric gear to reduce the forming load and improve the filling in the toothed corner portion. In the experimental study, they selected 45 steel without quenching as workpiece material, heated up mold and workpiece to 250 ^{0}C and 800 ^{0}C, respectively. The die surfaces were lubricated by graphite and a forming speed of 30 mm/s was used. By performing microstructure analysis of the gear they revealed that small grains evenly distributed in the region near the addendum of the gear and coarse grains unevenly distributed in the central region of the gear.

As can be understood from the literature review, no study has been conducted on precision forging of asymmetric spur gear. Therefore, this study has been carried out to fill the gap in this area.

CHAPTER 3

ASYMMETRIC GEAR TOOTH PROFILE GENERATION

3.1 Introduction

Gears are used to transfer uniform motion. On this purpose, different types of conjugate curves which are act on each other to result in smooth motion transfer at a constant ratio can be used [98]. Although there are many conjugate curves, only two of these are in common use; the cycloidal and involute profiles [99]. The curve that is used extensively in the spur and helical gear is the involute curve [98]. This is because of the involute curve allows transferring angular motion smoothly. In additionally involute curves are insensitive to the center distance between the gear pair when the gear pair works. So, in this chapter, the geometry of the involute curve and gear tooth will be explained. Also, the tooth profile of the asymmetric gear will be drawn by using a home-made software program.

3.2 Involute Profile Generation

Involute is a trajectory where the end of a tightly wrapped yarn traces when opened from a circle. In the case of spur gears, this circle is called the base circle of the gear and it is given Figure 3.1.

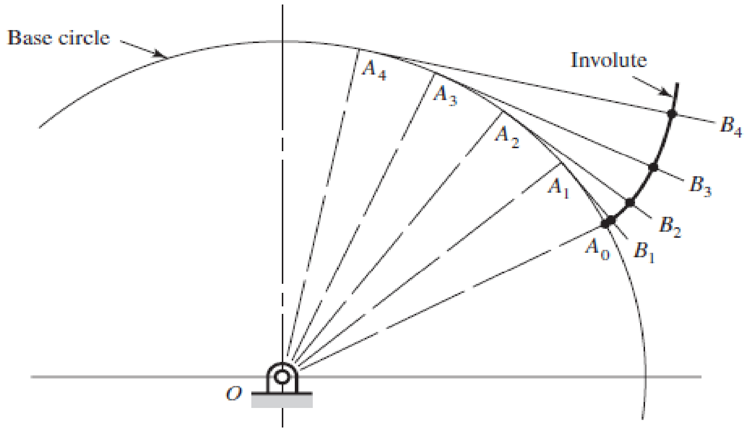

Figure 3.1 Involute and base circle [100]

If the radius of the base circle is known the involute curve is completely defined. Involute -Mathematically- can be defined as the vectorial angle θ in radians:

$$inv\phi = \theta = \tan\phi - \phi \tag{3.1}$$

where ϕ is the pressure angle of the interested point in radians
As can be seen in Figure 3.2, invϕ (θ) is the angle between any point considered and the starting point of the involute profile.

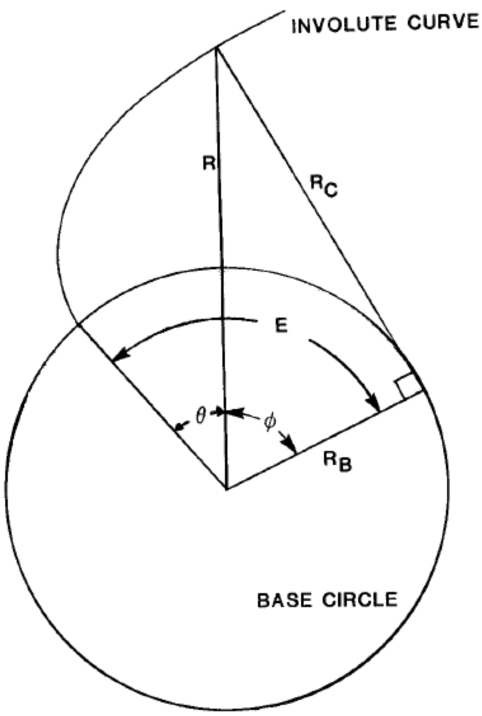

Figure 3.2 Involute curve [101]

R is the directed distance between the considered point and the center of the base circle or is the radius from the center of the base circle to the considered point. R_B is the radius of the base circle and R_C is the length of the unwrapped yarn when the base circle is rolled through E angle, also it is the radius of the curvature at the considered point. The relationships between these terms are given below.

$$R_C = R_B.E = \sqrt{R^2 - R_B^2} \quad (3.2)$$

$$R_B = R\,.Cos\,\phi \quad (3.3)$$

Before obtaining the X and Y Cartesian coordinate points of the involute profile, some information should be given such as module, pitch circle, etc. for the asymmetric spur gear. Nomenclature of the spur gear can be seen in Figure 3.3.

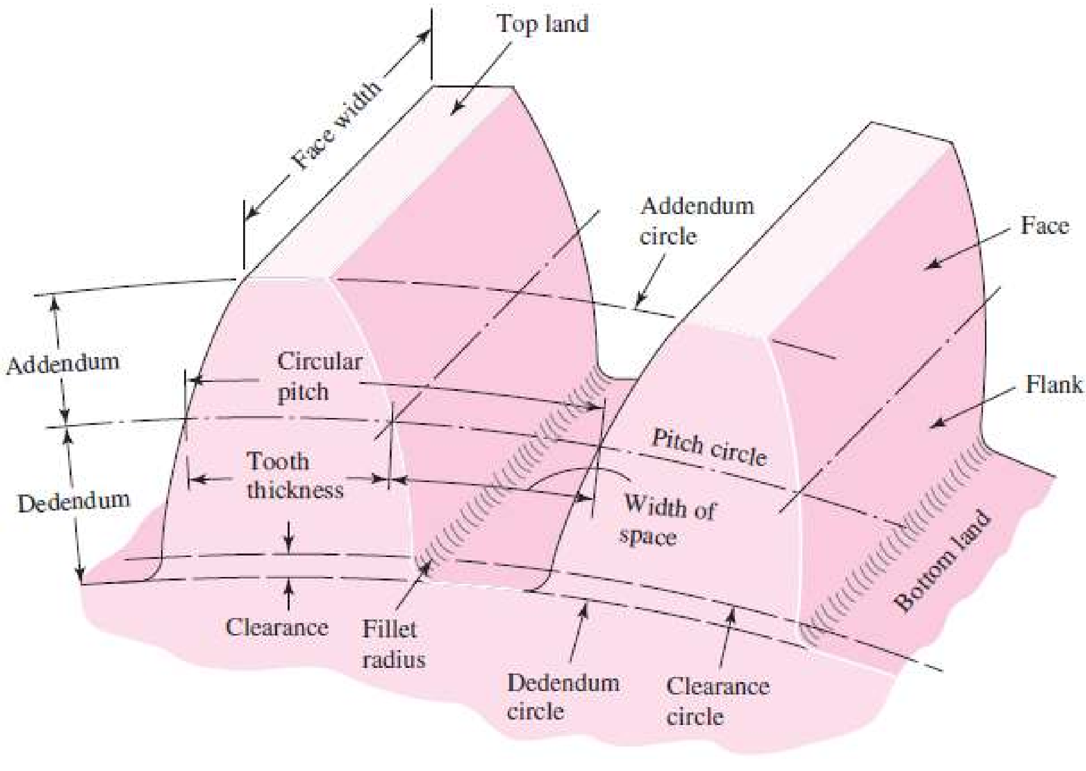

Figure 3.3 Spur gear tooth nomenclature [100]

Pitch circle is a theoretical circle that all calculations based on. As it is known an asymmetric gear has a different base circle for drive and coast-side because of the different pressure angle of the drive and coast-side but it has the same pitch diameter for the drive and coast side. The pressure angle is the profile angle of the involute at the point that coincides with the pitch circle. Representing the radii of the base circles of the drive and coast-sides by R_{BD} and R_{BC}, pitch circle radius by R_P, pressure angles of the drive side, and coast sides by ϕ_D and ϕ_C, relationships between these are given as below.

$$R_{BD} = R_P . cos\phi_D = \frac{1}{2} m . N . cos\phi_D \tag{3.4}$$

$$R_{BC} = R_P . cos\phi_C = \frac{1}{2} m . N . cos\phi_C \tag{3.5}$$

where N teeth number of the gear and m is the module which is the sign of tooth size in SI unit system.

$$R_P = R_{BC} / cos\phi_C = R_{BD} / cos\phi_D \tag{3.6}$$

From the equation (3.6), the tooth asymmetry factor K can be defined as

$$K = \frac{R_{BC}}{R_{BD}} = \frac{cos\phi_C}{cos\phi_D} \tag{3.7}$$

To determine X and Y Cartesian coordinates of the coast side involute profile, mathematical formulas and procedure is given in below for an arbitrary selected point a, and for this point geometric representation can be seen in Figure 3.4.

$$cos\phi_a = \frac{R_P}{R_a} . cos\phi_C \tag{3.8}$$

$$\phi_a = cos^{-1}\left(\frac{R_P}{R_a} . cos\phi_C\right) \tag{3.9}$$

Angle between Y axis and a point is;

$$\alpha_a = \frac{\pi}{2N} + inv\phi_C - inv\phi_a \tag{3.10}$$

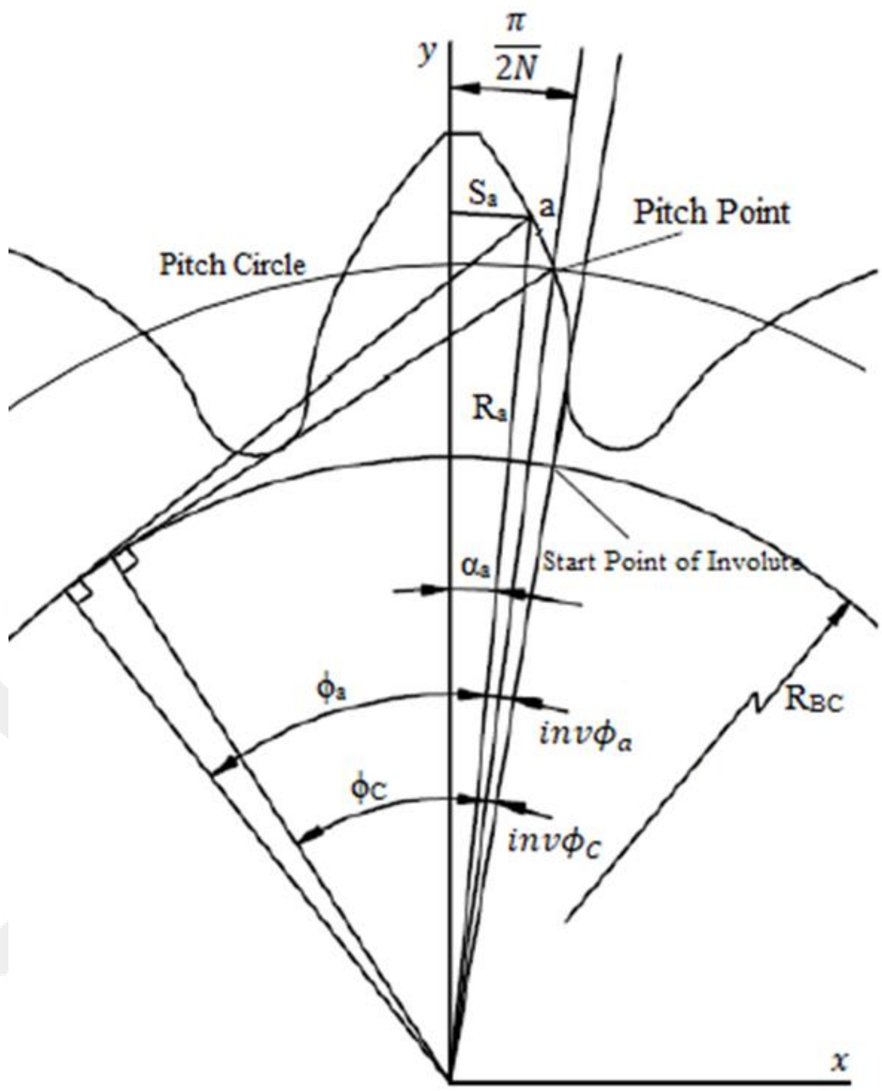

Figure 3.4 Geometric relationships of the coast side involute profile [102]

Then the S_a which is the arc length between point a and Y axis is

$$S_a = R_a \,.\, \alpha_a \tag{3.11}$$

or

$$S_a = R_a . \left(\frac{\pi}{2N} + inv\phi_C - inv\phi_a \right) \tag{3.12}$$

Finally, Cartesian coordinates of point a on the X and Y axis are

$$X_a = R_a . Sin\alpha_a \tag{3.13}$$

$$Y_a = R_a . Cos\alpha_a \tag{3.14}$$

To determine X and Y Cartesian coordinates of the drive side involute profile, the same procedure which is explained for coast side involute profile is applied. mathematical formulas and procedures are given below for an arbitrarily selected point b, and for this point, geometric representation can be seen in Figure 3.5.

$$cos\phi_b = \frac{R_P}{R_b} . cos\phi_D \tag{3.15}$$

$$\phi_b = cos^{-1}\left(\frac{R_P}{R_b} . cos\phi_D\right) \tag{3.16}$$

Angle between Y axis and b point is;

$$\alpha_b = \frac{\pi}{2N} + inv\phi_D - inv\phi_b \tag{3.17}$$

Then the S_b which is the arc length between point b and Y axis is

$$S_b = R_b \, . \, \alpha_b \tag{3.18}$$

or

$$S_b = R_b . \left(\frac{\pi}{2N} + inv\phi_D - inv\phi_b \right) \tag{3.19}$$

Finally, Cartesian coordinates of point a on the X and Y axis are

$$X_b = R_b . Sin\alpha_b \tag{3.20}$$

$$Y_b = R_b . Cos\alpha_b \tag{3.21}$$

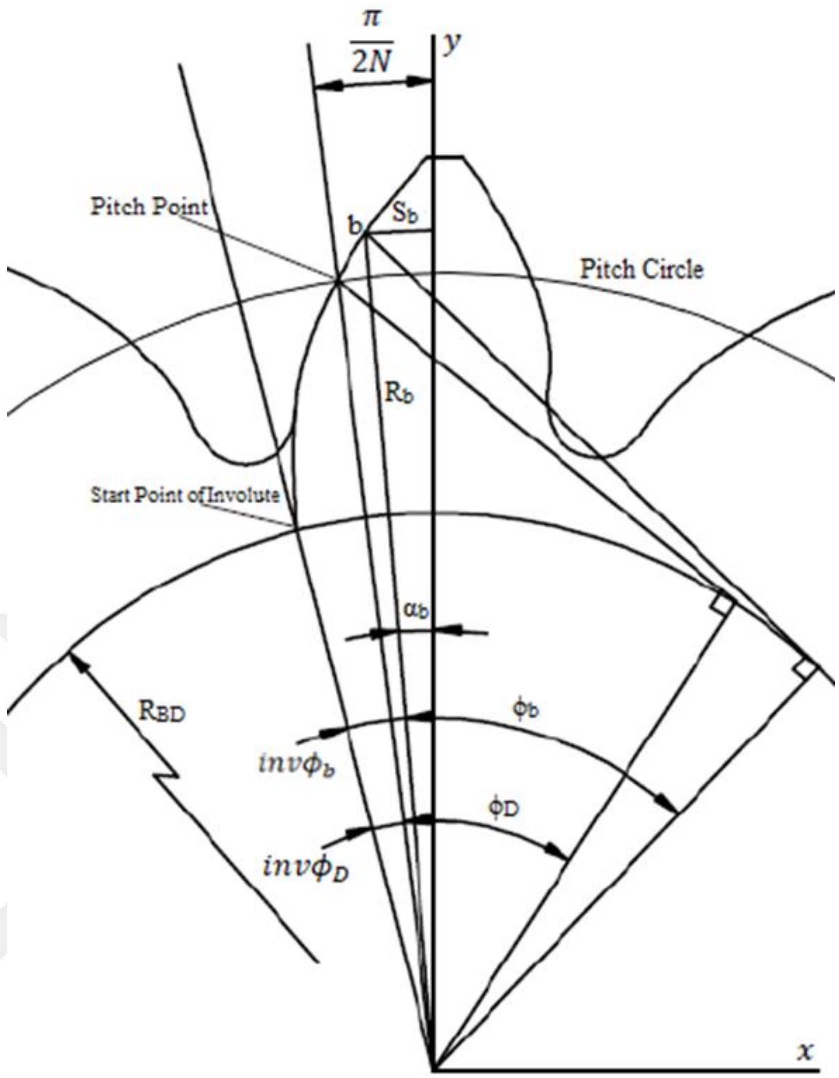

Figure 3.5 Geometric relationships of the drive side involute profile [102]

3.3 Asymmetric Gear Tooth Profile Generation

Gear design can be done by two different design types; indirect gear design (rack generation-based gear design) and direct gear design. In the indirect gear design rack cutters, parameters are defined and these parameters became the input parameters for gear. As to, in the direct gear design, the gears can be designed and optimized without using rack cutter parameters. Because symmetric gears have standard gear rack cutters, gear design of the symmetric gear is based on indirect gear design. In the case of asymmetric gear, there are no standard rack cutters, thus the direct gear design becomes naturally suitable for asymmetric gear design [2]. An asymmetric tooth consists of two involute flanks as can be seen in Figure 3.6.

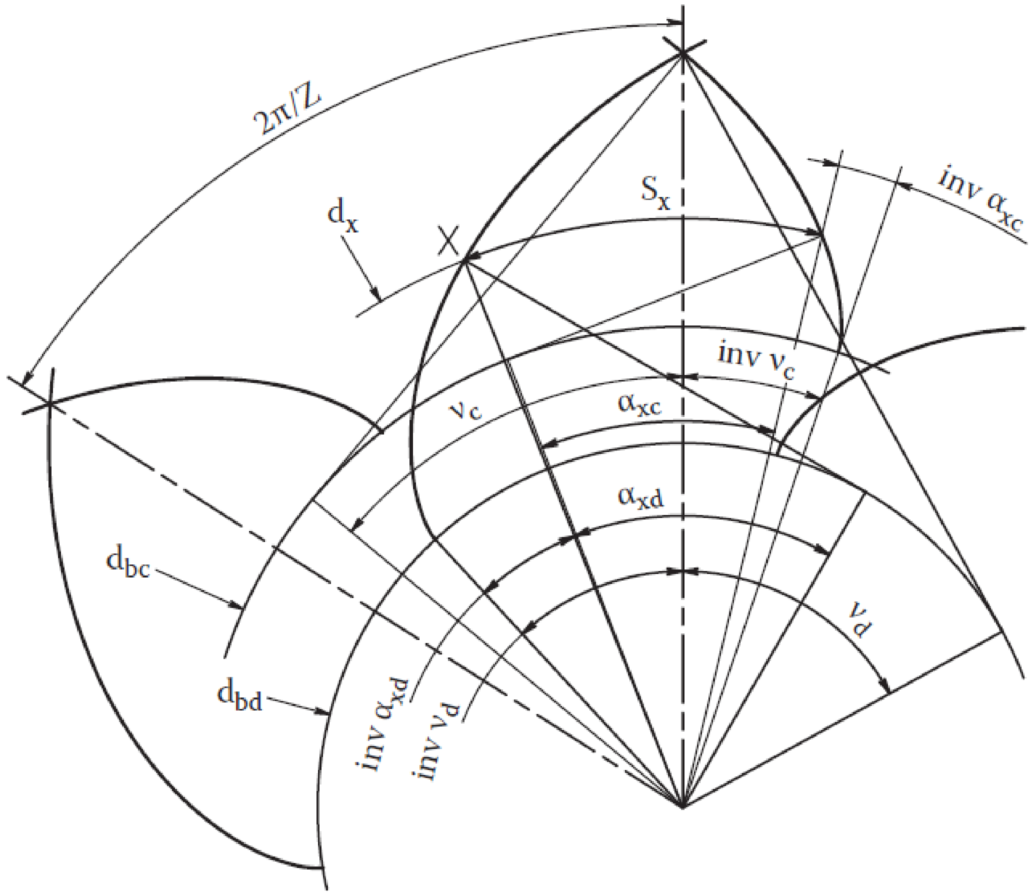

Figure 3.6 Involute flanks of external asymmetric gear [2]

Diameter of the any X point on the involute flanks can be found as;

$$d_x = \frac{d_{bd}}{Cos\alpha_{xd}} = \frac{d_{bc}}{Cos\alpha_{xc}} \tag{3.22}$$

Then the tooth asymmetry factor is

$$K = \frac{d_{bc}}{d_{bd}} = \frac{Cos\alpha_{xc}}{Cos\alpha_{xd}} \tag{3.23}$$

If the α_{xd} is greater than the α_{xd} then the d_{bc} will be greater than the d_{bd}. This means that tooth symmetry factor is greater than zero (K > 0).

Because the coast side base circle is greater than the that of the drive side, tooth base circle thicknesses should be determined at the coast side base circle.

$$S_b = \frac{d_{bc}}{2}\left[inv(V_d) + inv(V_c) - inv\left(arccos\left(\frac{1}{K}\right)\right)\right] \quad (3.24)$$

At the diameter d_x, tooth thickness can be found as

$$S_x = \frac{d_x}{2}\left[inv(V_d) + inv(V_c) - inv(\alpha_{xd}) - inv(\alpha_{xc})\right] \quad (3.25)$$

Or

$$S_x = \frac{d_{bd}}{2Cos\alpha_{xd}}\left[inv(V_d) + inv(V_c) - inv(\alpha_{xd}) - inv(\alpha_{xc})\right] \quad (3.26)$$

Also an asymmetric tooth profile should contain root fillet, tooth tip radius and tooth tip land as can be seen in Figure 3.7

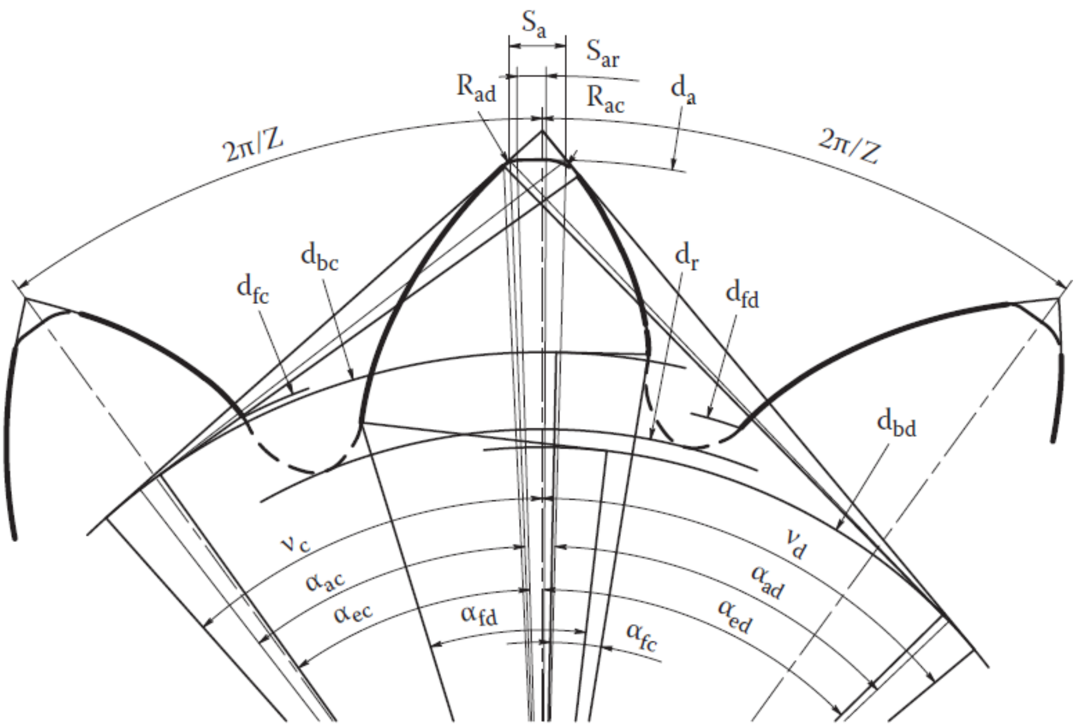

Figure 3.7 Asymmetric gear tooth [2]

To determine toot tip diameter, the equation 3.22 is applied for a point on the tooth tip diameter

$$d_a = \frac{d_{bd}}{Cos\alpha_{ad}} = \frac{d_{bc}}{Cos\alpha_{ac}} \tag{3.27}$$

If the tooth tip radius is considered as zero, tooth tip land thickness can be found as;

$$S_A = \frac{d_a}{2}\left[inv(V_d) + inv(V_c) - inv(\alpha_{ad}) - inv(\alpha_{ac})\right] \tag{3.28}$$

or

$$S_A = \frac{d_{bd}}{2Cos\alpha_{ad}}\left[inv(V_d) + inv(V_c) - inv(\alpha_{ad}) - inv(\alpha_{ac})\right] \tag{3.29}$$

If the tooth tip radius is not zero and tooth tip radiuses are determined as R_{ad} and R_{ac} for drive and coast side respectively, the profile angle of the start point of the tooth tip radius for drive side

$$\alpha_{ed} = \arctan\left[tan\left(arccos\left(\frac{d_{bd}}{d_a - 2R_{ad}}\right)\right) + \frac{2R_{ad}}{d_{bd}}\right] \tag{3.30}$$

For coast side

$$\alpha_{ec} = \arctan\left[tan\left(arccos\left(\frac{d_{bc}}{d_a - 2R_{ac}}\right)\right) + \frac{2R_{ac}}{d_{bc}}\right] \tag{3.31}$$

Then the real tooth tip land (S_{Ar}) can be found as;

$$S_{Ar} = \frac{d_a}{2}\left[\begin{array}{c} inv(V_d) + inv(V_c) - tan\alpha_{ed} - inv\alpha_{ec} \\ + arctan\left(tan\alpha_{ed} - \frac{2R_{ad}}{d_{bd}}\right) + arctan\left(tan\alpha_{ec} - \frac{2R_{ac}}{d_{bc}}\right) \end{array}\right] \tag{3.32}$$

After the tooth parameters are determined, asymmetric gear tooth rack determined. Asymmetric gear tooth rack can be seen in Figure 3.8. If the tooth tip radius assumed as zero, the tooth tip land can be found in the metric system as;

$$S_a = \frac{\pi m}{2} - H_a(tan\alpha_d + tan\alpha_c) \tag{3.33}$$

Actually, tooth tip radius has a value R_{ad} and R_{ac} for drive side and coast side respectively, then the real tooth tip land becomes as;

$$S_{ar} = \frac{\pi m}{2} - H_{aed} tan\alpha_d - H_{aec} tan\alpha_c - R_{ad} Cos\alpha_d - R_{ac} Cos\alpha_c \qquad (3.34)$$

Addendum of the rack tooth;

$$H_a = H_{aed} + R_{ad}(1 - Sin\alpha_d) \qquad (3.35)$$

or

$$H_a = H_{aec} + R_{ac}(1 - Sin\alpha_c) \qquad (3.36)$$

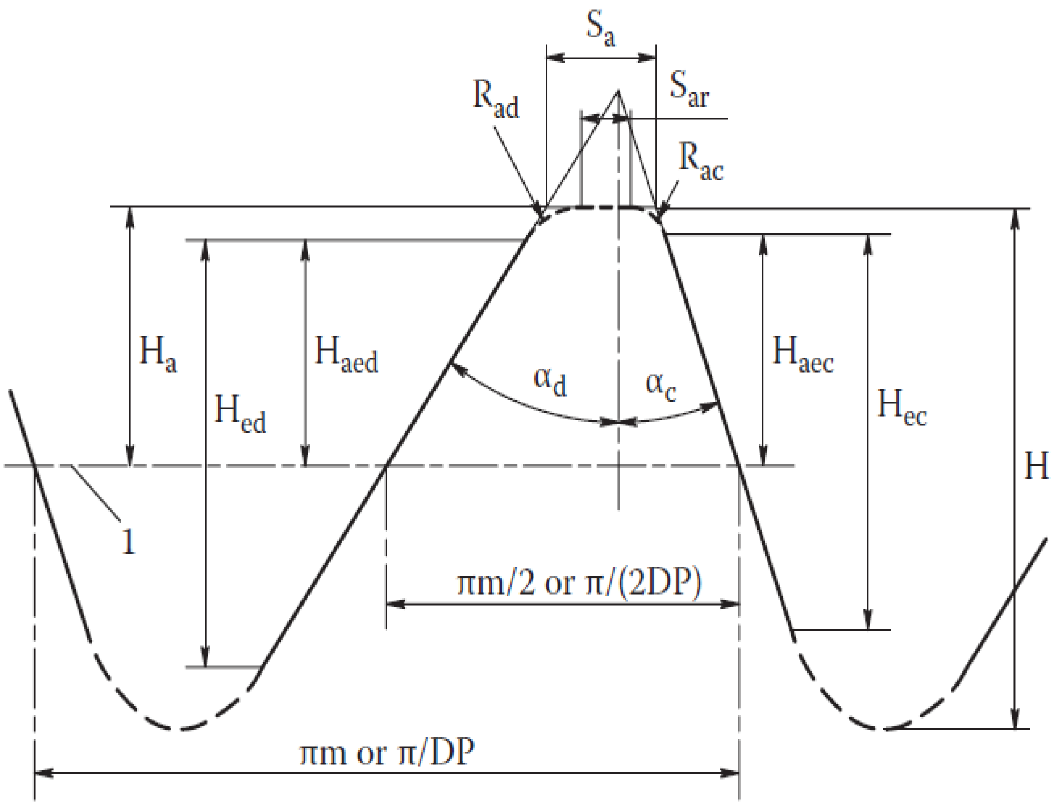

Figure 3.8 Asymmetric gear rack [2]

3.4 Root Fillet Optimization

The aim of the root fillet optimization is to minimize bending stresses and distribute along a large portion of the tooth root as well as possible, to obtain minimum stress concentration on the tooth root and to avoid interference between teeth of the mating gear pairs. Root fillet should be designed after tooth flank parameters are totally defined. In the optimization process firstly, the initial root fillet of the asymmetric gear is constructed. Asymmetric gear root fillet construction can be seen in Figure 3.9. In the figure; 2c and 2d are preliminary tooth flanks after hobbing, 1c and 1d represent final tooth flanks after grinding, 4 is the mating gear trajectory which is drawn in zero backlashes, 3c and 3d are temporary root flanks between preliminary tooth flanks and root fillet, d_{fd} and d_{fc} are form diameter of drive and coast-side respectively, d_{lpd} and dlpc are the diameters of the lowest point of contact and 5 is the initial root fillet which is a circular arc below the trajectory of the toot tip of the mating gear. Initial root fillet arc is tangential to 3c and 3d and also it assumed to be tangential to final tooth flanks (1c and 1d).

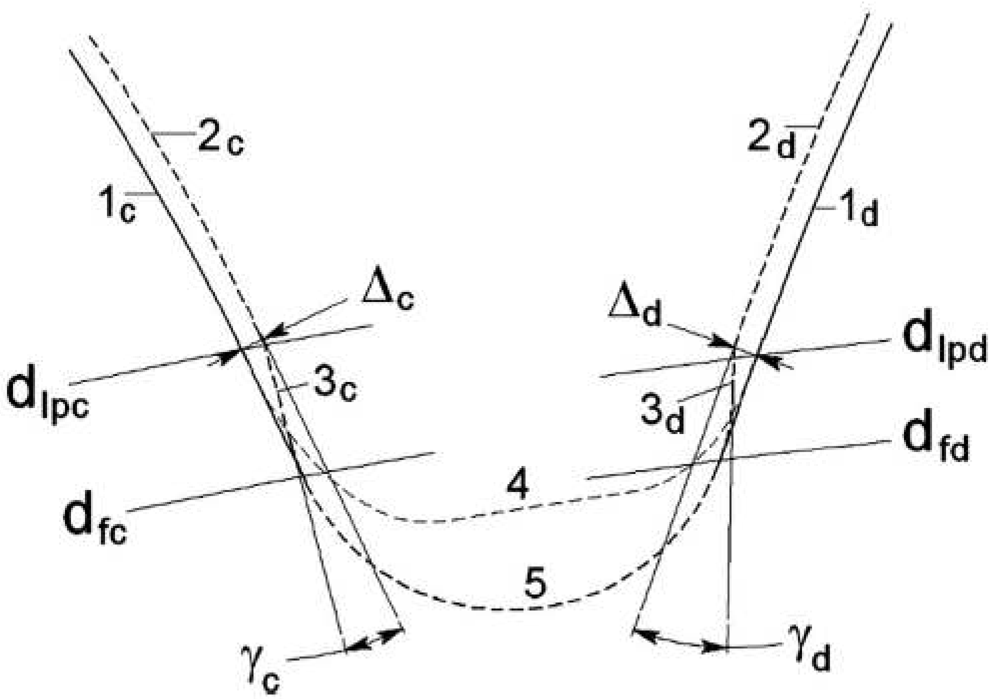

Figure 3.9 Initial root fillet of asymmetric gear [7].

After the initial root fillet is constructed, mathematical functions are defined in order to approximately determine the final root fillet profile. Then finite element analysis is performed to minimize stresses. In the finite element simulations, the first elements are located on the form diameter of the tooth flank of the drive and coast-side and these nodes are thought that they do not move during the analysis. Other elements are located along with initial root fillet and the center of the initial root fillet is assumed to connect with these finite element nodes. Then, these nodes are moved perpendicular to the initial root fillet, until minimum stresses values obtained (see in Figure 3.10).

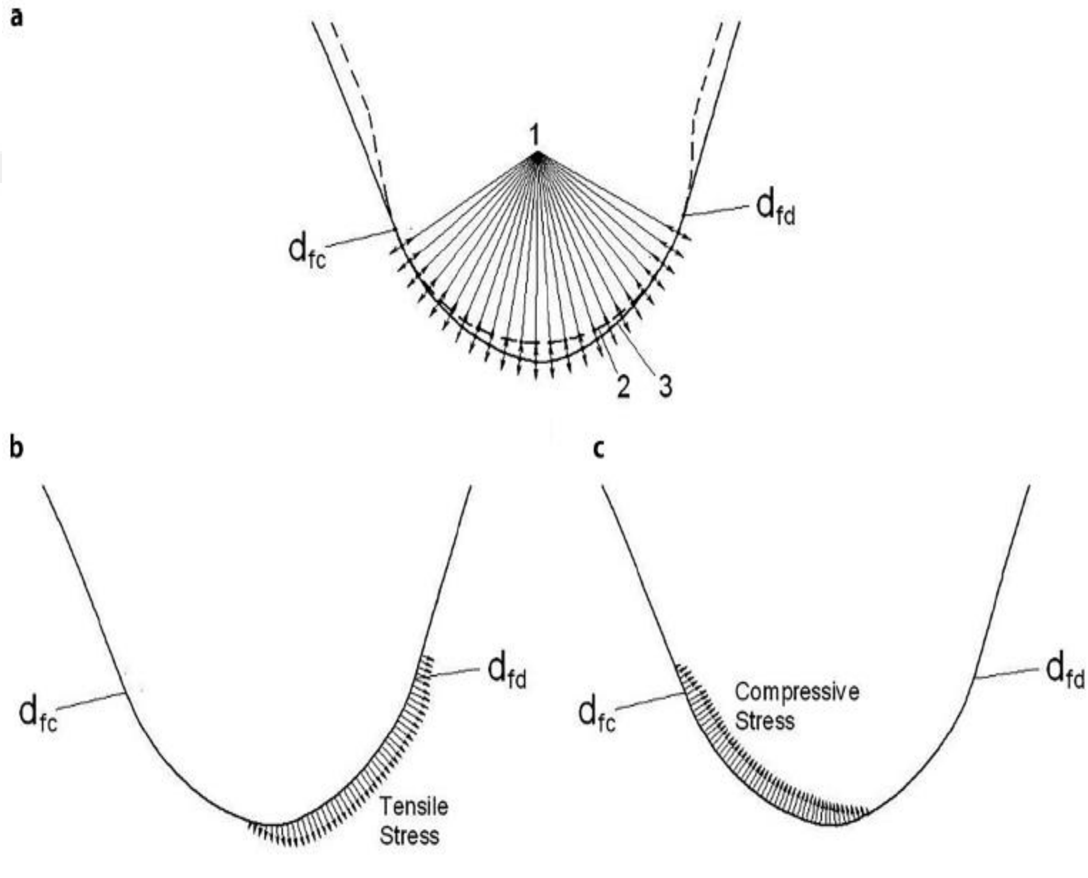

Figure 3.10 Root fillet optimization process a) fem simulations b) tensile stresses c) compressive stresses [7]

3.5. A Prototype Asymmetric Spur Gear Selection and Tooth Profile Generation

In order to conduct analytical and experimental studies, it is necessary to determine a prototype asymmetric spur gear. Design of asymmetric gear is out of the scope of this study. So, it is necessary to select an already designed and industrially applied one. In most of the industrial applications, the forgeable gear sizes are limited due to the required forming loads. The feasible pitch diameters are less than 200 mm for spur and helical gear forms. Thus the modules are generally restricted between 2 and 5 mm in the precision spur gear forging process. The gears that have modules less than 2 are difficult to machine on the die and those that have higher modules than 5 require much higher forging load during the forging. Also, it was shown that stresses have not considerable amounts of changes with the module changing between 2 and 4 for the spur gears have the same pitch diameter [80]. Taking all the above-mentioned restrictions into account, the sun gear of the first stage of TV7-117S turbo-prop motor was chosen as the prototype gear (see Figure 3.11). The TV7-117S turbo-prop motor gearbox is one of the famous asymmetric spur gear applications and its gears have been produced by traditional gear cutting methods [9]. The 3D model of the selected gear is given in Figure 3.12 and the gear parameters are given in Table 3.1[103].

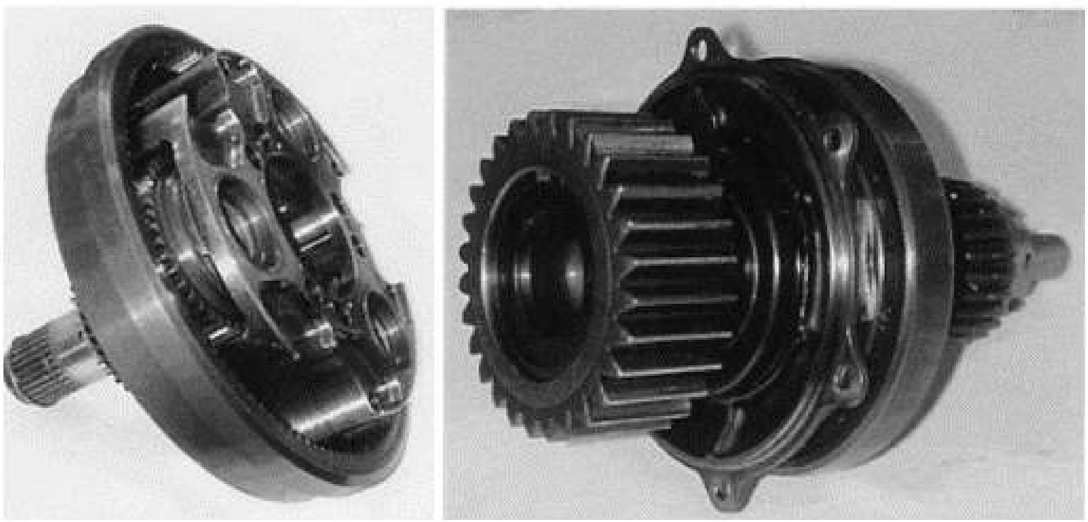

Figure 3.11 The first stage of TV7-117S turbo-prop motor gearbox a) carrier and ring gear assembly b) sun gear assembly [104]

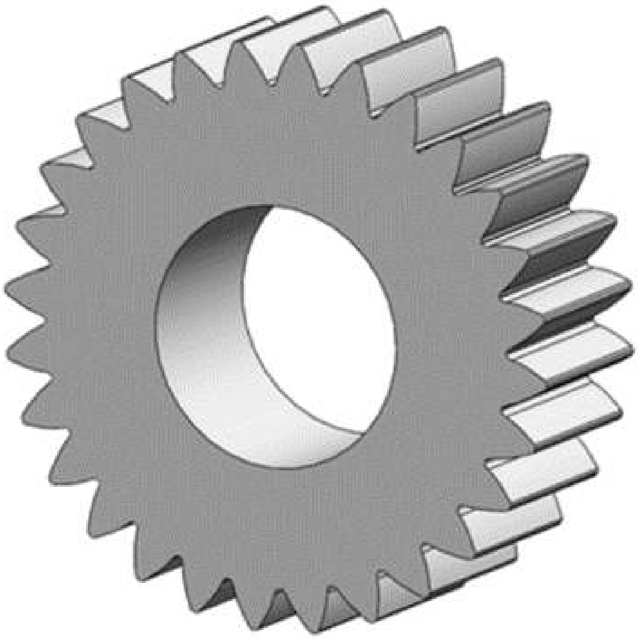

Figure 3.12 The 3D model of the selected gear model

Table 3.1 Parameters of asymmetric spur gear [103].

Definitions	**Value**
Teeth Number	28
Module	3
Drive Side Pressure Angle (°)	33
Coast Side Pressure Angle (°)	25
Pitch Diameter (mm)	84.00
Drive Side Base Diameter (°)	70.448
Coast Side Base Diameter (°)	76.13
Addendum Diameter (mm)	90.02/90.16
Root Diameter (mm)	76.55/77.05
Tooth Thickness on Pitch Circle (mm)	4.773/4.814
Face width (mm)	35
Hub diameter (mm)	40

After determining the gear parameters, software program was developed by using C++ program language. Gear parameters were used as the input parameters and involute tooth profile points were obtained as the outputs. The input parameters of the software can be seen in Figure 3.13.

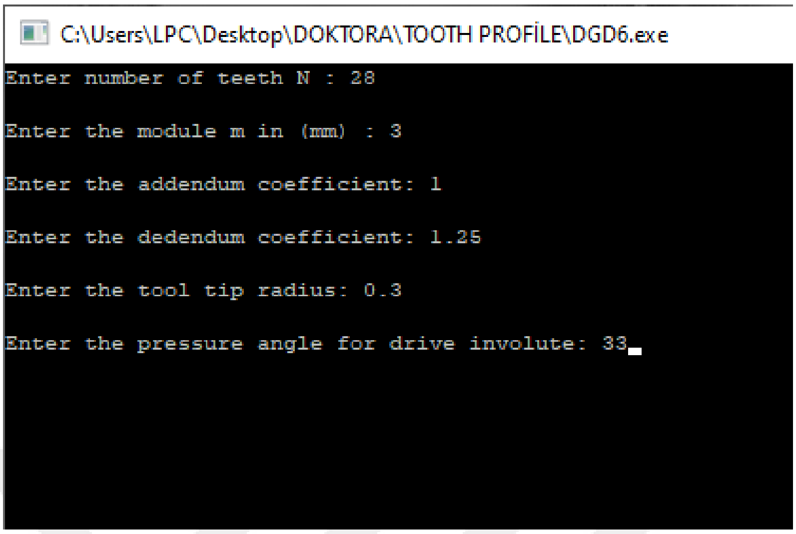

Figure 3.13 Input parameters of the developed software Program

Once getting the points of the tooth involute profile, these points were arranged by using Microsoft excel. Then using these points in SolidWorks the gear tooth profile (see in Figure 3.14) and the solid model of the gear was drawn (see in Figure3.15). Also, a solid model of the gear was obtained by using a 3D printer and this model can be seen in Figure 3.16.

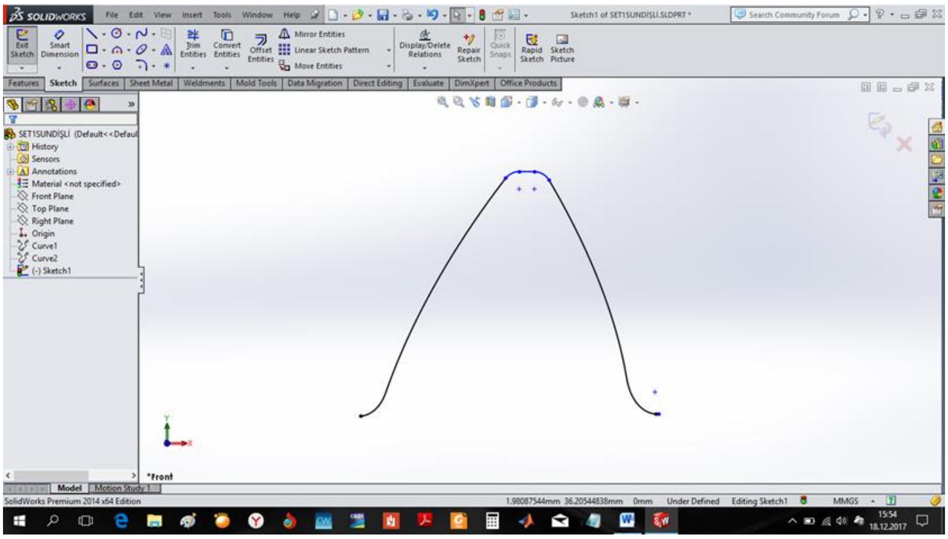

Figure 3.14 Tooth profile of sun gear drawn in SolidWorks

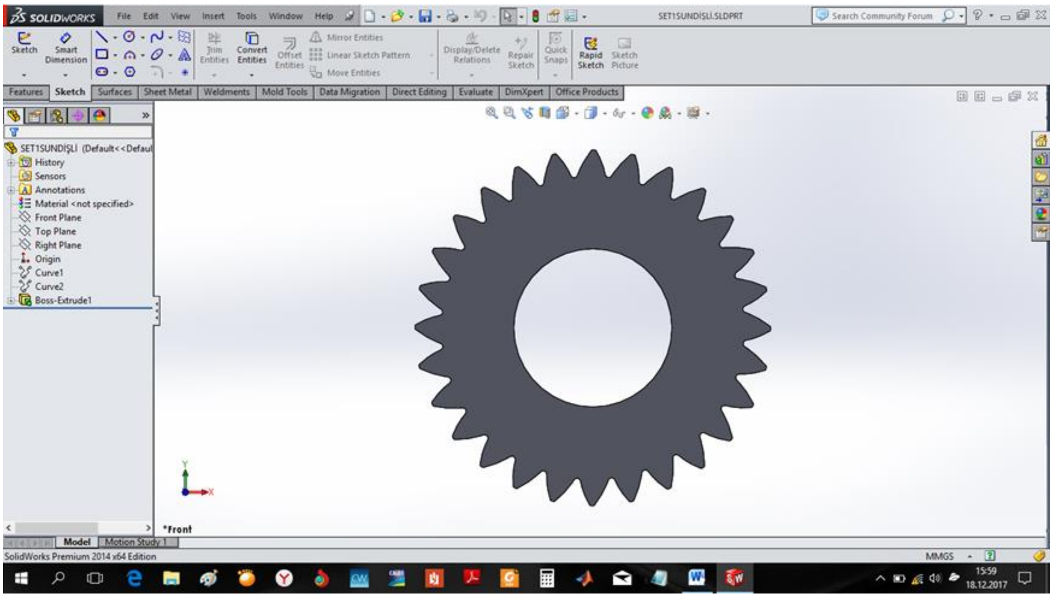

Figure 3.15 Sun gear drawn in SolidWorks

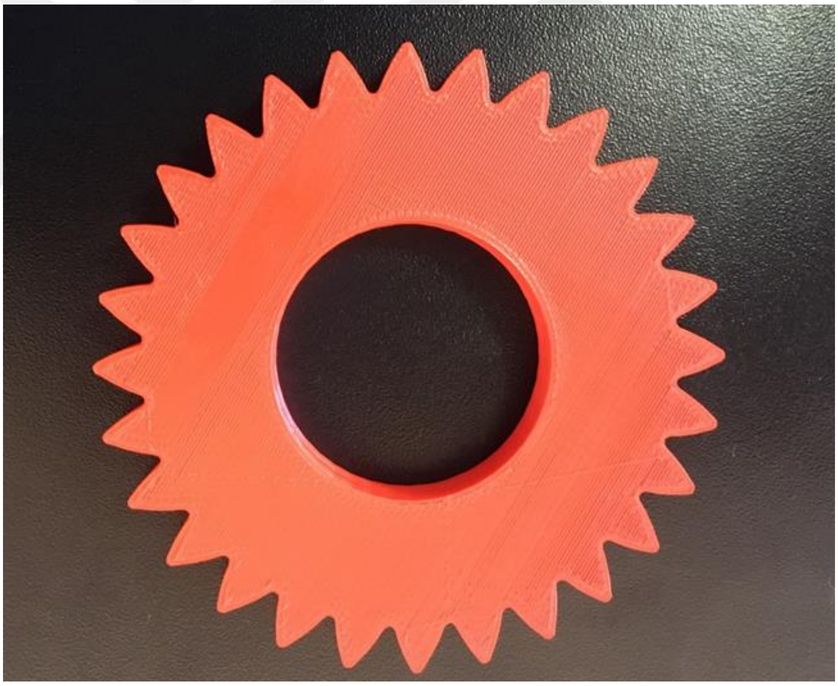

Figure 3.16 The 3D printed model of the prototype gear

CHAPTER 4

FINITE ELEMENT ANALYSIS OF ASYMMETRIC SPUR GEAR FORGING

4.1 Introduction

Finite Element Method is a numerical technique and recently used more commonly in order to solve engineering problems such as structural analysis, dynamic and static analysis, and forming. By using simulations, researchers obtain advantages such as what is possible or not, process and tool design, understanding the process deeply and saving time and cost.

In this chapter, finite element modeling of precision forging of asymmetric spur gear is presented. Firstly, the geometries of the workpiece and tool set were created by using SolidWorks software package then these geometries were transferred to finite element software. For the finite element simulations, SIMUFACT software package was used. Usually in most of the finite element simulations elastoplastic workpiece and rigid dies had been used although in the real situations dies are not rigid. However, Simufact offers to use both elastoplastic-rigid and elastoplastic-elastoplastic analyses.

4.2 Determination of Billet Geometry

One of the objectives of the precision forging process is to prevent or reduce waste material formation. Therefore, the dimensions of the billet, in other words, the volume of the workpiece are very important in the precision forging process. If the volume of the billet is less than the final gear volume, the die will not be completely filled so the product is not being as desirable. On the other hand, if the volume of the billet is higher than the final gear volume, the die is going to be subjected to overloading. The volume of the asymmetric gear which is to be produced was determined by using SolidWorks by assuming that the billet material is incompressible. After that, the billet was created by using SolidWorks as can be seen in Figure 4.1. The billet is a hollow cylinder whose inside diameter fitted the mandrel (i.e., shaft diameter), and with an outside diameter slightly less than the root diameter of the gear teeth, was suggested in a previous investigation [105]. The clearance between the outside diameter of the billet and the root diameter of the gear was carefully selected in order to compensate for the thermal expansion of the billet when heated and to enable it to be placed into the die cavity easily. The height of the billet is dependent on the face width of the forged gear and it can be calculated by using the volume constancy

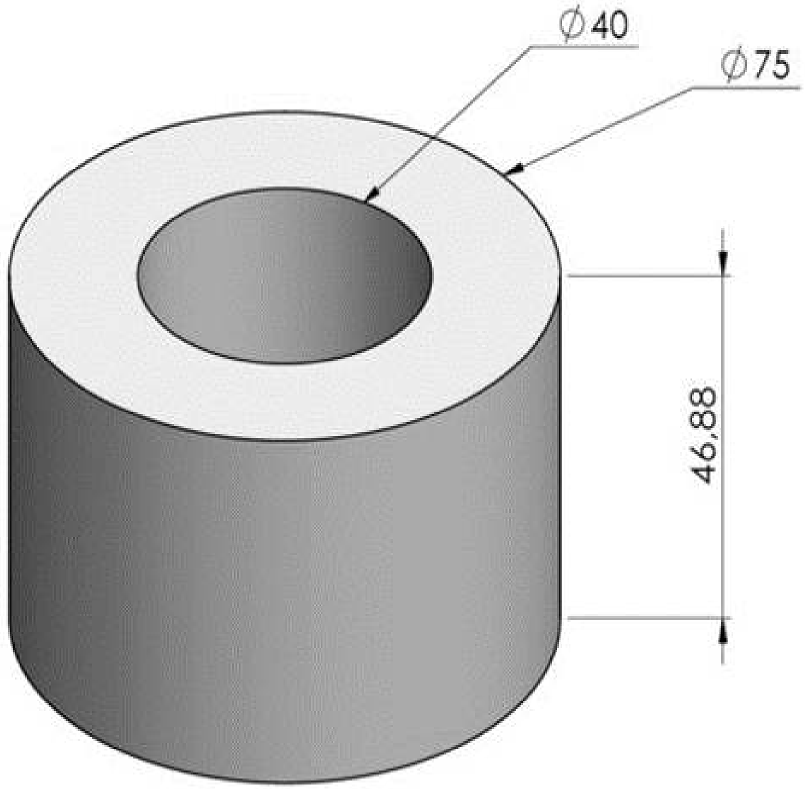

.

Figure 4.1 Geometry of the billet (dimensions are given in mm)

4.3 Finite Element Models

Finite element models were created by using SIMUFACT FORMING 16.0. Considering die type, forging temperature and workpiece material, six different types of models were prepared (see Table 4.1).

Table 4.1 FE models of asymmetric spur gear forging

Model	Forging temp	Billet Material	Billet	Die
I	Hot Forging (1200ºC)	AISI 4340 (DIN 34CrNiMo6)	Elasto-plastic	Rigid
II	Hot Forging (1200ºC)	AISI 4340 (DIN 34CrNiMo6)	Elasto-plastic	Elasto plastic
III	Warm Forging (800ºC)	AISI 4340 (DIN 34CrNiMo6)	Elasto-plastic	Rigid
IV	Warm Forging (800ºC)	AISI 4340 (DIN 34CrNiMo6)	Elasto-plastic	Elasto-plastic
V	Ambient Temperature Forging (20ºC)	Lead (asm_Lead_104)	Elasto-plastic	Rigid
VI	Ambient Temperature Forging (20ºC)	Lead (asm_Lead_104)	Elasto-plastic	Elasto-plastic

4.3.1 Hot and Warm Forging of AISI 4340 (DIN 34CrNiMo6)

In the finite element modeling first step is the selection of the process application type. When a new project is started, the process application module window opens and the options which can be selected appear. The process application module can be seen in Figure 4.2.

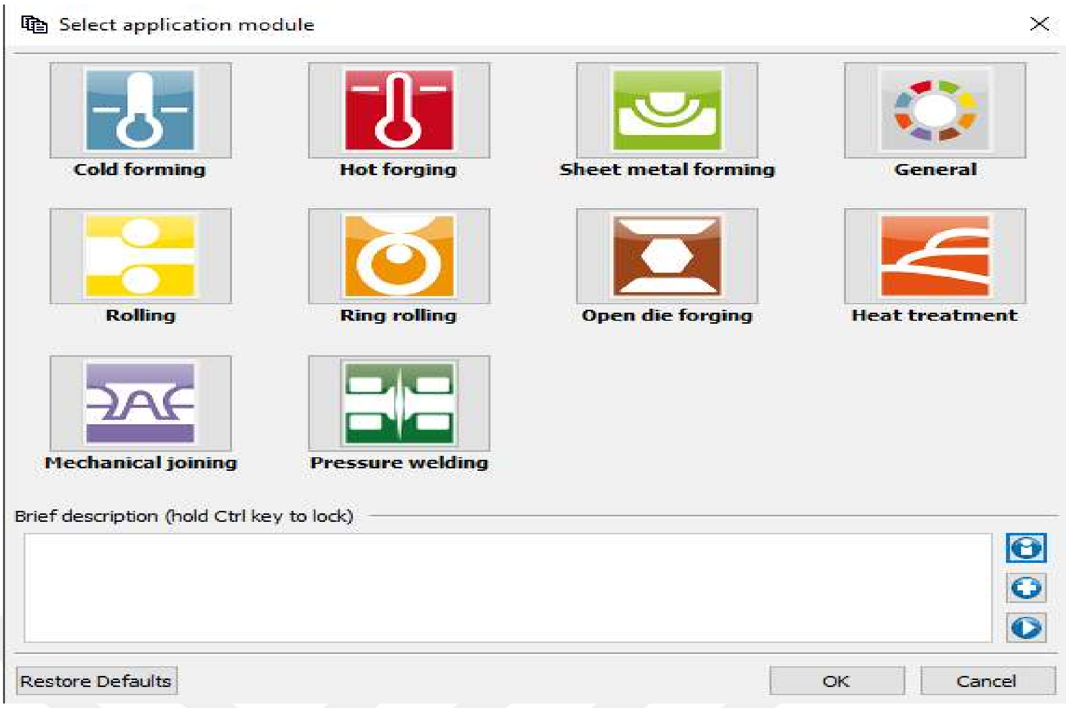

Figure 4.2 Process application module window of simufact

4.3.1.1 Pre-heating of the Workpiece

For the hot and warm forging, from the application module window, cold forming was selected as the process type in order to heat the workpiece up to the desired forging temperature. Then the process tree of the heating which can be seen in Figure 4.3 is created by the software program.

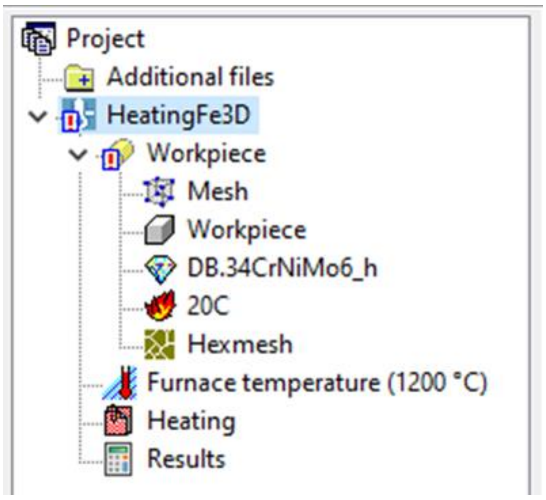

Figure 4.3 Process tree of the Heating

After the formation of the process tree, workpiece geometry was imported to the heating process by using the CAD import option. Workpiece material was selected as AISI 4340 (DIN 34CrNiMo6) steel form the Simufact Material Library. The mechanical properties of the AISI 4340 can be seen in Figure 4.4.

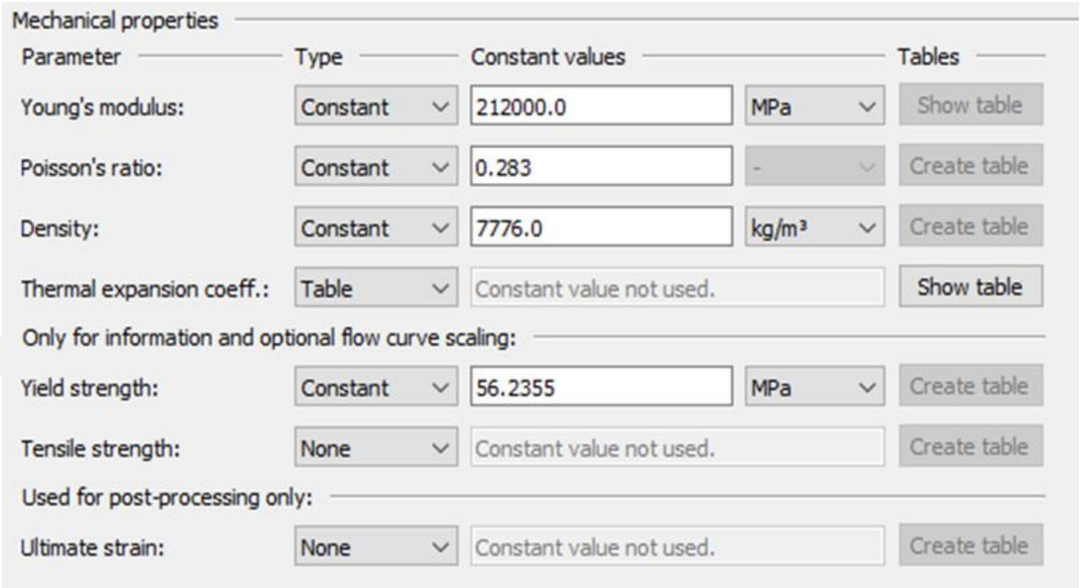

Figure 4.4 Mechanical properties of AISI 4340

Flow curves of the AISI 4340 can be seen in Figure 4.5 and 4.6 with respect to temperature and elastic strain, respectively. These curves were taken from the Simufact library.

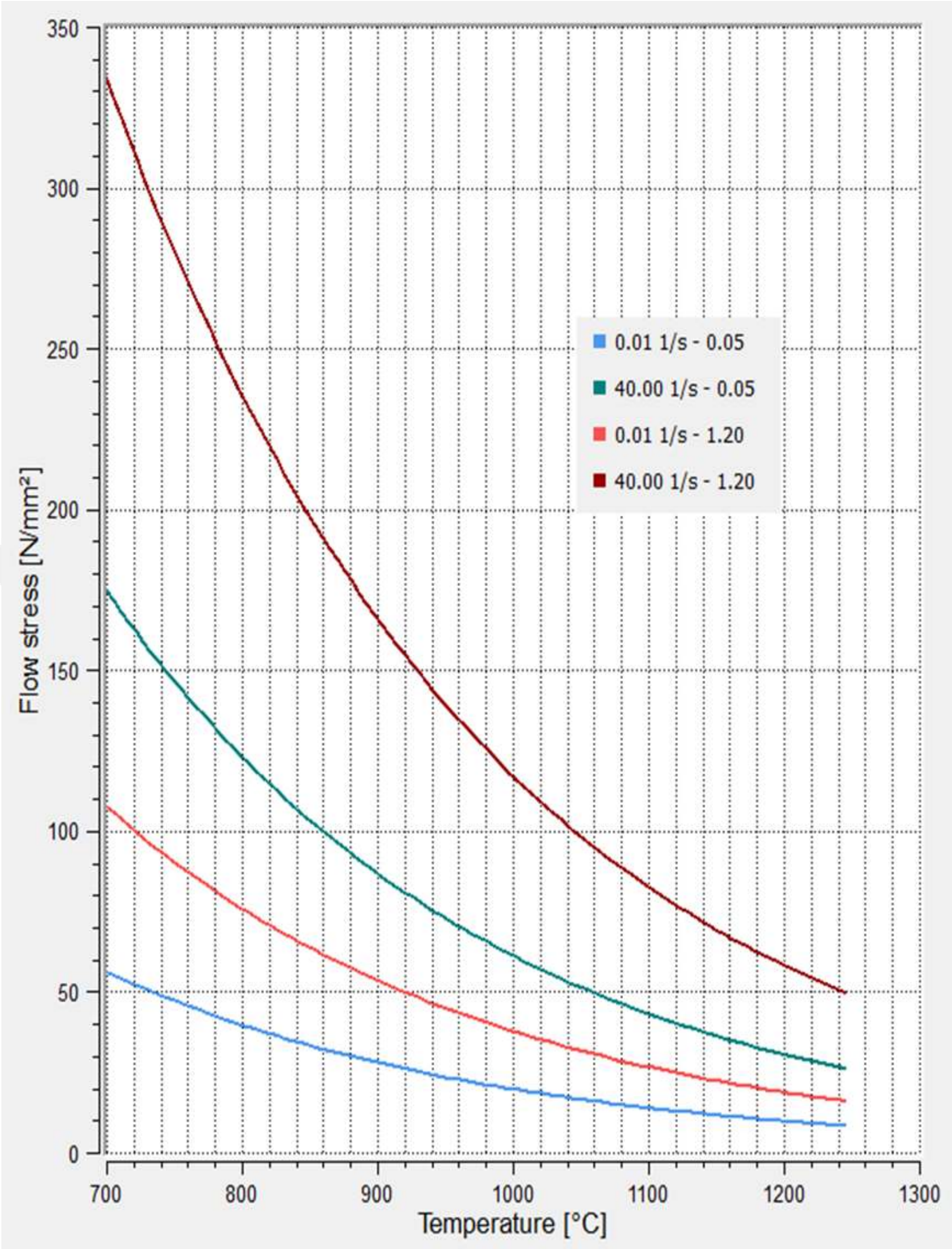

Figure 4.5 Flow stress-strain diagram of work piece material (AISI 4340) with respect to temperature

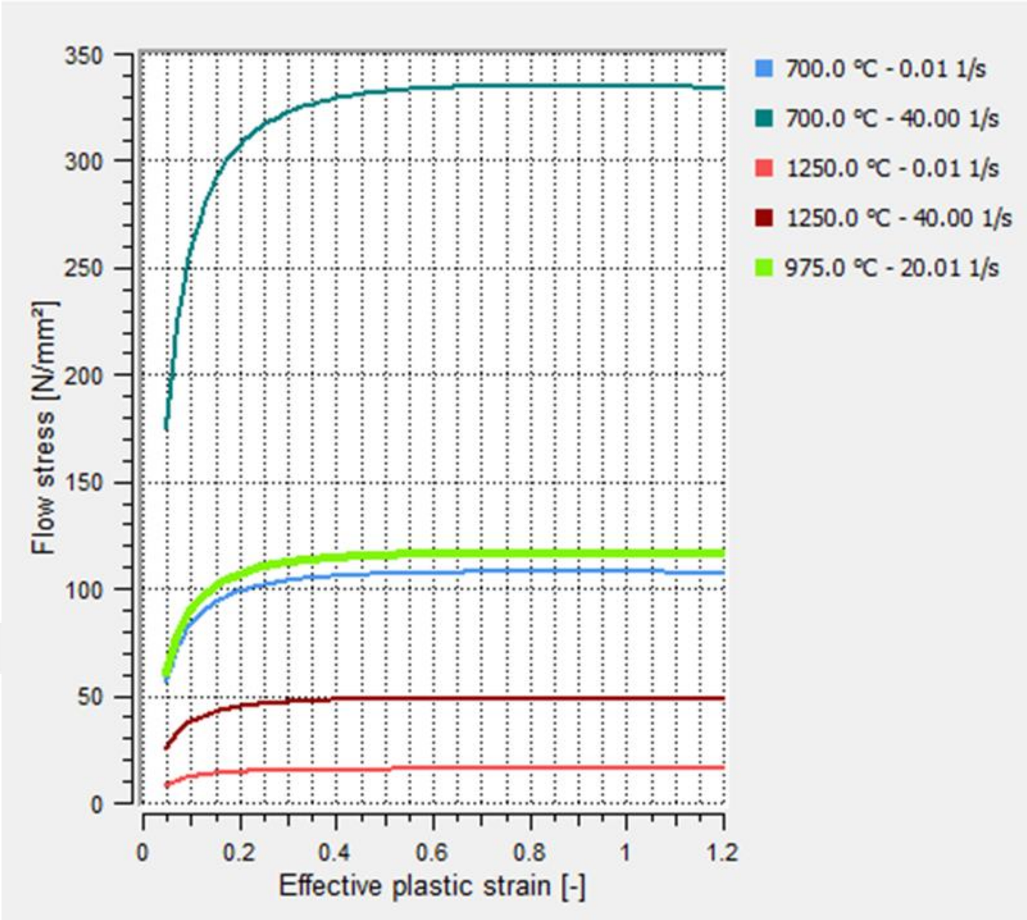

Figure 4.6 Flow curves of AISI 4340

Once the geometry and material of the workpiece were determined, the next step is the meshing of the workpiece (discretization). SIMUFACT provides many types of elements, but for the three-dimensional models SIMUFACT suggests hexahedral mesh type. Thus, the workpiece meshing process was done by Hexmesh. By using this mesh generator, the workpiece was divided into elements and 219318 elements were created. Because only the temperature of the workpiece is going to be change and elements will not be deforming, refinement boxes were not used. The initial temperature of the workpiece was selected as 20 ^{0}C for both processes hot and warm forging. Then the furnace temperature was selected as 1200 ^{0}C and 800 ^{0}C for hot and warm forging respectively. Finally, the heating conditions were determined and simulations were performed for the heating process. As can be predicted, after the Heating process dimensions of the workpiece changed because of the thermal expansion of the workpiece material. The final dimensions of the workpiece can be seen in Figures 4.7 and 4.8 for the warm and hot forging process, respectively.

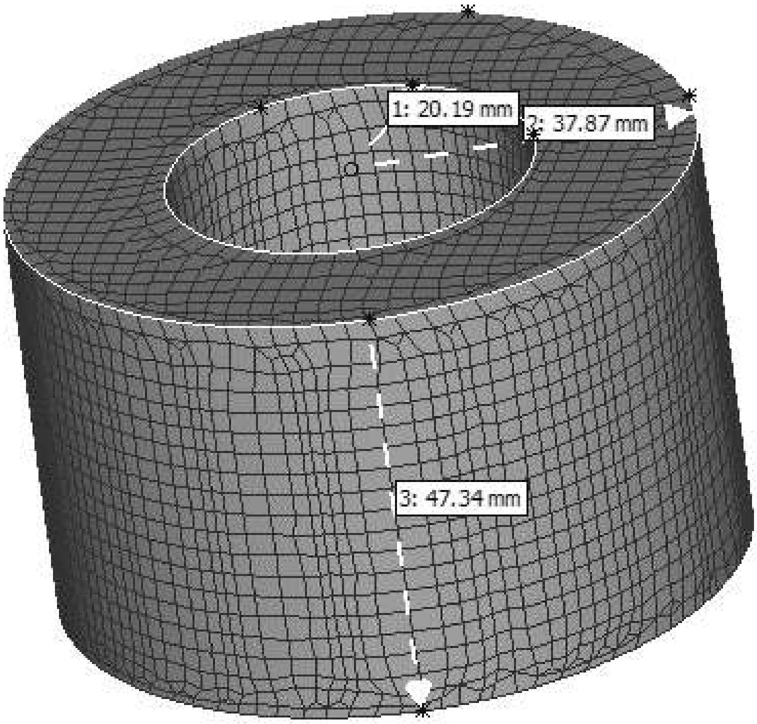

Figure 4.7 Dimension of the billet after heating up to 800 ^{0}C

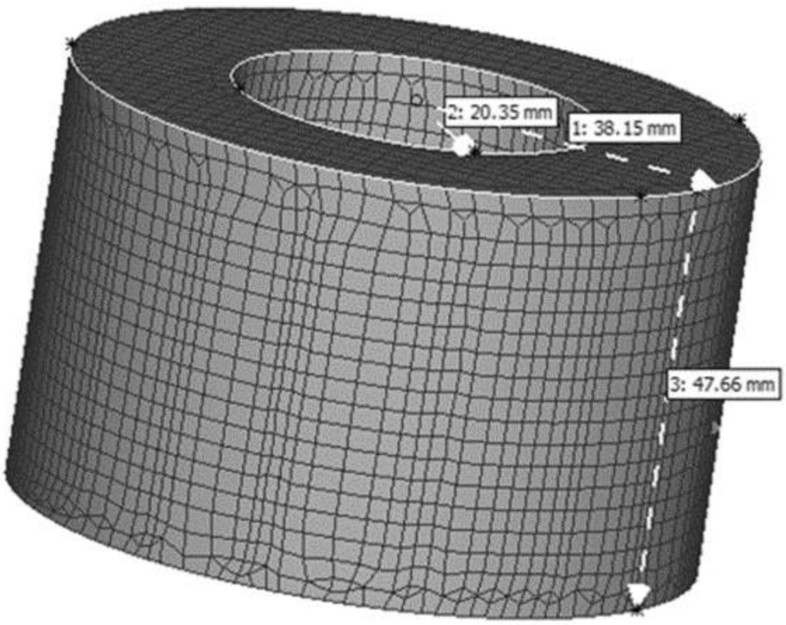

Figure 4.8 Dimension of the billet after heating up to 1200 ^{0}C

4.3.1.2 Forging Process Parameters for Hot and Warm Forgings

Modeling of the forging process started by selecting hot forging application from the process application window. Then the process definition window opened. In this window, the process type was selected as general forming, and the simulation type was chosen as three-dimensional finite elements. Also, by using this window number of dies and ambient temperature were determined as can be seen in Figure 4.9.

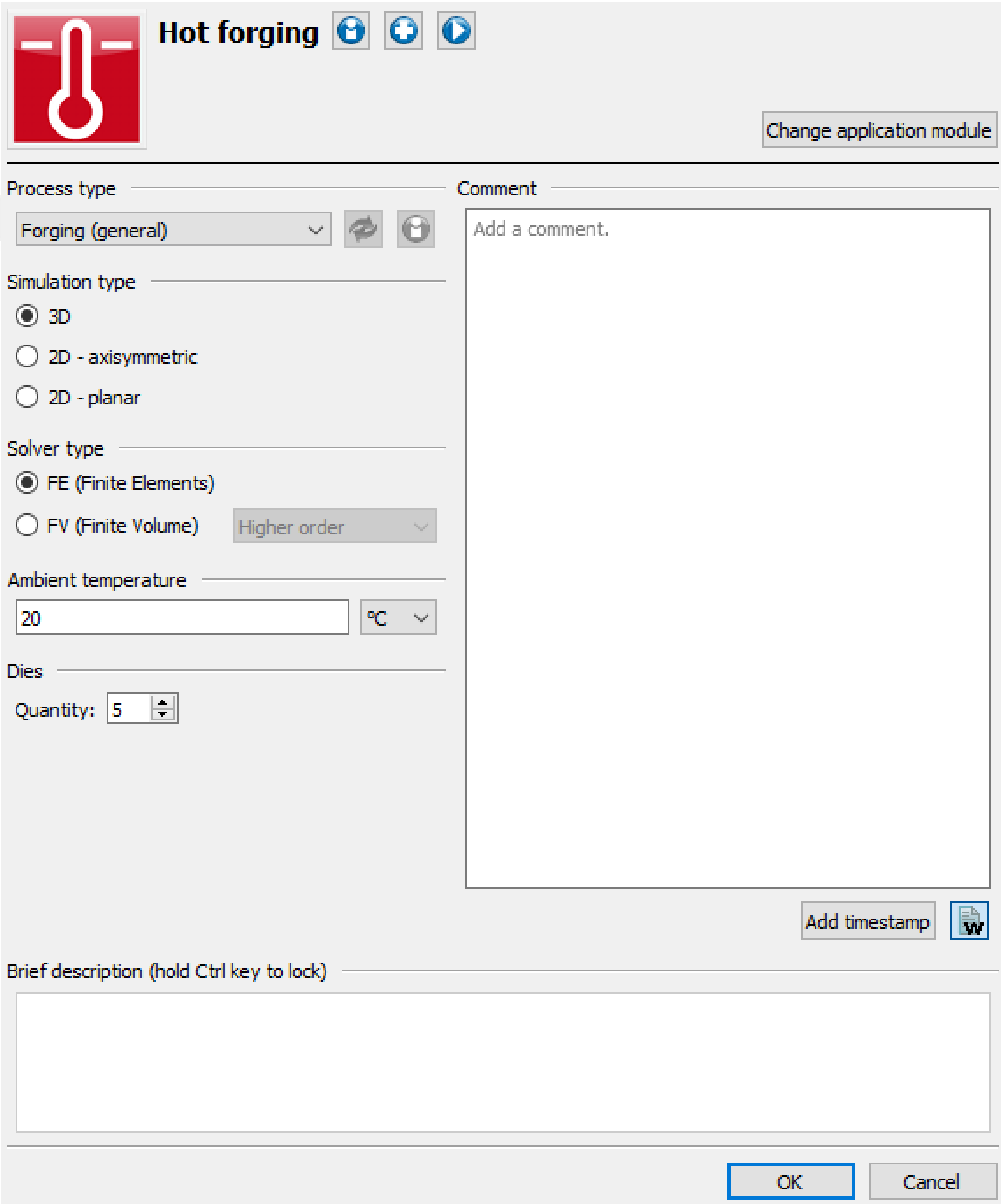

Figure 4.9 Process definition window

Then, the process tree was created. By using the process tree, geometries of the dies and workpiece were imported into the finite element model. Also, by using process tree, workpiece material, die and workpiece temperatures, environment temperatures, and forging settings were done. In addition, for elastoplastic dies, die material was determined by using the process tree. The next step is to define the press types. The crank press was selected from the SIMUFACT library and it was transferred into process tree and punch is attached to crank press. Velocity versus time graph of the selected crank press can be seen in Figure 4.10.

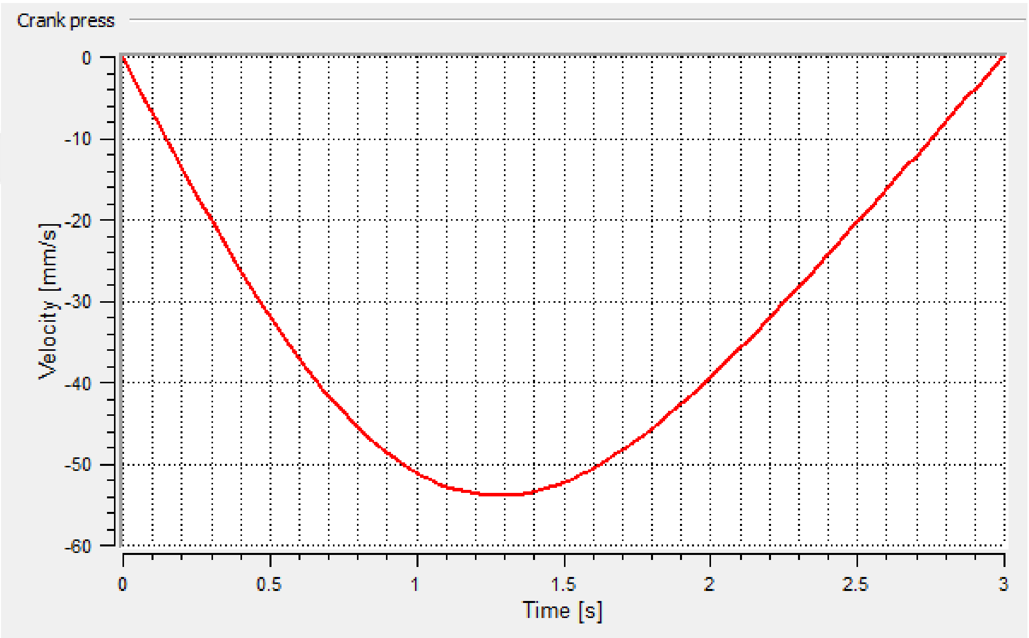

Figure 4.10 Velocity graph of the crank press

In order to provide more accurate and realistic results from the forging simulations, the boundary conditions and the consistency of the defined parameters are very important. As the material flow changes according to the mechanical properties of the material under load and the direction of the fibers, the analysis results also change. Thus, the material and the process parameters have to be selected carefully in the simulation and must be the same or closer to the real forging operation. The finite element parameters used in the analyses are given in Table 4.2. Also, in all models, the analyses were carried out for 99.5 % filling of the die so that the results can be compared with each other accurately.

Table 4.2 Finite Element forging simulation parameters for hot and warm forging

Work piece Material	AISI 4340
Die Material	H13
Work piece Temperature T_w (°C)	1200-800
Die Temperature T_d (°C)	100
Punch Speed (m/s)	50 mm/sec
Work piece Material Model	Elasto-Plastic
Punch Material Model	Rigid
Friction Coefficient	0.1
Work piece Mesh Type	Hexahedral
Work piece Mesh Size	219318 elements
Solver Machine	2 x Xeon 4114 CPU with 30 Solver Core – 32GB Ram

The number of elements used in the simulations have effects on the results, in order to achieve closer to real results in the simulations, it is necessary to use a large number of elements for the workpiece and the elastoplastic die type. A large number of elements increase the solution time of the finite element simulations. To optimize these conditions refinement boxes are used. Refinement boxes are appointed to the area where plastic deformation takes place. During the plastic deformation, elements get distorted and this can cause some errors. To prevent these errors and to obtain optimized results Simufact performs re-meshing automatically.

The die set for forging AISI 4340 consists of Punch, Ring, Gear toothed die, anvil, and mandrel as can be seen in Figure 4.11. The procedure that is used to determine the dimension of the die set is explained in Chapter 6. All parts of the die set are made from H13 tool steel. Punch and anvil are gear-shaped and the geometries are purposely designed to fit the die profile. Uni-directional forging operation is simulated, which means during forging, lower punch is fixed on the press bed while the upper punch is descending with the stroke of the press.

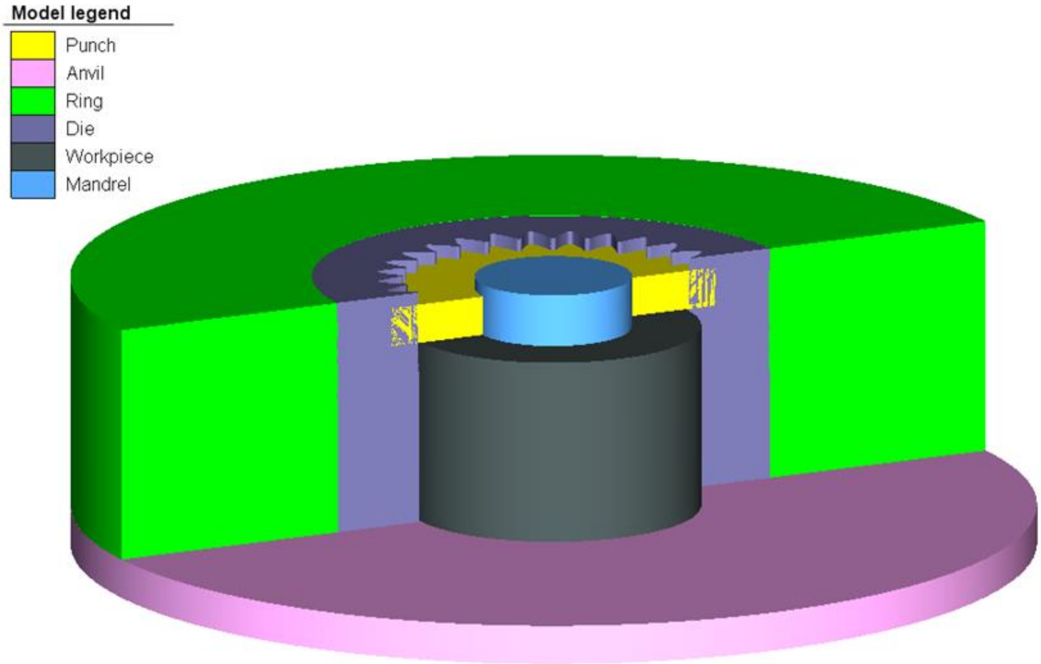

Figure 4.11 The die set and work piece for hot and warm forging of AISI 4340

Finite element simulations also were carried out according to die type. Considering all parameters which are mentioned in Table 4.1 are constant, firstly, die type was determined as the rigid. Then die type was determined as the elastoplastic. If the die type were determined as the rigid, there is no need to assign material to die, but if the die material were determined as the elastoplastic, then the material should be assigned to die. For the elastoplastic die type, AISI H13 tool steel was assigned as the die material. In addition to this when the die type is elastoplastic, the die should be divided into elements (Meshing). Simufact provides special mesh type which is called Tetrahedron (Element types 134) for elastoplastic die type [106].

4.3.2 Lead Asymmetric Spur Gear Forging at Ambient Temperature

For modeling of asymmetric spur gear at ambient temperature, lead (asm_Lead_104) was chosen as the workpiece material. The cold forging of AISI 4340 (DIN 34CrNiMo6) is not considered because of a very high forging load requirement, i.e., it is not industrially practical in terms of press capacity and tool (die) strength. The mechanical properties and flow curves of the asm_Lead_104 can be seen in Figures 4.12 and 4.13, respectively.

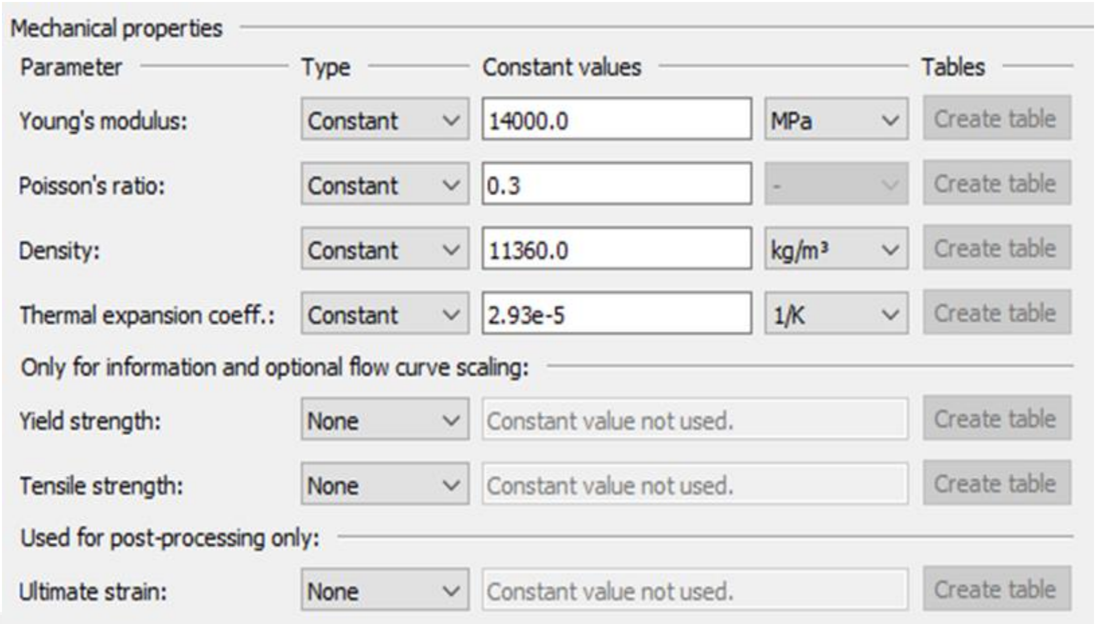

Figure 4.12 Mechanical properties of asm_Lead_104

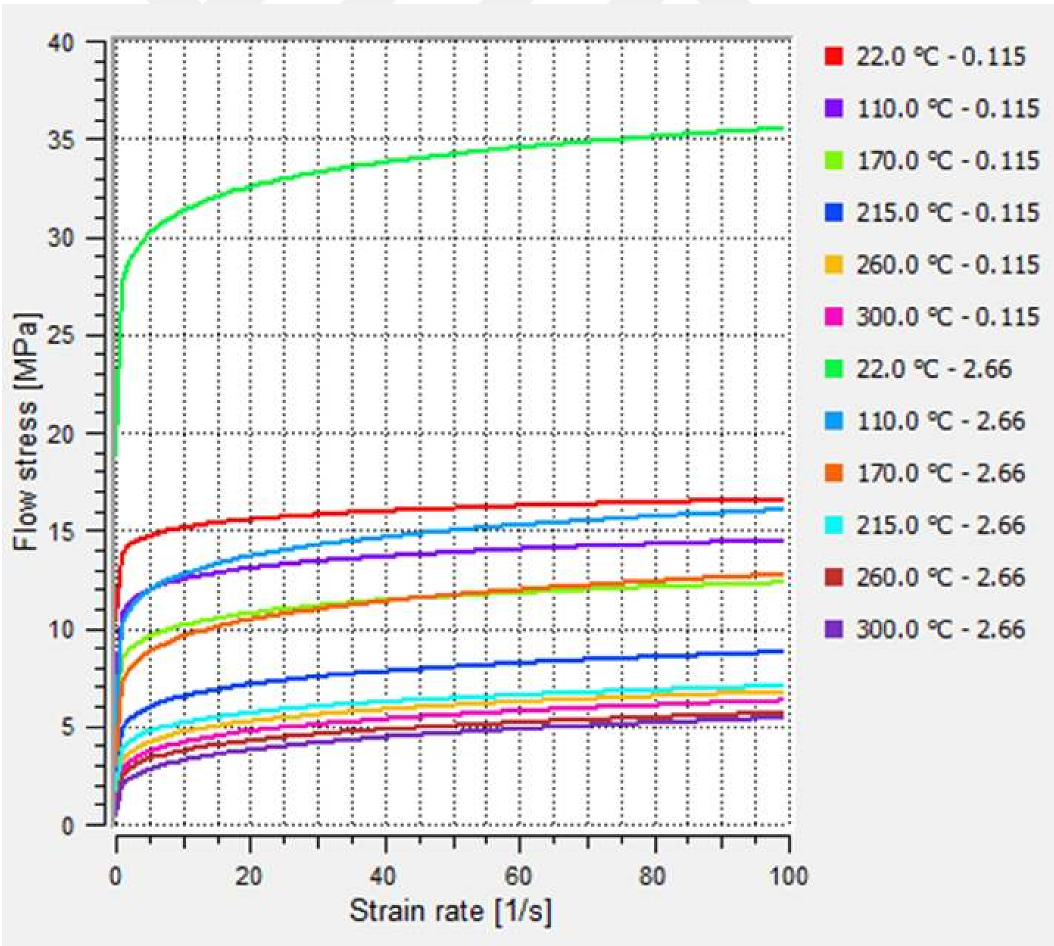

Figure 4.13 Flow curves of asm_Lead_104

Firstly, from the process application module, cold forming was selected as the process type, and then the process definition window opened. From this window, general forming for forging type and finite element for solver type was selected. Ambient temperature and number of die sets were determined as 20 ^{0}C and 4 respectively. Then the process tree was created as can be seen in Figure 4.14.

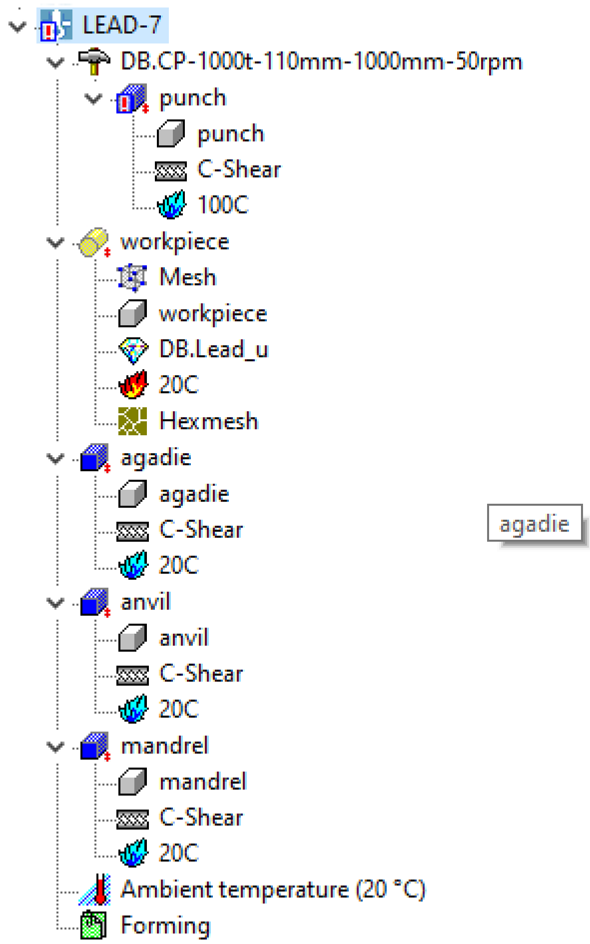

Figure 4.14 Process tree of the cold precision forging

Geometries of the die set and workpiece were imported into the finite element model by using process tree and forging temperature, workpiece temperature, and temperature of the die set parts were determined. In addition, friction conditions between die and workpiece were defined, and also forging settings were done. The view of the finite element model can be seen in Figure 4.15.

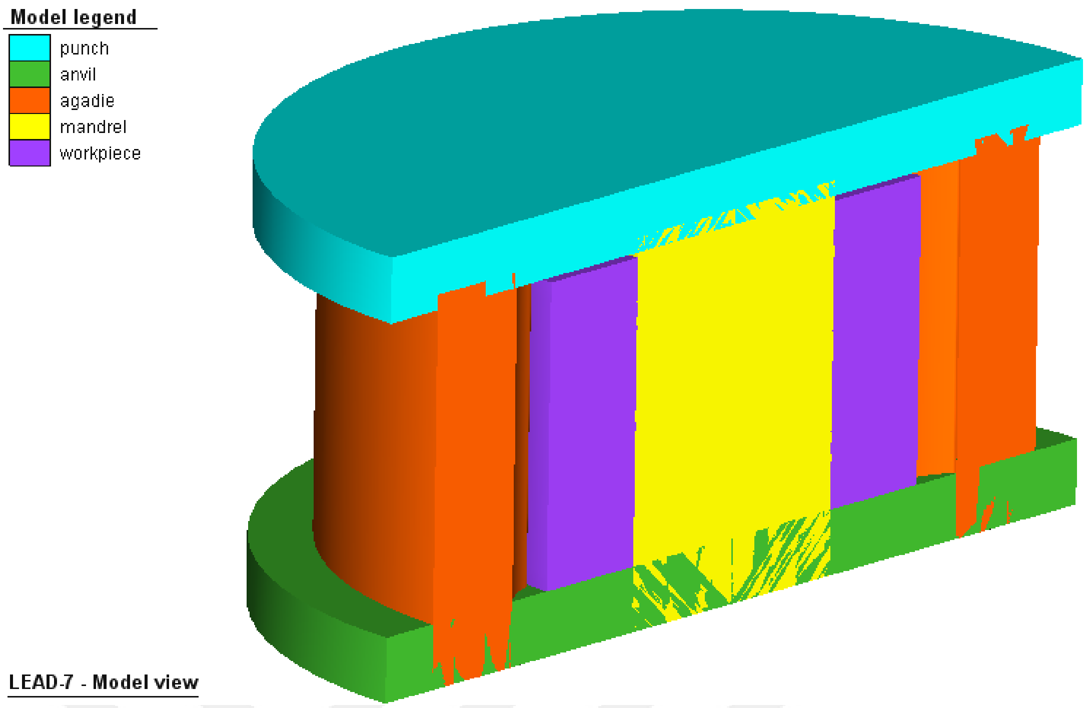

Figure 4.15 Finite model of the cold forging process

As can be seen in Figure 4.15, punch and anvil are designed as cylindrical forms. Because in the SIMUFACT software program, if the die set is rigid, die set pieces can interfere with each other, because of that, the punch and the anvil were designed as cylindrical forms to prevent flowing out the material [2]. If the die were taken as an elastoplastic type, by using contact tables the relationship between the die parts is determined.

Provided all other conditions remain the same, two different finite element models have been created taking into account the type of die. In the first model die type was selected as rigid. If the die type is rigid, die material can be determined or vice versa. In the second model die type was selected. Thus die material must be determined and die must be divided into finite elements. In this case, die material was determined as AISI H13 and by using tetrahedron (Element types 134) die divided into elements.

In the finite element models, if the element size decreases- in other words- element number increases, the solution time of simulations will increase but more accurate results will be obtained. In order to optimize simulation time and results, refinement boxes were used for the plastic deformation zone of the workpiece and for the region which is subjected load on the die surface. Thus the size of the elements in the refinement boxes will be smaller and element size in the region which is out of the refinement boxes will be greater. This causes to decrease element numbers and solution time and to get more realistic results. Differences between elements size which is outside and inside of the refinement box can be seen in Figure 4.16.

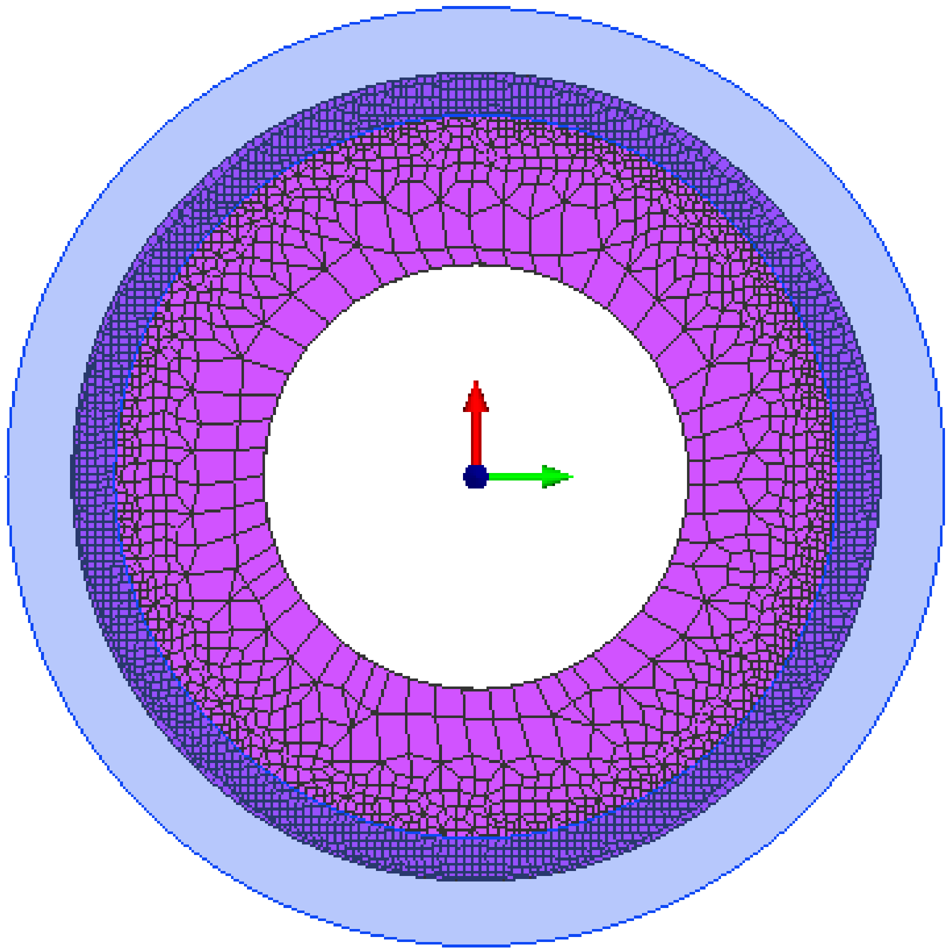

Figure 4.16 Differences between elements size which are outside and inside of the refinement box

A forging simulation can be successful when it reflects real forging. Therefore, simulation parameters must be defined carefully. The forging parameters of the ambient temperature precision forging of asymmetric gear were determined carefully and they are summarized in Table 4.3.

Table 4.3 Finite Element forging simulation parameters for ambient temperature forging

Work piece Material	Lead
Die Material	H13
Work piece Temperature T_w (ºC)	20
Die Temperature T_d (ºC)	20
Punch Speed (m/s)	35 mm/sec
Die Material Model	Rigid – Elasto-plastic
Work piece Material Model	Elasto-Plastic
Punch Material Model	Rigid
Friction Coefficient	0.1
Work piece Mesh Type	Hexahedral
Work piece Mesh Size	219318 elements
Solver Machine	2 x Xeon 4114 CPU with 30 Solver Core – 32GB Ram

CHAPTER 5

UPPER-BOUND ENERGY ANALYSIS OF ASYMMETRIC SPUR GEAR FORGING

5.1 Introduction

In the plastic deformation of metals, there are many non-linearities in the process and the material parameters. Therefore, forming loads cannot be calculated exactly by analytical formulations in metal forming processes. If the solution is kinematically and statically admissible, the solution can be considered as approximated to the exact solution. This means that the solutions must be geometrically self-consistent and must satisfy stress equilibrium in the deforming body. So, limit theorems that allow calculating forming load that is higher, equal, or lower than the required load are frequently used. These limit theorems are lower bound and upper bound energy analyses. Lower bound analysis based on ignoring geometrically self-consistency and satisfying stress equilibrium. The lower bound analysis gives the correct load or less than the required load. Upper bound energy analysis (UBEA) based on geometry-consistency and yield criteria [107]. The upper bound energy analysis gives the correct load or higher load than the required load.

In this chapter, upper bound energy analysis (UBEA) is applied to asymmetric gear. The UBEA was based on the analysis of symmetrical spur gear forging presented by Choi et al [108-109]. The analysis was evaluated for asymmetric gear forging by using twelve admissible metal flow fields.

5.2 Upper Bound Energy Analysis (UBEA) of Asymmetric Spur Gear Forging

Upper-bound analysis express that estimated force to deform plastically a material by making equal the rate of internal energy consumptions to the forces that are exerted externally will be equal or be greater than the required force [110]. In the Upper-Bound

method, flow fields that represent the shape change are determined; the rate of energy dissipation by the fields was calculated and made equal to the rate of external work made by external force [110].
In the upper bound energy analysis, some assumptions were made. These are;

- Material is isotropic
- Material is homogeneous
- During deformation, no strain hardening take place
- Two dimensional case were considered

In the case of asymmetric gear, the tooth of the gear was divided into twelve different flow fields as can be seen in Figure 5.1.

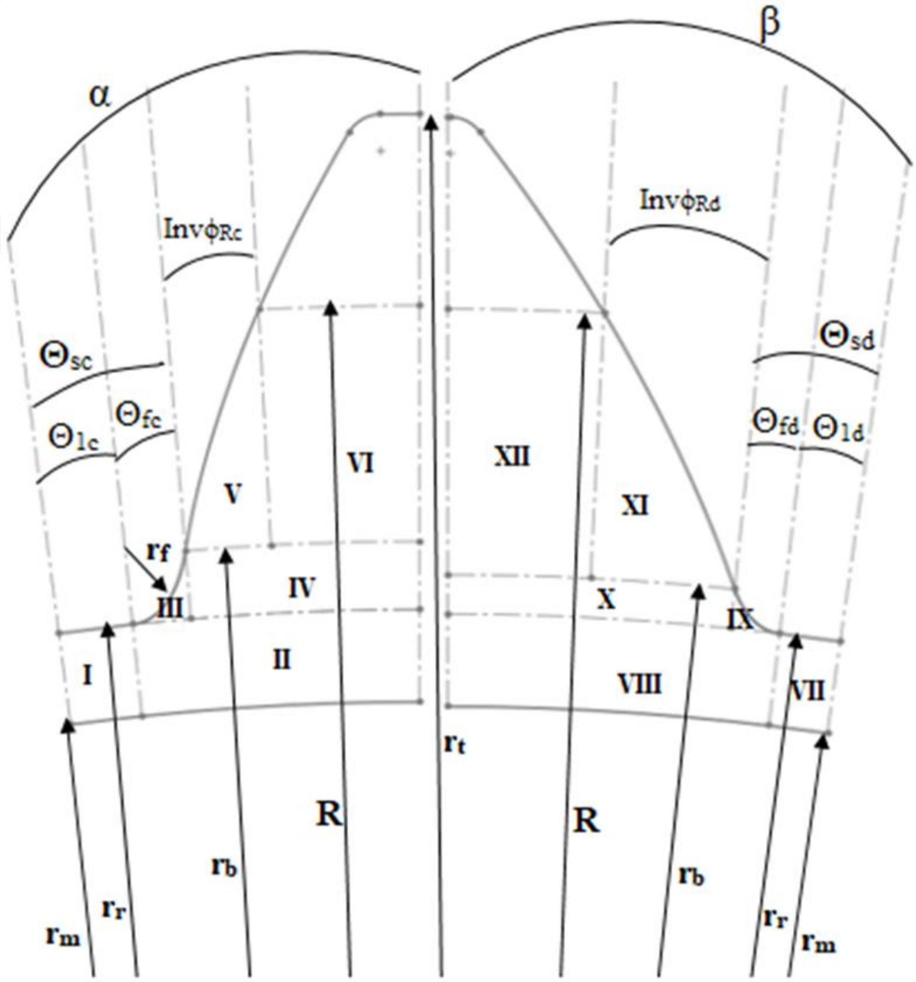

Figure 5.1 Flow Fields in the Asymmetric Gear Forging

For the drive side of the tooth, positive direction for angle –β- was selected as counterclockwise and for the coast side of the tooth, positive direction for angle –α- was chosen as clockwise and formulas were derived according to these directions. In the upper-bound analysis, polar coordinates were used and it was assumed that no material flow between die and punches so the volume of the material is constant. In additionally the drive side and coast side of the gear were considered as that they were independent of each other. Based on these assumptions, the flow field and their boundary conditions and formulas are given below.

5.2.1 Deformation Region of Coast Side of the Asymmetric Gear

5.2.1.1 First Deformation Region (rm < r < rr and 0 < θ < θ1c)

This region is bounded by the mandrel and die. Thus the radial velocity is zero and metal has only circumferential velocity.

$$U_{r1} = 0 \tag{5.1}$$

$$U_{\theta 1} = \frac{u\theta r}{h} \tag{5.2}$$

$$\dot{\varepsilon}_{rr} = 0 \tag{5.3}$$

$$\dot{\varepsilon}_{\theta\theta} = \frac{u}{h} \tag{5.4}$$

5.2.1.2 Second Deformation Region (rm < r < rr and θ1c < θ< α)

This region is bounded by mandrel, symmetry plane, the third region, and fourth region. Thus the circumferential velocity of the second region is zero at the symmetry plane and is equal to the circumferential velocity of the first region at the boundary of the first and second regions.

$$U_{r2} = \frac{u}{2h}\left(r - \frac{r_m}{r}\right)\left(\frac{\alpha}{\alpha-\theta_{1c}}\right) \tag{5.5}$$

$$U_{\theta 2} = \left(\frac{ur}{h}\right)\left(\frac{\theta_{1c}}{\alpha-\theta_{1c}}\right)(\alpha - \theta) \tag{5.6}$$

5.2.1.3 Third Deformation Region (rr < r < rb and Θsc < θ < α)

This region is bounded by the second deformation region, fourth deformation region and root fillet of the die. The formula of this region are;

$$U_{r3} = \frac{ur}{2h} + \frac{C_{II}}{r} \tag{5.7}$$

$$U_{\theta 3} = \left(\frac{ur}{2h} + \frac{C_{II}}{r}\right) Cot\varphi \tag{5.8}$$

$$Cot\varphi = \left(r_r + r_f\right)^4 - \left(r^2 - r_f^2\right) - \left(r^2 - r_r^2\right)\left[\left(2r_f + r_r\right)^2 - r^2\right] \tag{5.9}$$

$$C_{II} = \frac{ur_r}{2h}\left(\frac{\theta_{1c}}{\alpha - \theta_{1c}}\right) + \frac{ur_m^2}{2h}\left(\frac{\alpha}{\alpha - \theta_{1c}}\right) \tag{5.10}$$

5.2.1.4 Fourth Deformation Region (rr < r < rb and Θsc < θ < α)

For this region, the boundary conditions are; the circumferential velocity is zero at the symmetry plane of the coast side and is equal to the circumferential velocity of the third region at their boundary.

$$U_{r4} = \frac{ur}{2h} + \frac{C_I}{2hr(\alpha - \theta)} + \frac{C_{II}}{(\alpha - \theta_{sc})}\frac{C_{II}}{r} + \frac{C_{IV}}{r} \tag{5.11}$$

$$U_{\theta 4} = \frac{\alpha - \theta}{\alpha - \theta_{sc}}\left(\frac{ur}{2h} + \frac{C_{II}}{r}\right) Cot\varphi \tag{5.12}$$

$$C_I = \frac{1}{2}\sqrt{\left(r^2 - r_r^2\right)\left[\left(2r_f + r_r\right)^2 - r^2\right]} + 2r_f Sin^{-1}\left(\frac{\sqrt{\left(2r_f + r_r\right)^2 - r^2}}{2\sqrt{r_f\left(r_r + r_f\right)}}\right) \tag{5.12}$$

$$C_{II} = \frac{1}{2}\left(tan^{-1}A + tan^{-1}B\right) + Sin^{-1}\left(\frac{\sqrt{\left(2r_f + r\right)^2 - r^2}}{2\sqrt{r_f\left(r_r + r_f\right)}}\right) -$$

$$\frac{1}{4\left(r_r + r_f\right)^2}\sqrt{\left(r^2 - r_r^2\right)\left[\left(2r_f + r_r\right)^2 - r^2\right]} \tag{5.13}$$

$$C_{IV} = \frac{\pi r_f^2}{2h(\alpha-\theta_{sc})} - \frac{ur_m^2}{2h} \tag{5.14}$$

$$A = -\frac{(2r_f+r_r)\sqrt{(2r_f+r_r)^2-r^2+4r_f(r_r+r_f)}}{r_r(r^2-r_r^2)} \tag{5.15}$$

$$B = -\frac{(2r_f+r_r)\sqrt{(2r_f+r_r)^2-r^2-4r_f(r_r+r_f)}}{r_r(r^2-r_r^2)} \tag{5.16}$$

5.2.1.5 Fifth Deformation Region (rb < r < R and Θsc < θ < Θsc + invϕRc)

In this region, because the workpiece makes contact with the involute tooth profile, the velocity normal to die surface is zero. The formulae of this region are;

$$U_{r5} = \frac{ur}{3h} + \frac{C_V}{r^2} \tag{5.17}$$

$$U_{\theta 5} = \left(\frac{ur}{3h} + \frac{C_V}{r^2}\right)(\theta - \theta_{sc} + \phi_{Rc}) \tag{5.18}$$

$$\phi_{Rc} = tan^{-1}\left(\frac{\sqrt{(r^2-r_b^2)}}{r_b}\right) \tag{5.19}$$

$$C_V = \frac{ur_b^3}{6h} + \frac{r_b}{\alpha-\theta_{sc}}\frac{C_I^{''}}{2h} + \frac{C_{III}r_bC_{II}^{''}}{\alpha-\theta_{sc}} + C_{IV}r \tag{5.20}$$

$$C_I^{''} = [C_I]_{r=r_b} \tag{5.21}$$

$$C_{II}^{''} = [C_{II}]_{r=r_b} \tag{5.22}$$

5.2.1.6 Sixth Deformation Region (rb ≤ r ≤ R and Θsc + invϕRc ≤ θ ≤ α)

The boundary conditions of this deformation region are that circumferential velocity is zero at the symmetry plane of the coast side of the tooth and is equal to the circumferential velocity of the fifth deformation zone at the boundary of the sixth region with the fifth region.

$$U_{r6} = \frac{ur}{2h} + C_R\left(\frac{ur}{6h} - \frac{C_V}{r^2}\right) + C_R'\left[\frac{u}{3h}\left(\frac{r}{2}tan^{-1}R_{con} - \frac{r_b}{2r}R_{con}\right) + C_V\left(-\frac{1}{r}tan^{-1}R_{con} + \frac{R_{con}}{r^2}\right)\right] + \frac{C_{VI}}{r} \quad (5.23)$$

$$U_{\theta 6} = \frac{\alpha-\theta}{\alpha-(\theta_{sc}+inv\phi_{Rc})}\left(\frac{ur}{3h} + \frac{C_V}{r^2}\right)(inv\phi_{Rc} + \phi_{Rc}) \quad (5.24)$$

$$R_{con} = \frac{\sqrt{r^2-r_b^2}}{r_b} \quad (5.25)$$

$$C_R = \frac{inv\phi_{Rc}}{\alpha-(\theta_{sc}+inv\phi_{Rc})} \quad (5.26)$$

$$inv\phi_{Rc} = \frac{\sqrt{R^2-r_b^2}}{r_b} - tan^{-1}\left(\frac{\sqrt{R^2-r_b^2}}{r_b}\right) \quad (5.27)$$

$$C_R' = \frac{1}{\alpha-(\theta_{sc}+inv\phi_{Rc})} \quad (5.28)$$

$$C_{VI} = \left(\frac{1}{\alpha-\theta_{sc}}\frac{C_I''}{2h}\right) + \frac{C_{III}C_{II}''}{\alpha-\theta_{sc}} + C_{IV} - C_R\left(\frac{ur_b^2}{6h} - \frac{C_V}{r_b^2}\right) \quad (5.29)$$

5.2.2 Deformation Region of Drive Side of the Asymmetric Gear

5.2.2.1 Seventh Deformation Region (rm < r < rr and 0 < θ < θ1d)

This region is bounded by mandrel, symmetry plane and die. Thus the radial velocity is zero and metal has only circumferential velocity.

$$U_{r7} = 0 \quad (5.30)$$

$$U_{\theta 7} = \frac{u\theta r}{h} \quad 5.31)$$

$$\dot{\varepsilon}_{rr} = 0 \quad (5.32)$$

$$\dot{\varepsilon}_{\theta\theta} = \frac{u}{h} \tag{5.33}$$

5.2.2.2 Eighth Deformation Region (rm < r < rr and θ1d < θ< β)

This region is bounded by mandrel, symmetry plane, ninth region, and tenth region. Thus the circumferential velocity of the eighth region is zero at the symmetry plane and is equal to the circumferential velocity of the first region at the boundary of seventh and eighth region.

$$U_{r8} = \frac{u}{2h}\left(r - \frac{r_m}{r}\right)\left(\frac{\beta}{\beta - \theta_{1d}}\right) \tag{5.34}$$

$$U_{\theta 8} = \left(\frac{ur}{h}\right)\left(\frac{\theta_{1c}}{\alpha - \theta_{1d}}\right)(\beta - \theta) \tag{5.35}$$

5.2.2.3 Ninth Deformation Region (rr < r < rb and θ1d < θ < θsd)

In this region, the workpiece makes contact with the root fillet of the die. For this region formulae are;

$$U_{r9} = \frac{ur}{2h} + \frac{C_{IX}}{r} \tag{5.36}$$

$$U_{\theta 9} = \left(\frac{ur}{2h} + \frac{C_{IX}}{r}\right) Cot\varphi \tag{5.37}$$

$$Cot\varphi = \left(r_r + r_f\right)^4 - \left(r^2 - r_f^2\right) - \left(r^2 - r_r^2\right)\left[\left(2r_f + r_r\right)^2 - r^2\right] \tag{5.38}$$

$$C_{IX} = \frac{ur_r}{2h}\left(\frac{\theta_{1d}}{\beta - \theta_{1d}}\right) + \frac{ur_m^2}{2h}\left(\frac{\beta}{\beta - \theta_{1d}}\right) \tag{5.39}$$

5.2.2.4 Tenth Deformation Region (rr < r < rb and Θsd < θ < β)

The boundary conditions of this region are that circumferential velocity is zero at the symmetry plane of the drive side and is equal to the circumferential velocity of the ninth region at their boundary.

$$U_{r10} = \frac{ur}{2h} + \frac{C_{VII}}{2hr(\beta-\theta)} + \frac{C_{IX}}{(\beta-\theta_{sd})}\frac{C_{VIII}}{r} + \frac{C_X}{r} \tag{5.40}$$

$$U_{\theta 10} = \frac{\beta-\theta}{\beta-\theta_{sd}}\left(\frac{ur}{2h} + \frac{C_{IX}}{r}\right) Cot\varphi \tag{5.41}$$

$$C_{VII} = \frac{1}{2}\sqrt{(r^2 - r_r^2)\left[\left(2r_f + r_r\right)^2 - r^2\right]} + 2r_f Sin^{-1}\left(\frac{\sqrt{\left(2r_f+r_r\right)^2 - r^2}}{2\sqrt{r_f\left(r_r+r_f\right)}}\right) \tag{5.42}$$

$$C_{VIII} = \frac{1}{2}(tan^{-1}A + tan^{-1}B) + Sin^{-1}\left(\frac{\sqrt{\left(2r_f+r\right)^2 - r^2}}{2\sqrt{r_f\left(r_r+r_f\right)}}\right) -$$

$$\frac{1}{4\left(r_r+r_f\right)^2}\sqrt{(r^2 - r_r^2)\left[\left(2r_f + r_r\right)^2 - r^2\right]} \tag{5.43}$$

$$C_X = \frac{\pi r_f^2}{2h(\beta-\theta_{sd})} - \frac{ur_m^2}{2h} \tag{5.44}$$

$$A = -\frac{\left(2r_f+r_r\right)\sqrt{\left(2r_f+r_r\right)^2 - r^2} + 4r_f\left(r_r+r_f\right)}{r_r\left(r^2-r_r^2\right)} \tag{5.45}$$

$$B = -\frac{\left(2r_f+r_r\right)\sqrt{\left(2r_f+r_r\right)^2 - r^2} - 4r_f\left(r_r+r_f\right)}{r_r\left(r^2-r_r^2\right)} \tag{5.46}$$

5.2.2.5 Eleventh Deformation Region (rb < r < R and Θsd < θ < Θsd + invϕRd)

In this region, the workpiece makes contact with the involute profile of the drive side of the tooth. Thus velocity than normal to die surface is zero. Formulas for this region are;

$$U_{r11} = \frac{ur}{3h} + \frac{C_{XI}}{r^2} \tag{5.47}$$

$$U_{\theta 11} = \left(\frac{ur}{3h} + \frac{C_{XI}}{r^2}\right)(\theta - \theta_{sd} + \phi_{Rd}) \tag{5.48}$$

$$\phi_{Rd} = tan^{-1}\left(\frac{\sqrt{(r^2-r_b^2)}}{r_b}\right) \quad (5.49)$$

$$C_{XI} = \frac{ur_b^3}{6h} + \frac{r_b}{\beta-\theta_{sd}}\frac{C''_{VII}}{2h} + \frac{C_{IX}r_bC''_{VIII}}{\beta-\theta_{sc}} + C_Xr \quad (5.50)$$

$$C''_{VII} = [C_{VII}]_{r=r_b} \quad (5.51)$$

$$C''_{VIII} = [C_{VIII}]_{r=r_b} \quad (5.52)$$

5.2.2.6 Twelfth Deformation Region (rb ≤ r ≤ R and Θsd + invϕRd ≤ θ ≤ β)

For this deformation region, the boundary conditions are that circumferential velocity is zero at the symmetry plane of the drive side of the tooth and is equal to the circumferential velocity of the eleventh deformation zone at the boundary of the twelfth region with the eleventh region.

$$U_{r12} = \frac{ur}{2h} + C_R\left(\frac{ur}{6h} - \frac{C_{XI}}{r^2}\right) + C'_R\left[\frac{u}{3h}\left(\frac{r}{2}tan^{-1}R_{con} - \frac{r_b}{2r}R_{con}\right) + C_{XI}\left(-\frac{1}{r}tan^{-1}R_{con} + \frac{R_{con}}{r^2}\right)\right] + \frac{C_{XII}}{r} \quad (5.53)$$

$$U_{\theta 6} = \frac{\beta-\theta}{\beta-(\theta_{sd}+inv\phi_{Rd})}\left(\frac{ur}{3h} + \frac{C_{XI}}{r^2}\right)(inv\phi_{Rd} + \phi_{Rd}) \quad (5.54)$$

$$R_{con} = \frac{\sqrt{r^2-r_b^2}}{r_b} \quad (5.55)$$

$$C_R = \frac{inv\phi_{Rd}}{\beta-(\theta_{sc}+inv\phi_{Rd})} \quad (5.56)$$

$$inv\phi_{Rd} = \frac{\sqrt{R^2-r_b^2}}{r_b} - tan^{-1}\left(\frac{\sqrt{R^2-r_b^2}}{r_b}\right) \quad (5.57)$$

$$C'_R = \frac{1}{\beta-(\theta_{sd}+inv\phi_{Rd})} \quad (5.58)$$

$$C_{XII} = \left(\frac{1}{\beta-\theta_{sd}}\frac{C_{VII}^{''}}{2h}\right) + \frac{C_{IX}C_{VIII}^{''}}{\beta-\theta_{sc}} + C_X - C_R\left(\frac{ur_b^2}{6h} - \frac{C_{XI}}{r_b^2}\right) \tag{5.59}$$

5.2.3 Upper Bound Solution

By using deformation regions which are shown in Figure 5 and material flow velocities, internal power of deformation, shear power dissipated at the surface of velocity discontinuity and frictional power dissipation can be found.

Internal power of deformation

$$\dot{E}_{p,i} = \int_V \sigma\, \dot{\varepsilon}\, dV \tag{5.60}$$

Where i represent the deformation regions.

shear power dissipated at the surface of velocity discontinuity

$$\dot{E}_S = \int_S \frac{\sigma}{\sqrt{3}} |\Delta V|\, dS \tag{5.61}$$

Where S is the velocity discontinuity surface

Frictional power dissipation

$$\dot{E}_f = \int_{A_f} \frac{m\sigma}{\sqrt{3}} |\Delta V|\, dA \tag{5.62}$$

Where A_f surface area that friction occurs.

Total energy rate calculated by summing frictional power dissipation ($\dot{E}_f$), shear power dissipated at the surface of velocity discontinuity ($\dot{E}_{S)}$ and internal power of deformation ($\dot{E}_P$).

$$\dot{E}_T = \dot{E}_P + \dot{E}_S + \dot{E}_f \tag{5.63}$$

Punch load can be calculated as

$$P_{av} = \frac{\dot{E}_T}{Au} \tag{5.64}$$

In this equation, A, u and $\dot{E}_T$ represent, punch/workpiece contact area, punch velocity and total energy rate respectively.

5.3 UBEA Calculations with Python Programing Language and Software Development

In order to calculate the forging load of asymmetric spur gears, computer software was prepared by using Python programming language in order to numerically solve the equations that are obtained as a result of the analysis made using the upper limit energy theory. NumPy, SymPy, and SciPy modules was used whit the Python programming language. A user interface has been developed in Python's PyQt5 Gui Designer module for easy use. In this way, the parameters required for analysis can be easily defined in the program. The image of the user interface of the developed software is given in Figure 5.2. The user interface consists of 9 different sections. These sections are indicated in Figure 5.2 and the descriptions of the sections are given below.

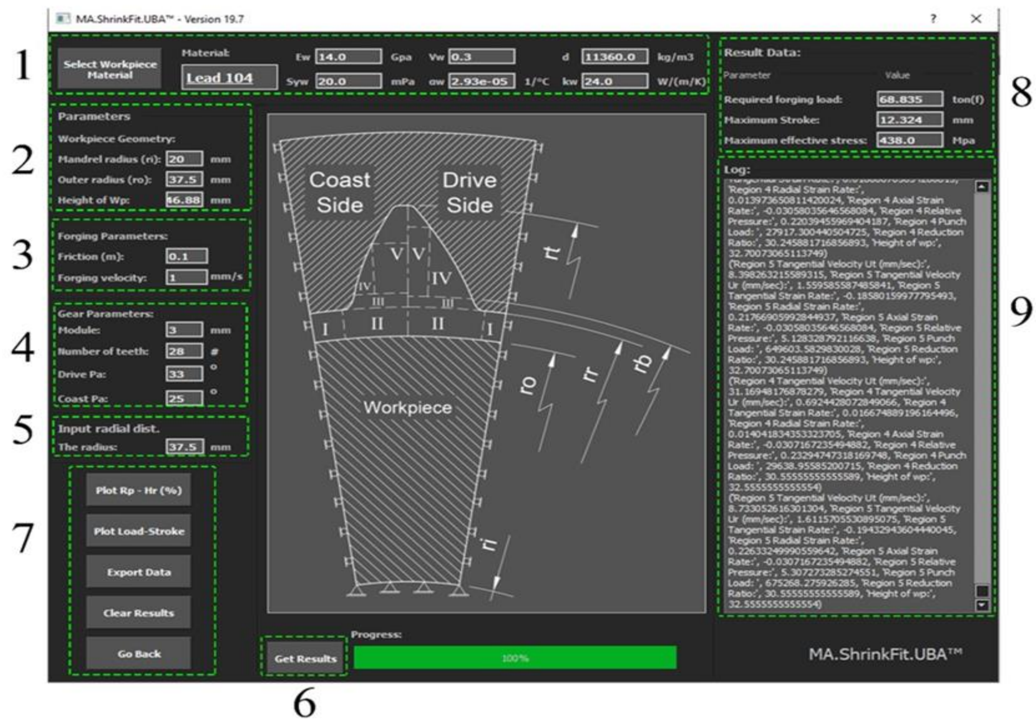

Figure 5.2 Developed software user interface

5.3.1 Section of Gear Material Selection

In this section, the material of the asymmetrical spur gear is selected. A material library was created in order to easily define the parameters of the material to be selected. The predefined materials will be able to select from the material library window opened by clicking on the "Select Workpiece Material" button (see Figure 5.3).

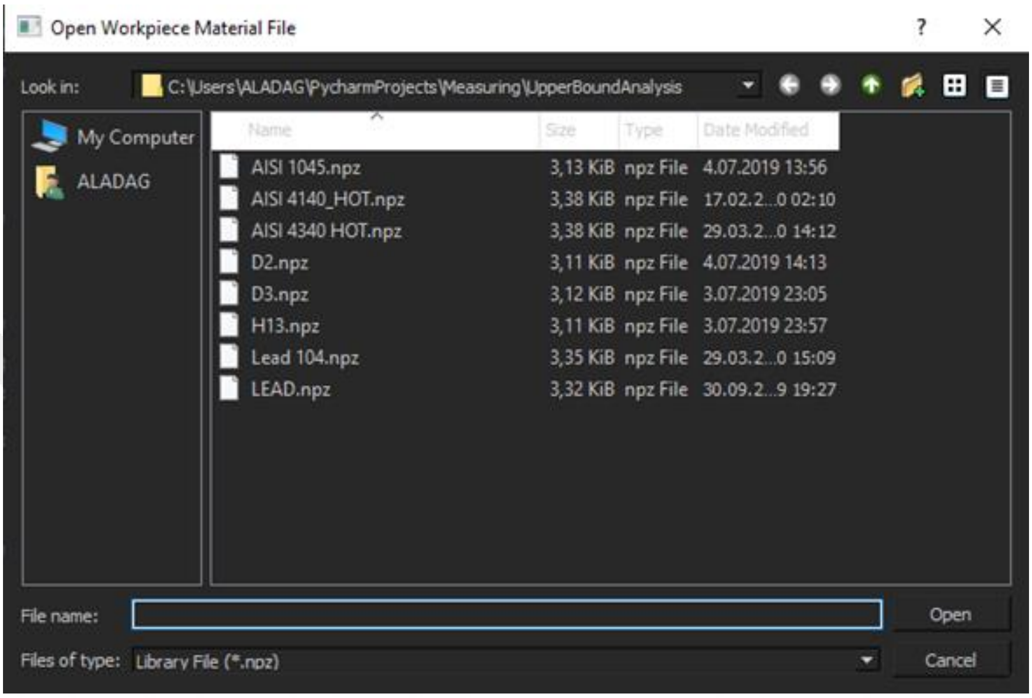

Figure 5.3 Material library window

In addition, an interface has been designed to create a new material library. This interface belongs to a different software developed to determine some parameters required in asymmetric spur gear forging. This developed software can exchange data whenever necessary. Thus, a single material library interface can also be used in upper bound analysis software. In this way, by defining a large number of materials, it was also possible to work with these materials (see Figure 5.4).

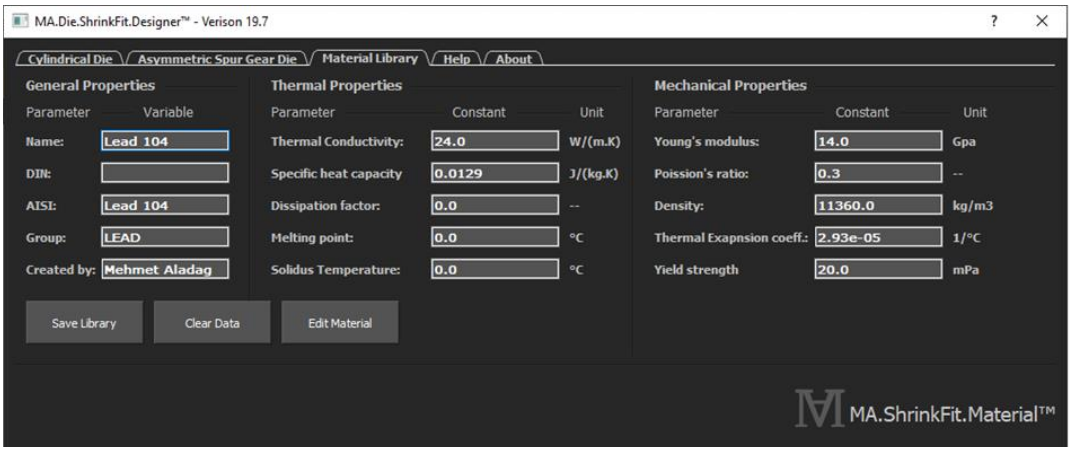

Figure 5.4 Material library creation and editing screen.

5.3.2 Section of Workpiece Geometry

In this section, the billet sizes of the gear to be forged are determined. In the precision forging of spur gears, the billet is designed as a cylindrical ring and is defined by the outer radius (r_o), inner radius (r_i), and height (h). For a gear with no center hole (full), the inner radius (r_i) value must be defined as zero "0". The purpose of this in practical application is to facilitate centering of the workpiece in the mold and to ensure symmetrical material flow through the mold section.

5.3.3 Section of Forging Parameters

In this section, punch speed (mm / sec) (Forging Velocity) and friction factor (m) are defined from forging parameters. Forging speed is used to determine the material flow rates in deformation zones, the hardening of the material is not taken into account in these calculations. The friction factor changes according to the lubrication conditions.

5.3.4 Section of Gear Parameters

It is the section that the gear parameters to be forged are defined. Teeth number and Module of the gear, pressure angles of the drive and coast side are included in this section. If the gear to be forged is symmetrical spur gear, the pressure angles will have the same value.

5.3.5 Radius Value Where Begin Upper Bound Analysis

Calculations in the program can be made starting from any given radius value. In the forging process, this radius is of course the outer radius of the billet and is generally equal to or smaller than the inner radius (bottom of the tooth) of the gear die.

5.3.6 Start Button

In this section of the user interface a button has been placed. By clicking this button, user stars the upper bound analysis.

5.3.7 Visualization of the Results

In this section, operations such as obtaining graphics from the obtained results or transferring the data to a table can be performed. With the top button (Plot Rp-Hr%) in the section, the ratio of the workpiece to height versus relative pressure can be plotted on a graph. With the second button (Plot Load-Stroke), the position of the punch can be plotted in response to the forged load (see Figure 5.5). Data obtained with the third button (Export Data) is converted into a table. In this way, different operations can be performed on the data with Excel or similar software. The fourth button (Clear Results) is the button to delete the previous results from memory for a new calculation. The fifth button (Go back) returns to the previous menu and the program is closed.

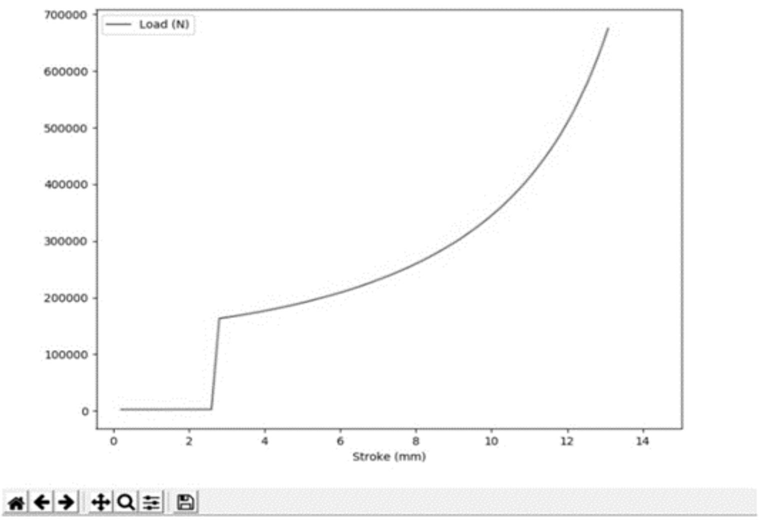

Figure 5.5 Sample of the load-stroke diagram

5.3.8 Results Data

In this section, the data obtained as a result of the calculation is directly shown. These data are as follows; the required forging load, the maximum movement of the punch and the highest stress value that occurs during forging.

5.3.9 Instant Data of the Analysis in Process

Data obtained instantly during the analysis process is displayed as output in this region. The data shown here are; tangential and radial flow rates of the material, tangential, radial and axial elongation rates of the material, relative pressure, forging load, instantaneous billet height and punch position data. Instant outputs can be followed here.

CHAPTER 6

THE DIE DESIGN AND THE GEAR TOOTH PROFILE MODIFICATIONS

6.1 Introduction

Precision forging gives the near net shape or net shape of the product. After precision forging, there is no need for further finishing operation or little finishing operation can be required. Also, die must resist loading conditions, and furthermore, in order to be a cost-effective process, die should have longer die life in the forging process. Thus in the precision gear forging, die design is significantly important. The accuracy of final forged gears is totally dependent on the accuracy of the die itself. Generally, the grade of the die must be 3 IT grades better than the forged gear [105]. In this chapter, the asymmetric spur gear forging die design and the modifications of the tooth profile are explained.

6.2 The Die Design

In a very short time period, die components are subjected to high load when the precision forging process takes place. Thus die components should resist high static and impact pressures, additionally die components should resist mechanical and thermal fatigue. The stresses encountered on the die components consist of tension, compression, and shear and it is a complex situation. These stresses occur as a result of the internal pressure exerted on the inner surface of the die. To determine internal pressure, the forging load must be known in advance. Thus it can be said that the first step of the die design is to determine forging load. The forging load can be generally found by using finite element or bound (upper or lower) analyses. In this study, both finite element analysis (see Chapter 4) and the upper bound analysis for asymmetric spur gear forging (see Chapter 5) were used for the determination of the forging load and the corresponding contact stresses required for the die design.

6.2.1 Interference Fitting Design for the Forging Die

Usually, in the precision gear forging to increase die strength against the internal pressure that exerted on it, the die is supported by an outer ring with some amount of interference. In the case of very high internal stresses where the single outer ring is inadequate, two rings or wound die may be used. The geometric representation of interference fit single ring gear forging die assembly is given in Figure 6.1.

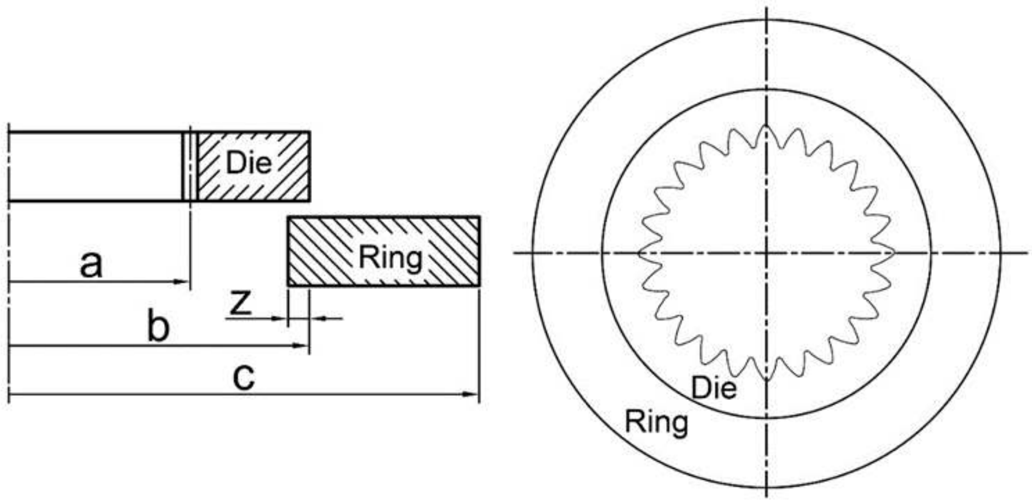

Figure 6.1 Geometric representation of interference fit single ring gear forging die assembly [80]

By applying the interference fit, the outside of the inner die is subjected to hoop stresses while the internal surface of the ring is subjected to internal pressure. The pressures and the radial- and tangential-stresses due to interference fit can be seen in Figure 6.2.

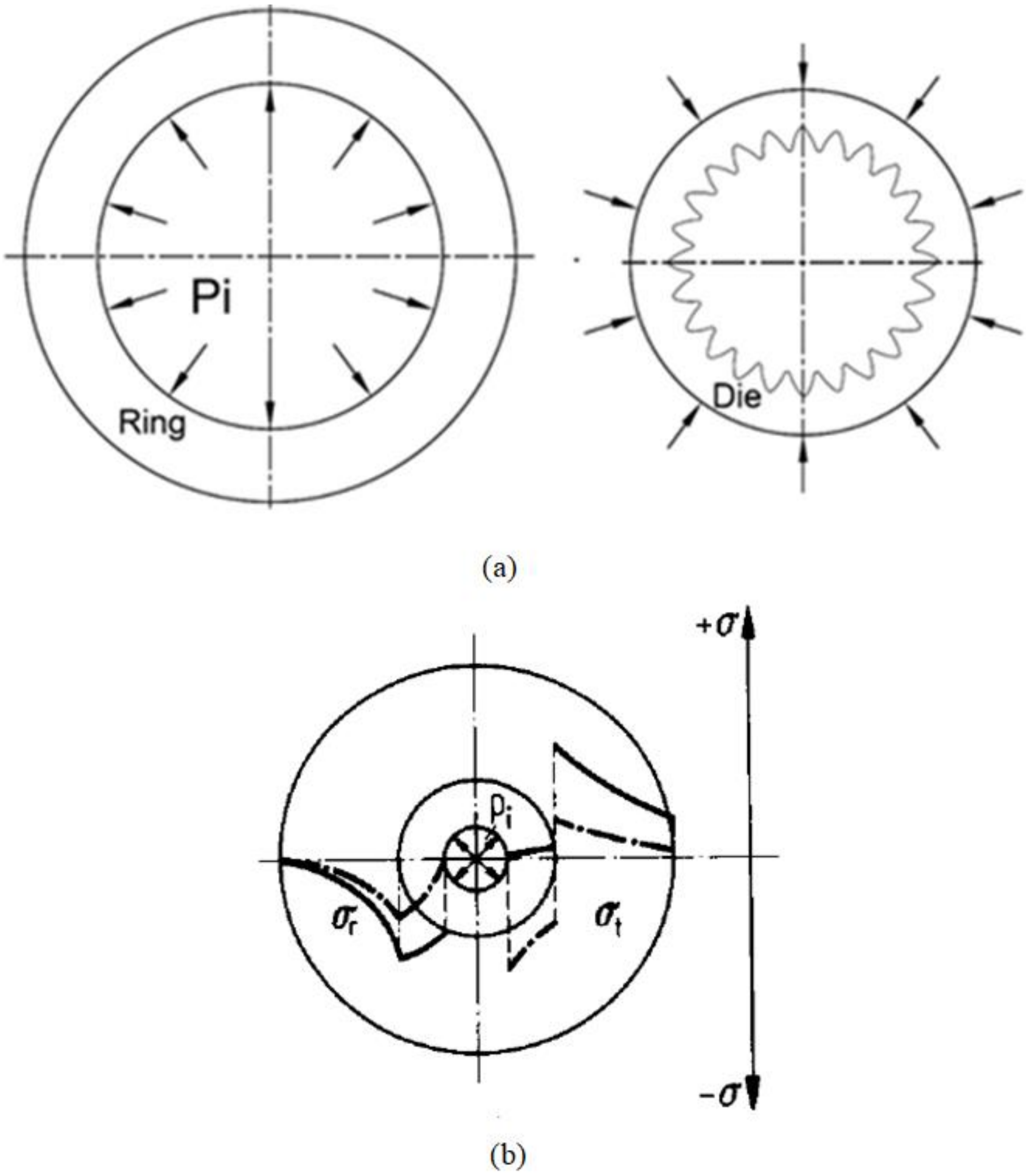

Figure 6.2 a) The pressures and b) the radial- and tangential-stresses due to interference fit.

Most of the interference fit applications are based on a thick-wall cylinder approach. However, it was shown that the design of the dies with gear teeth is beyond the thick-wall cylindrical approach [93]. Therefore, a new set of formulae were derived and suggested for the symmetric gear forging die design [80]. These formulae are given below.

$$p' = \frac{P_i}{S_y} \tag{6.1}$$

where P_i internal pressure and S_y yield stress

$$K_1 = \frac{S_{y(die)}}{S_{y(ring)}} \tag{6.2}$$

$$Q_1 = \sqrt{\frac{1}{2}\left(1 + \frac{1}{K_1}\right) - p'} \tag{6.3}$$

$$Q_2 = Q_1\sqrt{K_1} \tag{6.4}$$

$$Q = Q_1 Q_2 \tag{6.5}$$

$$a = \frac{mN}{2} \tag{6.6}$$

where m module of the gear and N teeth number of the gear.

$$b = \frac{a}{Q_1} \tag{6.7}$$

$$c = \frac{1.8a}{(\left(\frac{1}{2}\right)\left(1+2.62\left(\frac{1}{K_1}\right)\right)-2.24p')\sqrt{K_1}} \tag{6.8}$$

$$z = \frac{bS_y}{E}(1.17\frac{1}{K_1} - 0.7Q_1^2) \tag{6.9}$$

where E is elastic modulus of the die material.

From the formulae (6.1-6.9) it can be seen that the dimensions of the die set are not (or less) dependent on the pressure angle of the gear. This means that dimensions of the die set are can be determined by using the effective parameters; yield strength of the die material, the module, and the teeth number of the gear. Therefore, these formulas can be used for asymmetric spur gear dies. In this study, the die dimensions (outer diameter of the die and outer- and inner-diameters of the ring) and the amount of interference can be found using the presented method [80].

6.2.2 Profile Modification of the Asymmetric GearTooth

During precision forging, some changes take place on the tooth profile of the die. These changes result from the contraction of the die when the die interference fitted to the outer ring, the expanding of the die under load, the contraction of the die when the load is removed, the expansion due to increase in temperature, the manufacturing type of the die, the expansion of the workpiece when it is removed from the die and the cooling of the workpiece to room temperature. Hence the tooth profile should be modified according to all these factors. The geometric representation of the effects of these factors is demonstrated in Figure 6.3. These factors and their effects on the tooth profile are explained briefly in the following sections.

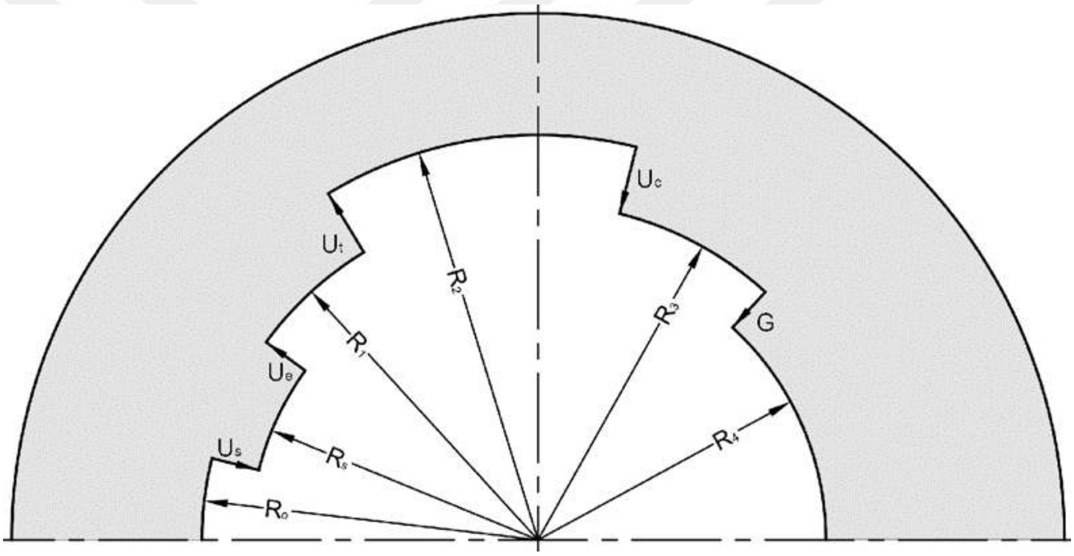

Figure 6.3 Geometric representation of the tooth profile modifications factors.

6.2.2.1 Calculation of Contraction due to the Interference Fit (U_s)

When the die is interference fitted into the ring, the inner diameter of the die gets smaller in radial direction because of the compressive forces exerted by the ring on the outer surface of the die. To calculate the amount of the radial contraction at any radius on the tooth profile (Ur), the radial and tangential stresses should be found in advance according to the thick-wall cylinder approach. The radial stress;

$$\sigma_r = \frac{P_i a^2 - P_o b^2}{b^2 - a^2} - \frac{P_i - P_o}{r^2} \cdot \frac{a^2 b^2}{b^2 - a^2} \tag{6.10}$$

And the tangential stress;

$$\sigma_\theta = \frac{P_i a^2 - P_o b^2}{b^2 - a^2} + \frac{P_i - P_o}{r^2} \cdot \frac{a^2 b^2}{b^2 - a^2} \tag{6.11}$$

where Pi and Po are the internal and external pressures, respectively. By using the stress- strain relationship;

$$U_r = \frac{r}{E_d}(\sigma_\theta - \nu_d \sigma_r) \tag{6.12}$$

where E_d is elastic modulus and ν_d is Poisson’s ratio of the die material.

By subsutiting equations 6.10 and 6.11 into equation 6.12;

$$U_r = \left(\frac{1-\nu_d}{E_d} \frac{P_i a^2 - P_o b^2}{b^2 - a^2}\right) r + \left(\frac{1-\nu_d}{E_d} \frac{a^2 b^2 (P_i - P_o)}{b^2 - a^2}\right) \frac{1}{r} \tag{6.13}$$

If $P_i = 0$, $P_o = P_p$ and r =a, radial contraction at the bore radius of the die (U_s) can be found as;

$$U_s = \frac{-2ab^2}{E_d(b^2 - a^2)} P_p \tag{6.14}$$

Thus the inner radius of the die is less than the original inner radius of the die at an amount of U_s.

6.2.2.2 Calculation of the Elastic Deformation (Ue)

There are three distinct elastic deformations which affect the final product dimensions. These are; elastic deformation of the die under loading condition, elastic deformation of the die when the forging load is removed and elastic deformation of the workpiece when it is ejected from the die.

The die expands when the forging load is applied and subsequently contracts when the forging load is released. When the workpiece is removed from the die, it will expand again. Thus they affect the workpiece dimension in different ways. By summing these values, the total effect of the elastic deformation can be found. The calculation of these conditions is discussed in the following sections.

6.2.2.3 The Elastic Deformation of the Die Under Maximum Forging Load

To calculate this elastic deformation, the die set was assumed to be a simple cylindrical shape and external pressure on the die set is zero. When the maximum forging load is applied the workpiece takes the shape of the die cavity by means of plastic deformation and so that the workpiece exerts an internal pressure on the internal surface of the die. Therefore, in addition to interference pressure, interfacial stress (nPi) is formed between the die and the ring (see in Figure 6.4).

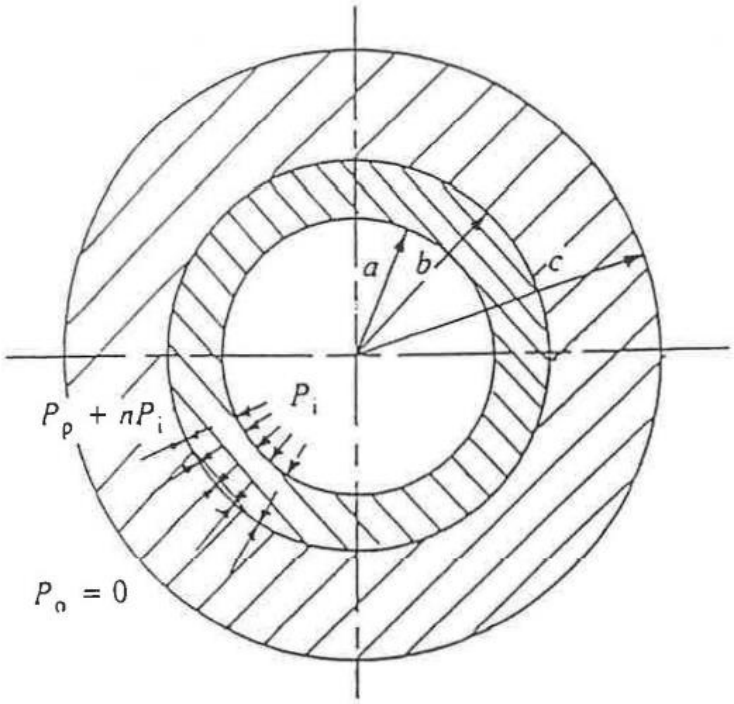

Figure 6.4 Interference pressure between the die and the ring under forging load [3]

For the continuity, the tangential strains of the ring and die must be equal to each other at the interface between them and they calculated as;

$$\varepsilon_{\theta 1} = \frac{Pi\left(1-\frac{nb^2}{a^2}\right)}{\frac{b^2}{a^2}} \frac{1-\nu_{d1}}{E_{d1}} + \frac{Pi(1-n)}{\frac{b^2}{a^2}-1} \frac{1+\nu_{d1}}{E_{d1}} \tag{6.15}$$

$$\varepsilon_{\theta 2} = \frac{nPi}{\frac{c^2}{b^2}} \frac{1-\nu_{d2}}{E_{d2}} + \frac{nPi\left(\frac{c^2}{b^2}\right)}{\frac{c^2}{b^2}-1} \frac{1+\nu_{d2}}{E_{d2}} \tag{6.16}$$

where subscripts 1 represents the die and 2 represents the ring. Thus;

$$n = \frac{2\frac{E_{d2}}{E_{d1}}\left(\frac{c^2}{b^2}-1\right)}{x+y\left(\frac{b^2}{a^2}\right)+z\left(\frac{c^2}{b^2}\right)+w\left(\frac{c^2}{a^2}\right)} \tag{6.17}$$

where

$$x = -\left(1-\nu_{d2}+\frac{E_{d2}}{E_{d1}}(1-\nu_{d1})\right) \tag{6.18}$$

$$y = 1-\nu_{d2}-\frac{E_{d2}}{E_{d1}}(1-\nu_{d1}) \tag{6.19}$$

$$z = -\left(1+\nu_{d2}-\frac{E_{d2}}{E_{d1}}(1+\nu_{d1})\right) \tag{6.20}$$

$$w = 1+\nu_{d2}+\frac{E_{d2}}{E_{d1}}(1-\nu_{d1}) \tag{6.21}$$

By using equation 6.13 and replacing P_o with (P_p+nP_i) and equating instant radius to a, elastic deformation amount at the inner radius of the die can be found as;

$$U_a = \frac{a\left(a^2(1-\nu_{d1})+b^2(1+\nu_{d1}-2n)\right)P_i-2ab^2P_p}{E_{d1}(b^2-a^2)} \tag{6.23}$$

6.2.2.4 The Elastic Deformation of the Die When Forging Load is Removed

When the forging load is removed, the die set compresses the workpiece. Using Tresca's yield criterion, the relationship between the radial stress (σ_r) and the punch pressure (σ_z) is;

$$\sigma_r = \sigma_z + 2S_y \tag{6.24}$$

Because the forging load is removed, the punch pressure will be zero. Therefore, equation 6.24 will be

$$\sigma_r = 2S_y \tag{6.25}$$

at the radius **a,** this radial stress will be equal to P_i and by replacing this value into equation 6.23, total elastic deformation of the die can be found as;

$$U_a = \frac{a\left(a^2(1-\nu_{d1})+b^2(1+\nu_{d1}-2n)\right)2S_y - 2ab^2P_p}{E_{d1}(b^2-a^2)} \tag{6.25}$$

6.2.2.5 The Elastic Deformation of the Workpiece After Removed from the Die

When the forging load is released, the radial stresses are still acting on the workpiece. On ejection, its radius will expand elastically and the amount of recovery can be calculated by assuming a cylindrical state of stress. The radial and tangential stresses (σ_r and σ_θ) will be equal to each other. By using the stress-strain relationship;

$$\varepsilon_\theta = \frac{1-\nu_w}{E_w}\sigma_\theta = \frac{s}{r} \tag{6.26}$$

where E_w and ν_w are the elastic modulus and the Poisson's ratio of workpiece material, respectively.

By replacing **r** with a and $\boldsymbol{\sigma_\theta}$ with $\mathbf{2S_y}$, elastic expansion of the workpiece can be calculated as;

$$s = \frac{1-\nu_w}{E_w}2S_y a \tag{6.27}$$

The total elastic deformation due to the die expansion, die contraction and workpiece expansion can be found as,

$$Ue = Ua + s \tag{6.28}$$

6.2.2.6 Calculation of the Thermal Die Expansion (U_t)

To perform hot and warm precision forging, the die is heated to a predefined temperature to prevent cracking of the die components and to reduce the cooling rate of the workpiece. Also, heat is transferred from the workpiece during forging which further heats the die. The combination of these two sources of heat causes the die to expand. Thus, the expansion of the inner radius of the die due to preheating is;

$$U_{tp} = \lambda_d a\,(\text{Tpreheat-Tenvironment}) \tag{6.29}$$

where λ_d is the termal expansion coefficient of the die material.

During the plastically deformation of the workpiece, heat will be generated. Therefore die dimension will be affected. The amount of this change can be calculated as explained in the below.

If T_i-T_p is the temperature increase on the die surfac and asuming the temperature increasing on the outer surface of the die is zero (T_o-T_p = 0) temperature at the any selected radius value can be found as

$$T = -\frac{\delta T}{(b-a)} r + \frac{(T_i - T_o)}{(b-a)} b \tag{6.30}$$

Where T_i inner temperature of the die, T_p is the preheat temperature, $-\frac{\delta T}{(b-a)}$ is the temperature gradient with respect to radius and T_o is the outer surface temperature of the die.

The radial and tangential stresses depending on the temperature are;

$$\sigma_{rt} = \frac{\lambda_d E_d \delta T}{3(b-a)} \left(\frac{a^2 b^2}{a+b} \frac{1}{r^2} - 2r + \frac{b^3 - a^3}{b^2 - a^2} \right) \tag{6.31}$$

and

$$\sigma_{\theta t} = \frac{\lambda_d E_d \delta T}{3(b-a)} \left(\frac{-a^2 b^2}{a+b} \frac{1}{r^2} - r + \frac{b^3 - a^3}{b^2 - a^2} \right) \tag{6.32}$$

By replacing these equation in to equation 6.12 radial displacement of the die at any radius can be found as

$$U_{ts} = \frac{\lambda_d \delta T}{3(b-a)} \left[\frac{-(1+v_d)a^2b^2}{a+b}\frac{1}{r} + (2v_d - 1)r^2 + \frac{(1-v_d)(b^3-a^3)}{b^2-a^2}\right] \qquad (6.33)$$

Total die expansion due to temperature is;

$$U_t = U_{ts} + U_{tp} \qquad (6.34)$$

6.2.2.7 Calculation of the Thermal Workpiece Contraction (U_c)

When the workpiece is removed from the die and cools to room temperature, its dimensions contract. The amount of the contraction simply can be found as;

$$U_c = \lambda_w a\,(T_{forgingt} - T_{environment}) \qquad (6.35)$$

6.2.2.8 WEDM Spark Gap (G)

In this study die will be machined by using a wire electrical discharge machining (WEDM) process. After determining the contractions and expansions of the die, the spark gap of the WEDM must be taken into account. Tool path of the WEDM must be smaller than the determined radius of the die at the amount of the spark gap.

6.2.2.9 Die Profile Changing Due to Finishing of the Die by AFM process (U_{AFM})

The WEDMed surfaces are relatively rough and contain a certain amount of white layer. The white layer has micro-cracks, so it must be removed from the die surface. In order to get a smooth surface and to remove the white layer, a finishing process is required. In recent years, there has been an increased interest in the finishing of forging dies by Abrasive Flow Machining (AFM). AFM is a relatively novel and non-usual surface finishing process that is performed by the movement of abrasive media through the surface. Due to the material removal during the process, the dimension of the die will change. Assuming that the material removal is uniform, the effect of the AFM on the die dimension can be calculated as below.

The material removed by an abrasive particle is

$$W_a = \rho A_g L_m \tag{6.36}$$

where ρ is the density of the die material, A_g is area of groove and L_m is length of the abrasive media.

In one cycle, many of the abrasive particle remove material from the surface of the die and the number of the particle that pass in one cycle can be found as;

$$N_s = C N_a L_w L_m \tag{6.37}$$

in which C is the concentration of the media, N_a particle number per area and L_w is length of the workpiece

Amount of the material that removed in one cycle can be found as

$$W_t = N_s W_a \tag{6.38}$$

Total material which is removed after n cycle can be found as

$$W = n W_t \tag{6.39}$$

Then the change of the die dimension (the amount of finishing allowance) caused by AFM can be calculated as

$$U_{AFM} = \frac{W}{L_w h_w \rho} \tag{6.40}$$

where h_w is the hight of the die.

CHAPTER 7

EXPERIMENTAL STUDIES

7.1 Introduction

The finite element modeling and upper bound analysis of the precision forging of asymmetric spur gears were presented in the previous chapters. Also, a design procedure for the die was suggested including gear tooth modifications. For validation of the suggested die design criteria and the presented numerical analyses, experimental studies were carried out. The experimental procedure, working materials and manufacturing of die components are explained in this chapter.

7.2 Preform Material and Manufacturing

The preform was designed as a cylindrical ring with an outer diameter of 75 mm and an inner diameter of 40 mm, in accordance with the selected prototype asymmetric gear parameters. Here, the inner diameter is equal to the mandrel diameter and the outer diameter is equal to the root diameter. The height of the billet was determined to equal the volume of the forged gear and was calculated as 46.88 mm from the 3D model to obtain a gear with a 35 mm face width.

To observe the material flow during gear forging, the preform was produced as two halves having square grids on the section faces as shown in Figure 7.1. The preform halves were manufactured by using casting and a metal mold (see Figure 7.2) was designed and manufactured. The halves of the preforms were joined by a water-soluble adhesive for ease of positioning into the forging die cavity. The adhesion was kept weak enough to separate from each other after forging.

Figure 7.1 Two halves preform with grids

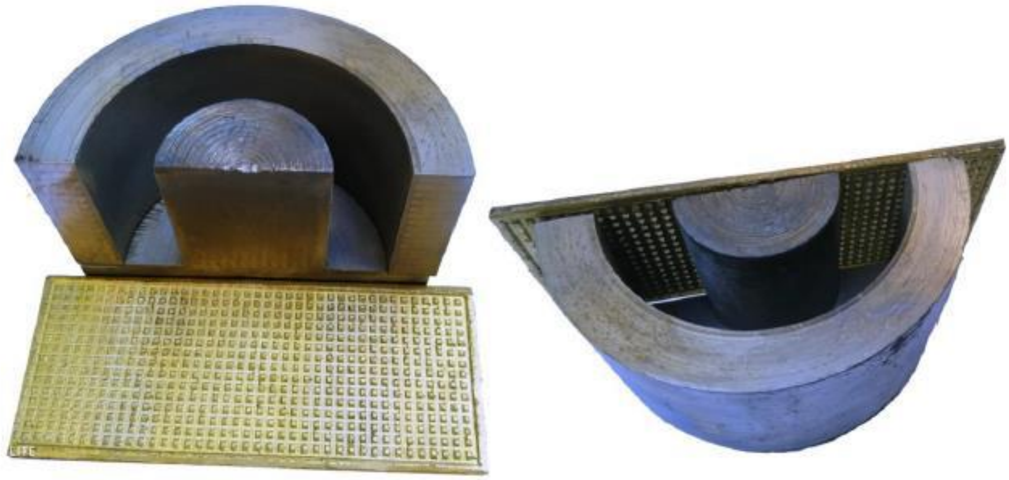

Figure 7.2 The preform casting mold.

The preforms were cast from lead. For this purpose, lead billets were obtained from the market and material properties were determined by performing material tests. The results are compared with the values in the Simufact Forming Finite Element Software's existing material library. The stress-strain diagram of the lead material and the flow stress diagram of the material "asm_Lead_104" in the Simufact material library are given in Figure 7.3 It was decided to supply the sample which is compatible with the "asm_Lead_104" features in the Simufact material library and to use it in experimental studies. The properties of the lead material are given in Table 7.1 and Flow curve diagram is given in Figure7.3

Table 7.1 Properties of Lead

Lead (asm_Lead_104)	
Elastic Modulus	1.4e+10 Pa
Poisson's ratio	0.3
Density	11360.0 kg/m³
Thermal Conductivity	24.0 W/(m·K)
Specific Heat Capacity	129.0 J/(kg·K)
Thermal Expansion Coefficient	2.96e-5 1/K
Melting Temperature	327.5 ^{0}C

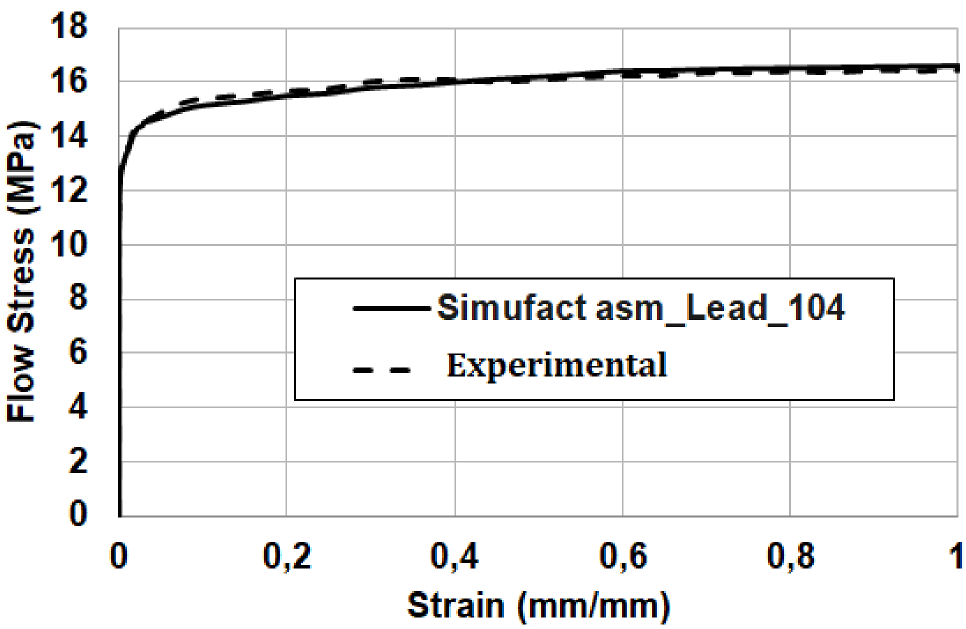

Figure 7.3 Flow curves of Lead

7.3 Forging Die Manufacturing

The dimensions of the die components were determined based on the design criteria given in the previous chapter. The die material was selected as Uddeholm Orvar Supreme (AISI H13) and it was provided from the market. Mechanical properties and chemical composition of the die stock material can be seen in Table 7.2 and Table 7.3 respectively.

Table 7.2: Properties of Die Material (Uddeholm Orvar Supreme -AISI H13-)

Property	**Value**
Tensile strength, ultimate (@ 20ºC, varies with heat treatment)	1200 – 1590 MPa
Tensile Strength, yield (@ 20ºC, varies with heat treatment)	1000 – 1380 MPa
Reduction of area (@20°C)	50.00%
Modulus of elasticity (@20°C	215 GPa
Poisson's ratio	0.27-0.30
Thermal expansion	10.4 x 10^{-6}/ºC
Thermal conductivity	28.6 W/mK

Table 7.3 Chemical Composition of the Die Material

Cr	**Mo**	**Si**	**V**	**C**	**Ni**	**Cu**	**Mn**	**P**	**S**
5.2	1.4	1.0	0.9	0.39	0.3	0.25	0.2-0.5	0.03	0.03

Before manufacturing, die was subjected to heat treatment in order to obtain 52-55 HRC. Then die stock was machined by using VT 80 C-Axis CNC Lathe in Gaziantep University CAD/CAM Innovation Center in order to prepare for the Wire Electro Discharge Machining process (WEDM). To machine die set, tool path was generated for each part of the die set (die, punch, and anvil) by using computer-aided manufacturing (CAM) package software program (TopsolidCam), and G codes were obtained for each part. WEDM process was performed by using the process parameters given in Table 7.4.

Table 7.4 Process Parameters of WEDM

Gap set Voltage	Cutting Speed	Peak Current	Pulse on Time	Pulse off Time	Wire Tension	Wire Feed
V	Mm/min	A	µs	µs	4	4
10	3.5	90	108	40	12	4

The outer ring and the mandrel were machined by using VT 80 C-Axis CNC Lathe to the required dimensions and hardened to 52-55 HRC. The die and the outer ring was interference fitted by heating the ring to 200 ^{0}C and cooling the die by using liquid nitrogen. The components of the die set are shown in Figure 7.4.

Figure 7.4 The components of the forging die set

After machining and interference fitting, the gear toothed die was finished by using an abrasive flow machining process (AFM). The two-way AFM machine which was designed and constructed at Gaziantep University (see Figure 7.5) was used. The machining parameters of the AFM process are given in Table 7.5.

Table 7.5 Process Parameters of AFM

Abrasive Type	Abrasive Media	Viscosity	Density	Concentration	Working Pressure
		Pa s	gr/cm^3	%	MPa
SiC	Polyborosloxane	60	3.2	70	6

Figure 7.5 The two-way AFM machine.

7.4 Measurements

After AFM finishing, dimensions and tooth profiles of the die were measured. The measurement of the asymmetric spur gear die is a difficult task because of its geometry. Because the asymmetric gear die will be used in precision forging, dimensional accuracy of the die is very important and die should be manufactured precisely. Thus, to measure the dimension of the asymmetric gear die tooth, an optical profilometer and a 3D coordinate measurement machine CMM were used. The Leitz Wetzlar optical profilometer was used to magnify the tooth profile as shown in Figure7.6. The tooth profile was magnified by 20 times and gauge blocks were used to scale. Then the image of the scaled tooth was transferred to AutoCAD in order to see differences between technical drawing and the manufactured profile.

Figure 7.6 Magnified tooth profile by using Leitz Wetzlar optical profilometer

The measurements were also performed by using the Kemco 3D Coordinate Measuring Machine (CMM) available in the metrology laboratory (see Figure 7.7). The measurements were done by using a 1 mm radii Renishaw touch probe for comparison.

Figure 7.7 The Kemco 3D Coordinate Measuring Machine (CMM)

The surface roughness was measured by using a Mitutoyo SJ 401 surface measuring machine (see Figure 7.8). The cut off length was 0.8 mm and three measurements were taken repeatedly for each condition and the averages of them were taken.

Figure 7.8 Mitutoyo SJ 401 Surface roughness tester

7.5 Experimental Procedure and the Forging Press

Experimental studies were conducted in the laboratory of the Mechanical Engineering Department of Gaziantep University. For experimental studies, a hydraulic press that has 200 tons' capacity was used. The press can be seen in Figure 7.9 and the technical features are given in Table 7.6.

Figure 7.9 View of the press

Table 7.6 Technical Features of the Press

TECHNICAL FEATURES	
Capacity (ton)	200
Working Size	1300x450
Stroke (mm)	400
Motor Power (KW)	7.5
Pump (liters)	22
Down Speed (mm/s)	6.4
Return Speed (mm/s)	11.04
Overall Dimensions (LxWxH,mm)	1200x2020x2800
Weight (kg)	2350

The press has a 170 mm diameter cylinder and punch was attached to the press cylinder. By controlling the hydraulic oil pressure, the forging load was predicted step by step. Incremental forging tests were carried out to observe the metal flow and comparing them with the FE simulation results.

Experimental studies were performed at room temperature. To perform the precision forging process, die and anvil were placed on the press table and fixed. The surfaces of the asymmetric gear die, the mandrel and the upper and lower punches were carefully coated with molybdenum disulfide (MoS_2) lubricant by using a small brush. Then the preform was placed into the die cavity carefully.

CHAPTER 8

RESULTS AND DISCUSSION

8.1 Introduction

In this chapter, the results of the upper-bound energy analysis (UBEA), the FEM, and the experimental studies are presented. The forging loads for hot-and warm-forging of AISI 4340 determined by UBEA and FE analyses were compared and the calculated results of the final forging die dimensions and the amount of interference were given. The rigid-die and elastoplastic-die FE models were compared. The temperature distribution and the stresses formed on the preform during forging were also discussed for both hot- and warm-forging. The experimental gear forging was carried out for the lead and the material flow patterns during forging for the experimental and FEA were shown. The measurement results of tooth profile deviations from the designed forging die and the theoretical gear are discussed.

8.2 The Results of Hot- and Warm-Forging of AISI 4340 Gear

8.2.1 Forging Load

The FEM simulations (Chapter 4) and the UBEA (chapter 5) of the hot- and warm-precision forging of asymmetric gear were performed for AISI 4340 steel. The load-stroke diagrams of the FEM simulations and UBEA are given in Figure 8.1. In the FEM simulations, the forging load increases with the punch stroke slowly until the preform touching the tooth tip of the die. Then it increases asymptotically at the final filling of the die. The trends are similar for both the hot- and the warm-forgings. The UBEA results show the load increases very slowly at the very beginning of the forging where the preform expands radially. Then the load is increasing sharply, which is due to the initial touching the preform to the die walls (there is a difference between the outer diameter of the preform size and the root diameter of the die). The load increases with the stroke slowly until the final stage where the increase of the load is very sharp (asymptotic). Again, the trends are similar for both the hot- and the warm-forgings. However, the upper bound analysis results give higher forging load values than the experimental results as expected due to the nature of the upper bound method. The maximum forging loads were found as 345 tonf and 280 for UBEA and FE study, respectively, for hot-forging. For the warm-forging, the maximum forging loads were 695 ton force and 670 ton force for UBEA and FE study, respectively, the presented UBEA is recommended for the asymmetric spur gear die design and determination of press capacity in order to stay in the safe zone. The difference of maximum forging loads of the UBEA and FE is less than 4% and 15% for warm- and hot-forgings, respectively. Here, the maximum load is required for the die design and press capacity. The higher differences in the mid-stroke come from the barreling effect which is neglected in the UBEA. If the barreling effect is included, i.e. 3D analysis is applied, this deviation will be smaller. The load stroke diagram can be obtained by using the developed software based on the UBEA in a very short time (3 seconds in this analysis).

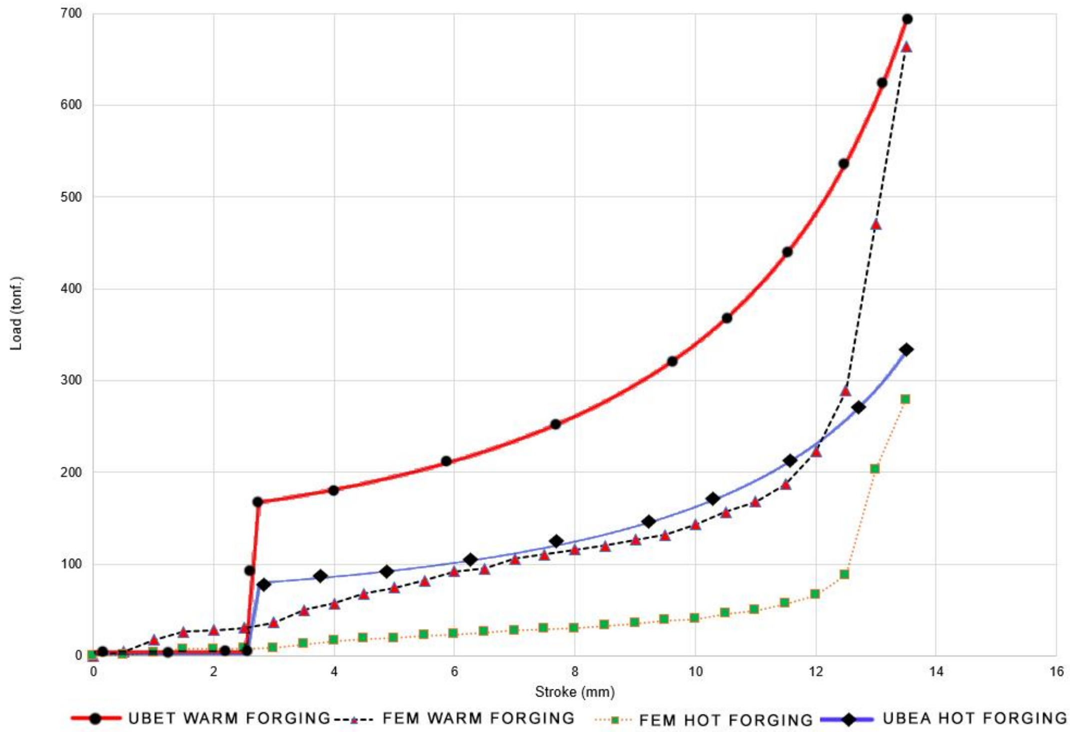

Figure 8.1 Forging loads comparison of fem simulations and upper-bound analysis, for hot and warm forging

8.2.2 Internal Pressure Exerted on the Inner Surface of the Die (Contact Pressure)

In order to determine contact stresses (internal pressure Pi), finite element simulation for hot-forging were used. When the contact surface area between the preform and die reaches 99.5% of the total area, the simulation was stopped and the corresponding contact pressure was determined. The contact pressure distribution of forged gear is shown in Figure 8.2. As it can be seen in Figure 8.2 that maximum contact pressure occurs at the root diameter of the gear and tip of the gear teeth. Contact pressure (internal pressure) is approximately 590 MPa.

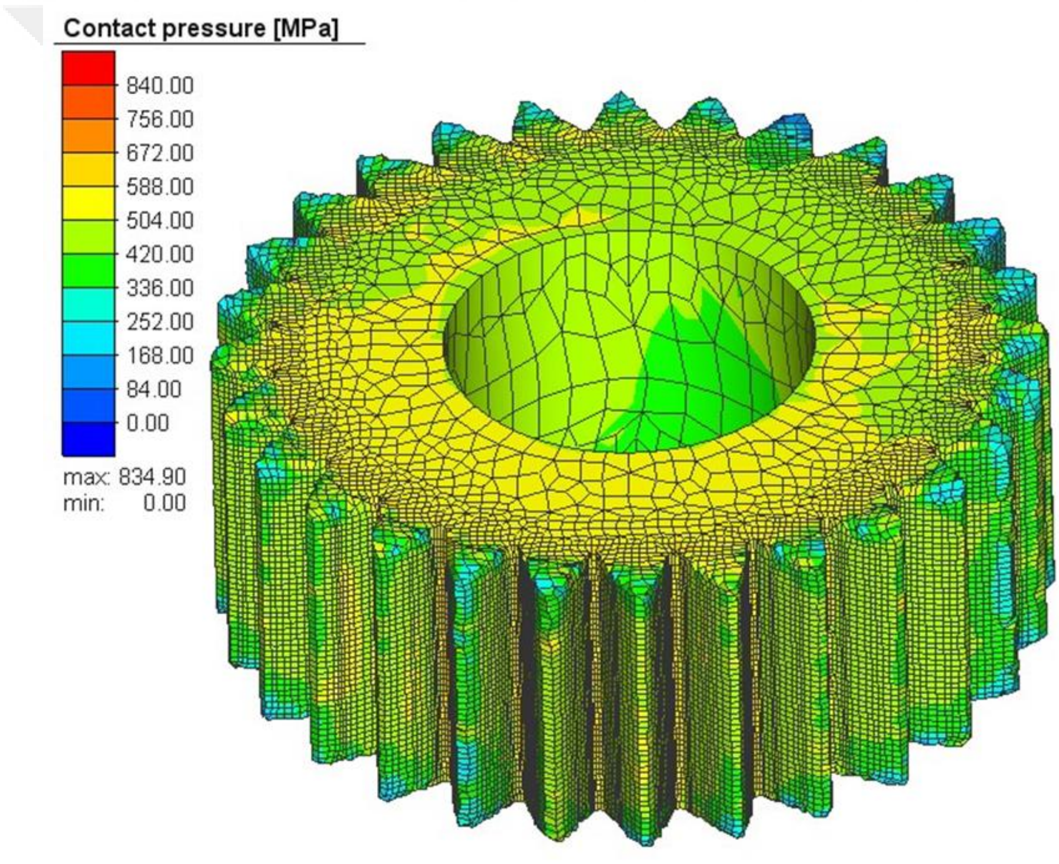

Figure 8.2 Distribution of contact stresses on forged asymmetric spur gear.

8.2.3 The Dimensions of the Asymmetric Gear Forging Die

The dimensions of the gear die were calculated by the method suggested by Eyercioglu [80]. The results of the method were verified in a study that is a part of this project for asymmetric spur gear forging dies [111]. The dimensions of the asymmetric gear forging die and the amount of interference are given in Table 8.1.

Table 8.1 Dimensions of the forging die

Inner Pressure	Outer Diameter of the inner die	Inner Diameter of the ring	Outer Diameter of the ring	Amount of Interference
MPa	(mm)	(mm)	(mm)	(mm)
590	64.13±0.05	142.21±0.05	142.47±0.05	0.268

8.2.4 Temperature Distribution

The results of temperature distributions on the forged asymmetric spur gear at the final die filling stage (99.5%) are shown in Figure 8.3. for hot- and warm-forging simulations. The die components were at 100 ^{0}C and the preforms were at 1200 ^{0}C and 800 ^{0}C for hot- and warm-forging, respectively, at the beginning of the forging operation. During forging time heat was transferred from preform to the die components and environment. Although some amount of heat is generated during deformation, the temperature drops by the time pass. As it is expected, the rate of temperature drop is higher for hot forging due to the higher temperature gradient (see Figure 8.4). Cooling of the preform is faster after the punches touch to it. Although the total forging time is less than a second for both cases, a considerable amount of cooling takes place. The preform temperature drops from 1200 ^{0}C to 850 ^{0}C during hot forging and from 800 ^{0}C to 550 ^{0}C for warm forging case.

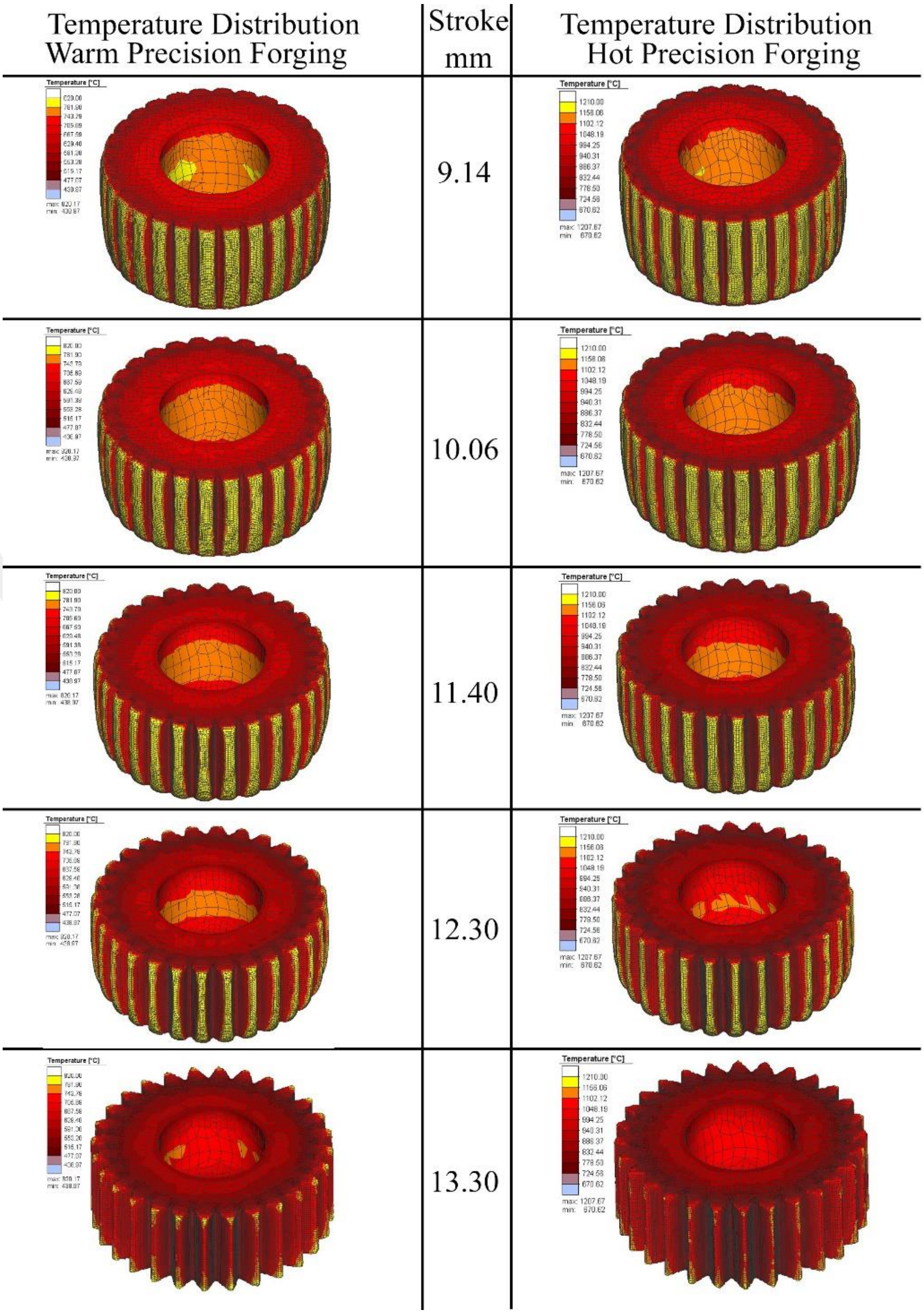

Figure 8.3 Temperature distributions with respect to punch stroke for warm- and hot-forging.

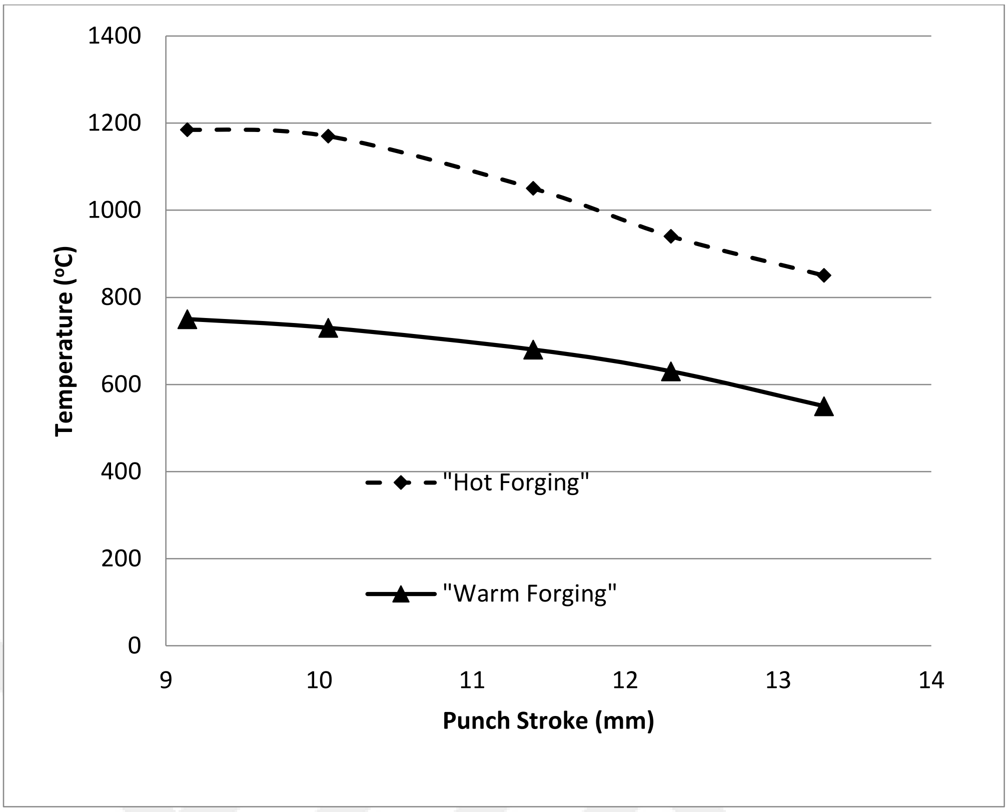

Figure 8.4. Cooling of preform with respect to punch stroke for warm- and hot-forging.

8.2.5 Effective Stress Distribution

The effective (von Mises) stress distributions with respect to punch strokes are given in Figure 8.5. The flow stress increases as the workpiece cools. Therefore, higher effective stresses are encountered in warm forging simulations. The effective stress increases with the stroke for both warm- and hot-forging simulations as shown in Fig. 8.6. The stresses are increasing asymptotically at the final filling stages because of the difficulty of metal flow at the tooth region. The involute profile of the gear causes more friction effect and inhomogeneous metal flow. The gear tooth shape is forming at the upper part of the workpiece before the bottom part because of bi-linear forging (i.e. only upper punch is moving).

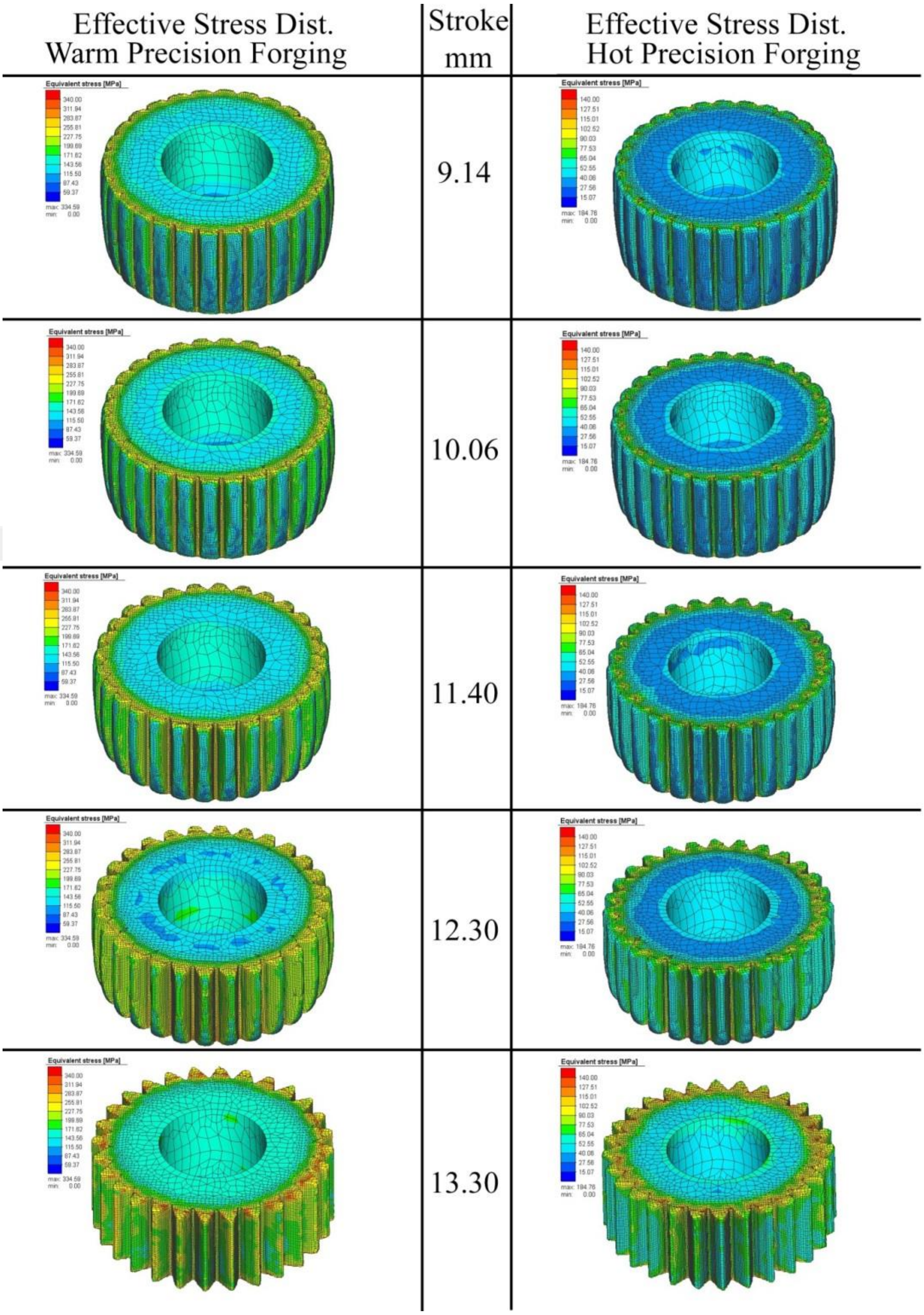

Figure 8.5 Effective stress distributions with respect to punch stroke for warm- and hot-forging.

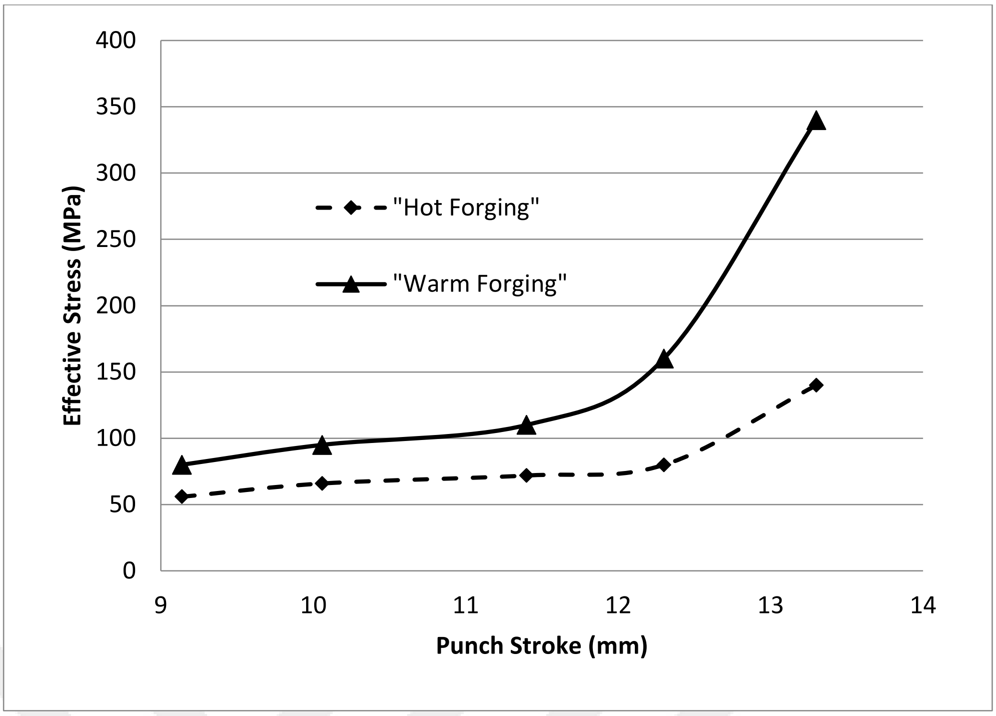

Figure 8.6 Effective stress with respect to punch stroke for warm- and hot-forging.

8.2.6 Tooth Profile Modifications

The gear tooth profile modifications of the forging die calculated by the developed software based on the analyses given in Chapter 6 and the results those obtained from the hot-forging FE simulations are shown in Table 8.2. As it can be seen from the table,

Table 8.2 The gear tooth profile modifications of the forging die

Parameter	Equation No	Calculated (mm)	Determined by FE (mm)
Contraction due to the Interference Fit (U_s)	6.14	-0.153	-0.150
Elastic Deformation (Ue)	6.28	-0.084	-0.075
Under Maximum Forging Load	6.23	0.020	0.025
When Forging Load is Removed	6.25	-0.120	-0.110
After ejection from die	6.27	0.016	0.010
Thermal Die Expansion (U_t)	6.34	0.070	0.072
Due to preheat	6.29	0.010	0.010
Due to preform contact	6.33	0.060	0.062
Thermal Workpiece Contraction (U_c)	6.35	0.059	0.061
AFM finishing allowance	6.40	0.080	0.078*

*measured by CMM

8.3 Results of Experimental, FEA and UBEA for Lead Gear Forging

8.3.1 Forging Load

The load-stroke diagrams obtained from the upper bound analysis (UBEA), the FE and experimental study are shown in Figure 8.7. In the figure, the dashed line shows the experimental results, the continuous line with the point represents the result of rigid die FE analysis and the continuous line shows the results obtained from the upper bound energy analysis. The fact that both curves show similar changes proves the suitability of the upper bound energy analysis presented in this study and the proposed strain regions. As can be seen in Figure 8.7, the upper bound analysis results give higher forging load values than the experimental results, due to the characteristic of the upper bound method. The maximum forging loads were found as 68.8 tonf and experimental 63 tonf for UBEA and experimental study, respectively. In order to stay in the safe zone, the presented UBEA can be recommended for the asymmetric spur gear die design and determination of press capacity. In this analysis, the maximum forging load was determined with a difference of less than 10%. The higher differences in the mid-stroke come from 2D analysis, i.e. barreling effect is neglected. If the barreling effect is included in the analysis (3D analysis), this deviation will be further reduced. With the software developed, solutions can be obtained in a very short time (3 seconds in this analysis).

The Rigid die FE results are in good agreement with the Upper bound energy analysis results. However, FE gives an amount of lower loads through the punch descends, the maximum loads are about the same.

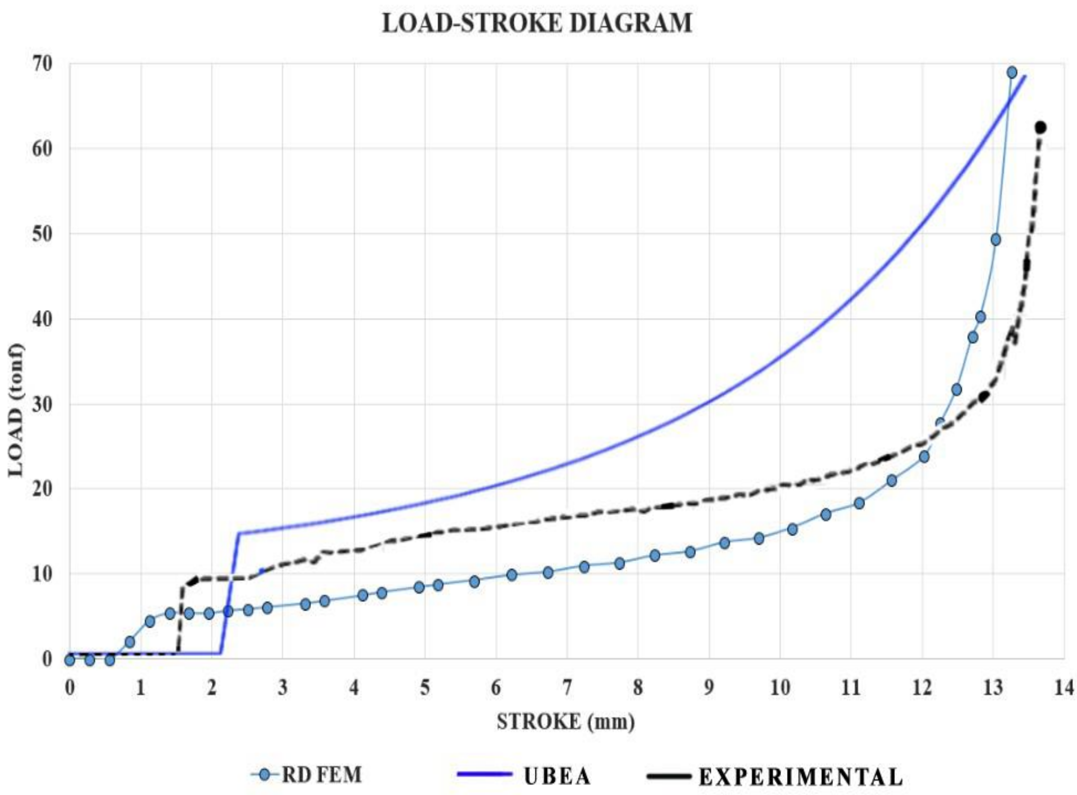

Figure 8.7 Load-Stroke Diagrams of lead forging (UBEA, Experimental and Rigid Die FEM)

8.3.2 Material Flow

The photograph of the experimentally forged asymmetric spur gear is given in Figure 8.8. The section line is the interface of the two halves and some amount of fin formation on the upper surface of the gear is visible. It is a difficult task to completely eliminate the fin formation complete filling is aimed. At the beginning of the forging process gear-shaped punch is fitted to gear-shaped die precisely. When the die subjected to load, die will expand and clearance will occur between die and punch. Thus some material flows in this clearance and fin comes off. The metal flow pattern forging was obtained from the incremental forging tests. After separating the two halves of the forgings, the material flow was revealed step by step and the results are shown in Figure 8.9 and the corresponding load stroke diagram is given in Figure 8.10.

Figure 8.8 Asymmetric spur gear resulting from forging

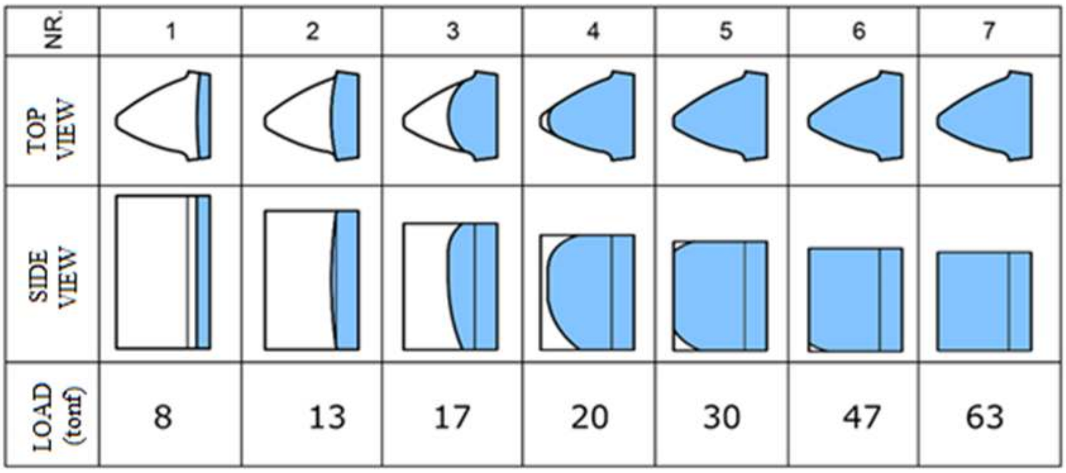

Figure 8.9 Schematic representation of material flow in asymmetric spur gear forging

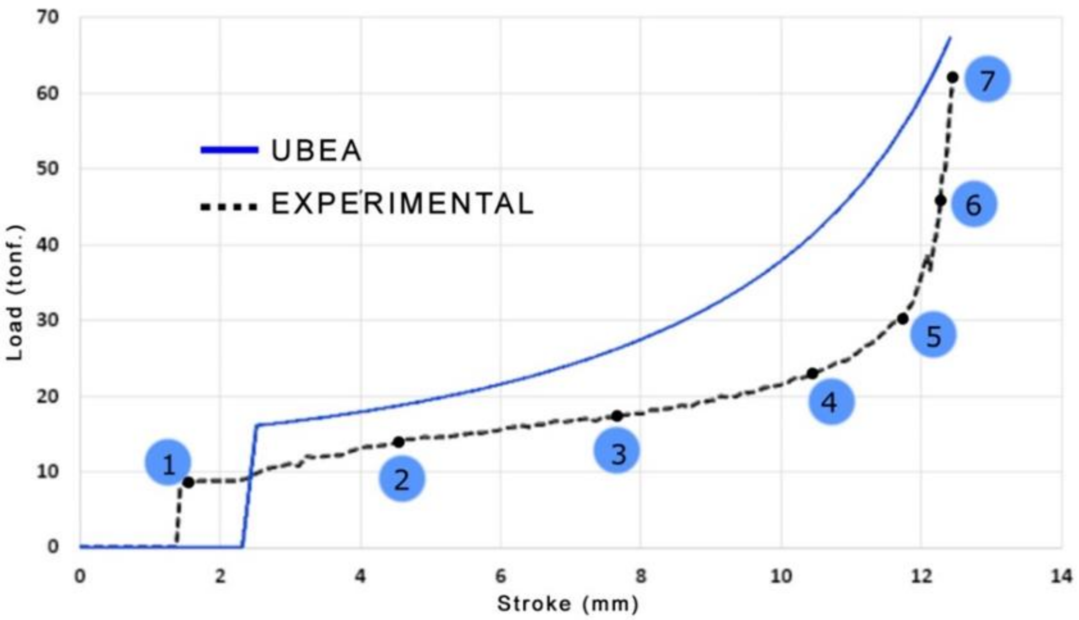

Figure 8.10 The load-stroke diagrams of UBEA and experimental study.

The comparison of the experimental and FE metal flow is given in Figures 8.11 and 8.12, for side and top views of the preform, respectively. Due to uni-directional forging (the upper punch moving and the lower punch stationary), bulging takes place on the upper half of the preform height. So as the upper corners of the die are filling earlier than the bottom corners. The results show that the FE model is successful to predict the metal flow and the forging load; however, slight differences in the images are due to the inevitable deviations of the experimental and simulation conditions

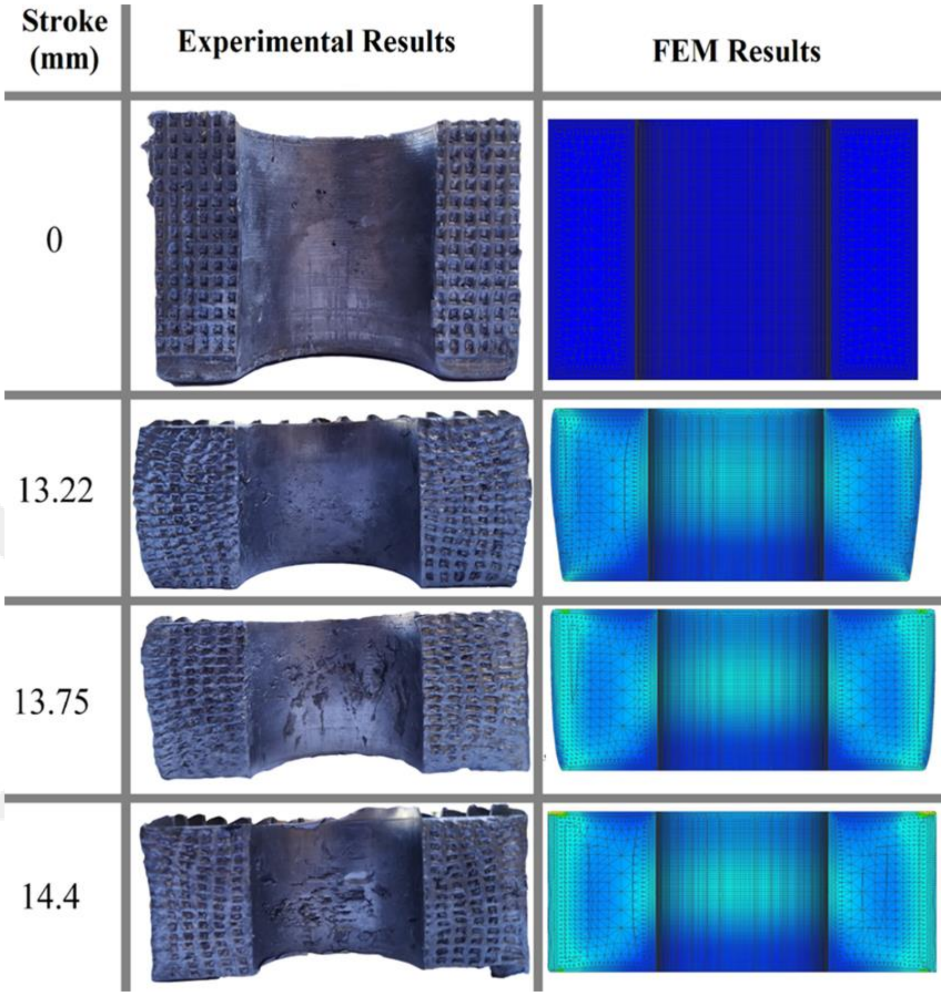

Figure 8.11 Cross sectional view of material flow in finite element and in experimental study.

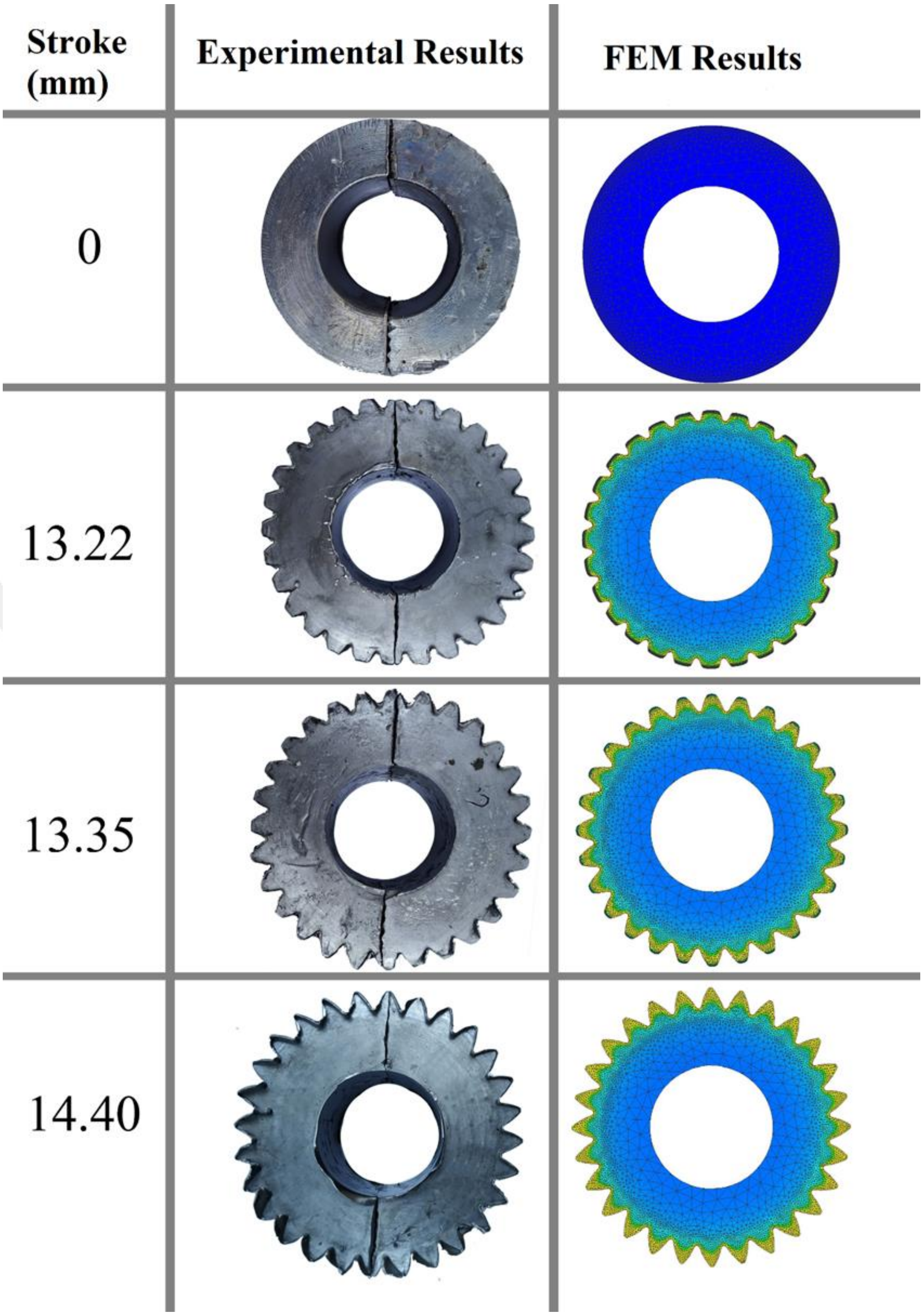

Figure 8.12 Top view of material flow in finite elements and in experimental study.

8.3.3 Comparison of Rigid- and Elastic-Die FE Models

In the classical method in FE forging analysis, the die is assumed as a rigid material while the workpiece is elastoplastic. This makes the modeling of interference between the die and workpiece and computation easier in the analysis. The die stresses are determined by further simulation where the die is assumed as elastic and the inner contact pressure is transferred from the workpiece. Although this approach is easier and requires less computing time, in reality, both the die and the workpiece are elastoplastic. However, the strength of the die is much higher than the workpiece material, the die may be considered as elastic. Therefore, the analysis can be simulated as elastoplastic (die)-elastoplastic (workpiece). In this study, both rigid-elastoplastic and elastoplastic-elastoplastic FE models were simulated and the results were compared. Figure 8.13 shows the dimensional differences of the forged gears between the two models. As can be seen in the figure, the maximum deviation is at the tip radius of the gear tooth and the value is approximately 0.286 mm. In the root radius of gear, the deviation is approximately 0.069 mm.

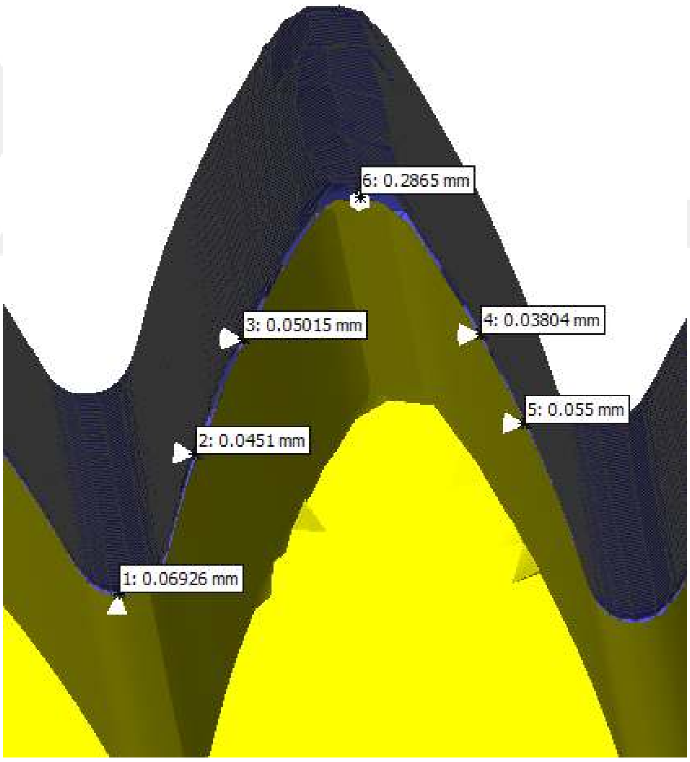

Figure 8.13 Dimensional Differences between Forged Gear in the FEM simulations

The final punch strokes and the corresponding forging loads have differences between the two models. As can be seen in Figure 8.14 and Figure 8.15, the length of punch stroke of the elastoplastic-die model (13.68 mm) is higher than the rigid-die (13.26

mm) one. This is due to the expansion of the die under load for the elastoplastic material property. On the contrary, the corresponding forging load (68.99 tonf) is greater for the rigid-die than the elastoplastic-die model (62.95 tonf.). The reason is the elastic expansion of the die allows the flow of the material with lower forces.

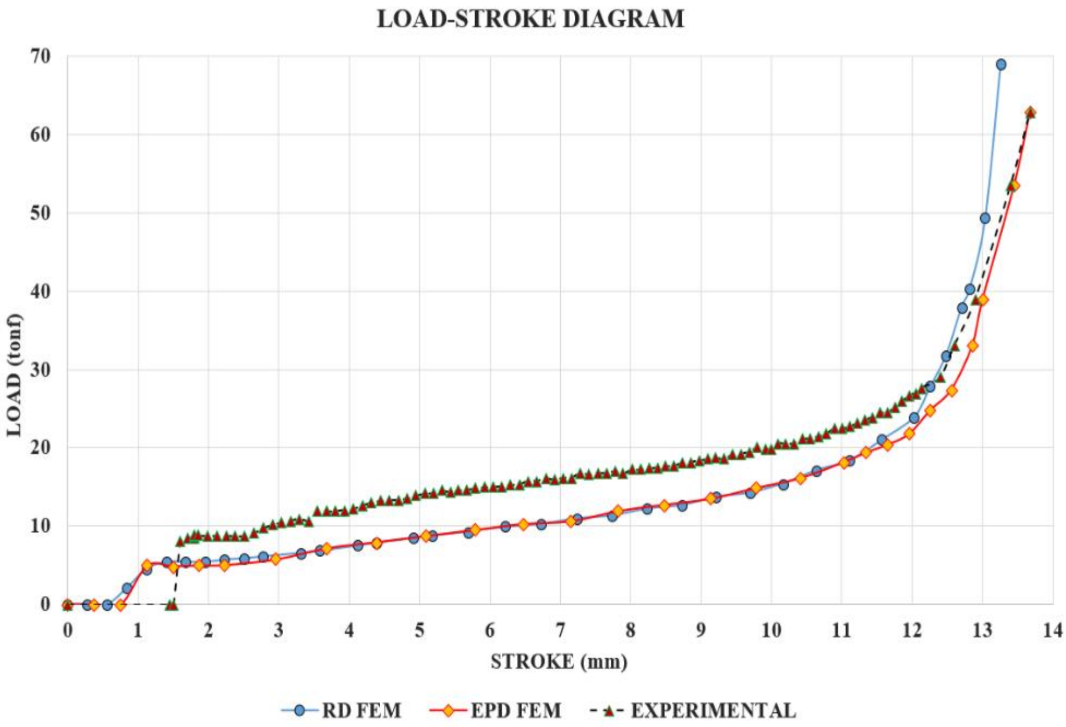

Figure 8.14 The load stroke diagrams for the experimental and the rigid-die and elastoplastic-die FE models.

Figure 8.15 Punch Stroke and Forging Load Differences of the Simulations a) Rigid die b) elastoplastic die

8.3.4 Tooth profile and Surface Roughness Measurements of the Manufactured Die

The design procedure and the tooth profile modifications of the asymmetric spur gear die were explained in chapter 6. After generation of the modified profile, the die profile was cut by WEDM and then finished by AFM. The WEDM as-cut and AFM finished surfaces of the die are shown in Figure 8.16. The surface roughness values are given in Table 8.3. The as-cut surface is uniform and rough; however, the surface after AFM finishing is polished and directionally different in quality. A finer surface was obtained along the Facewidth of the gear (Ra = 0.06 µm) than the transverse direction, i.e. through involute (Ra = 0.5 µm) due to the flow direction of the AFM media. The overall surface roughness is improved by AFM.

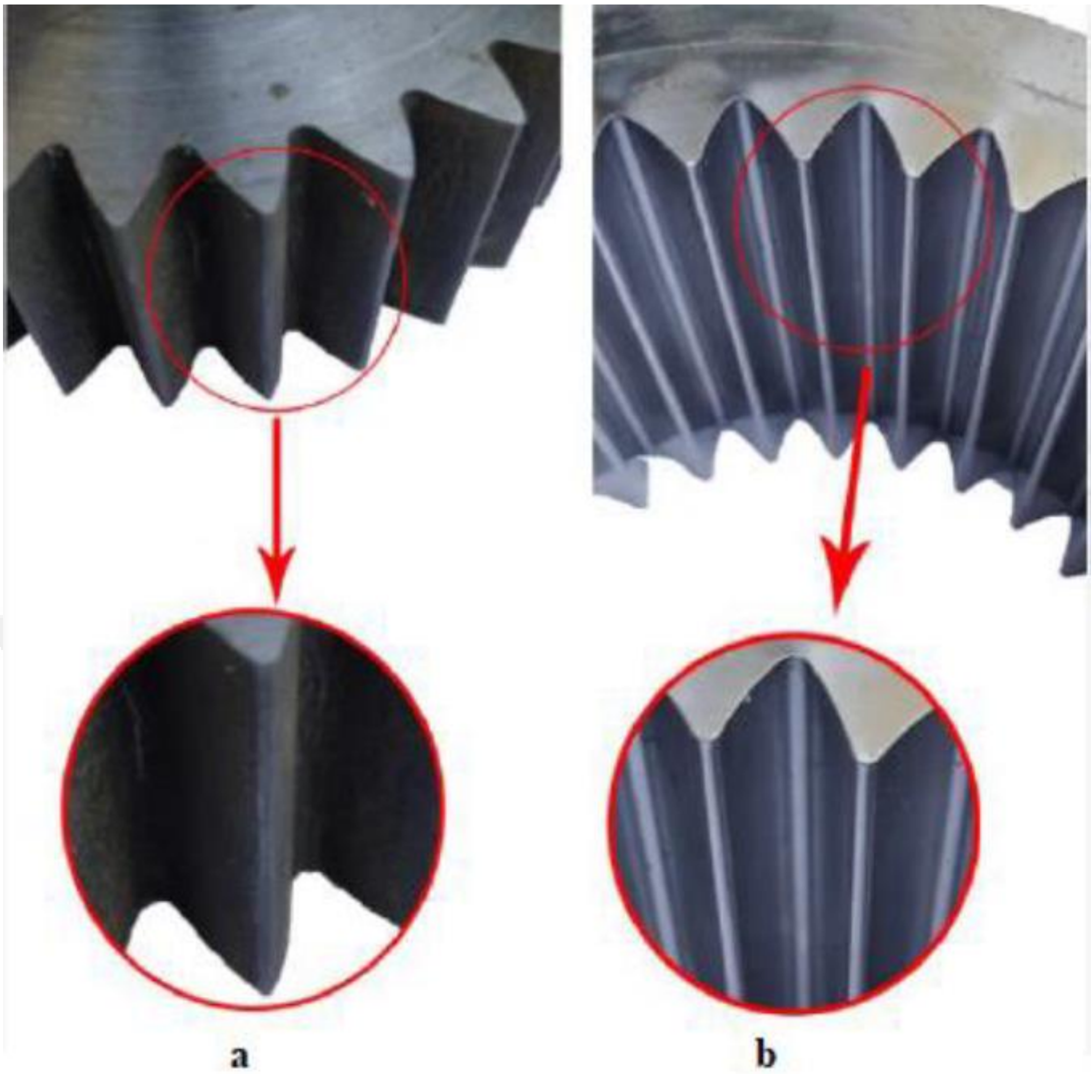

Figure 8.16 Surface Differences (a) As-cut by WEDM (b) Finished by AFM

Table 8.3 Surface roughness measurements of the die.

Surface Parameter	As-cut (after WEDM)		Finished by AFM	
	Along Facewidth	Through involute	Along Facewidth	Through involute
Ra (µm)	3.07	3.03	0.06	0.5
Rz(µm)	18.60	17.48	0.5	1.6

The tooth profile of the forging die was measured by using Leitz Wetzlar optical profilometer and Kemco 3D Coordinate Measuring Machine (CMM). A scaled photo of the tooth of the die obtained from the optical profilometer is given in Figure 8.17. The image taken from the profilometer was transferred to the AutoCAD environment. The deviations of the x- and y-coordinates of the image from the theoretical (calculated) ones are processed in the AutoCAD software package and the deviations from the designed tooth profile were shown in Figure 8.18. The measurements were carried out by using a Kemco 3D Coordinate Measuring Machine (CMM) using a 1 mm radii touch probe of Renishaw for comparison and the scattering of the results are also shown in Figure 8.18. The measured errors of the asymmetric spur gear die are given in Table 8.4.

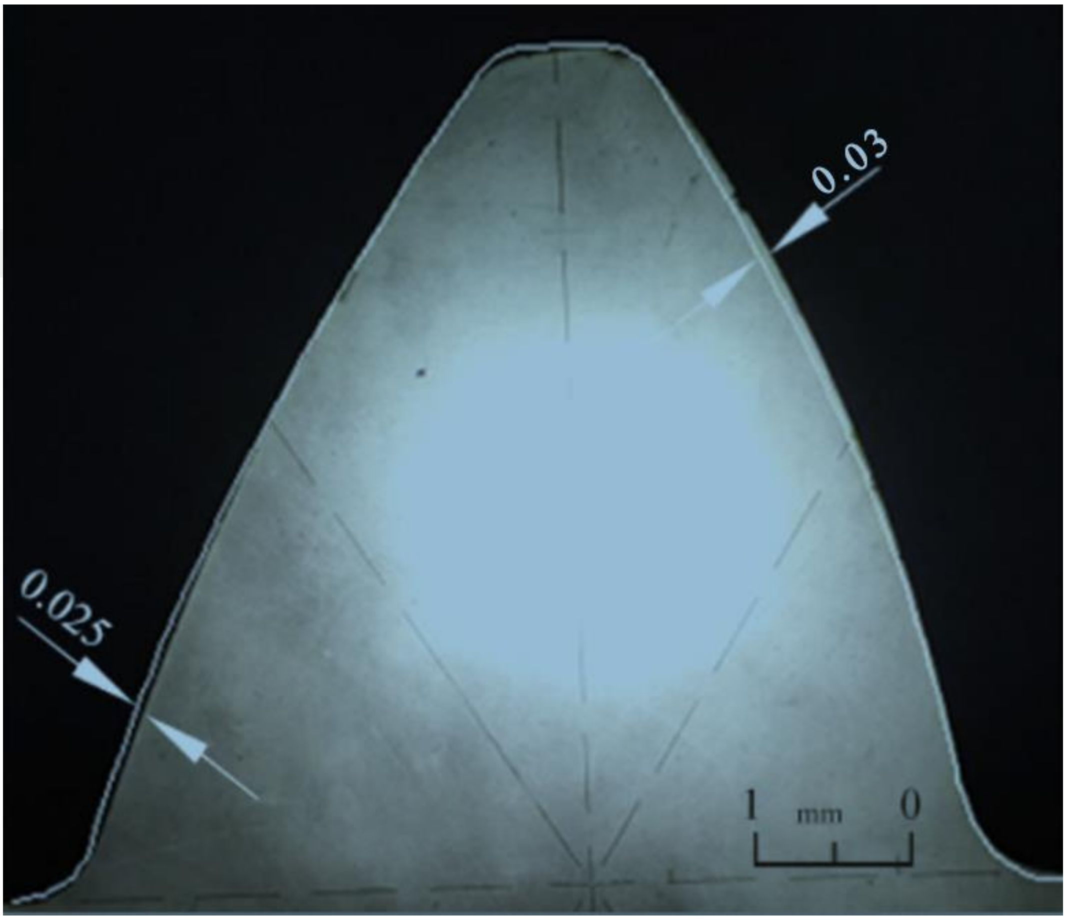

Figure 8.17 Differences of tooth profile of the forging die between scaled and AutoCAD drawing.

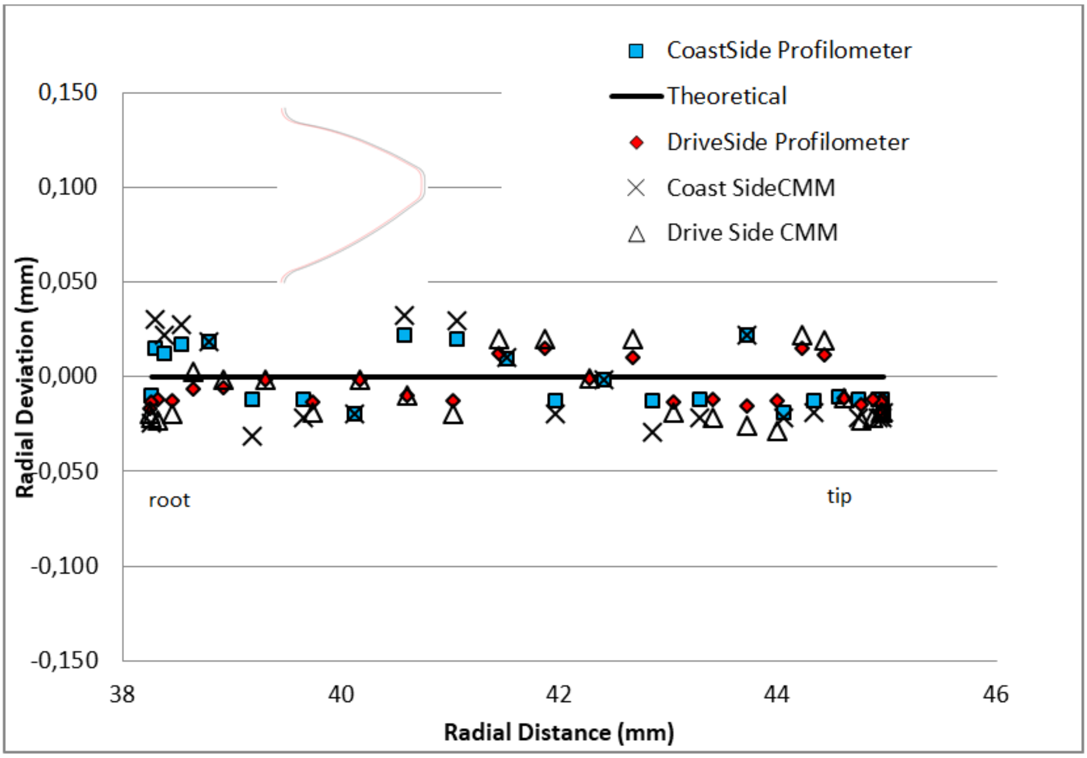

Figure 8.18 Differences between measured and designed tooth profile of the forging die

Table 8.4 Measured errors of the asymmetric spur gear die.

Parameter	Theoretical size (mm)	Measured by CMM (mm)	CMM Deviation from theoretical (mm)
Da	45.16	45.17	0.01
Do	42.16	42.18	0.02
Df	38.40	38.42	0.02
p	9.42	9.43	0.01
h_t	6.78	6.79	0.01

8.3.5 Dimensional Accuracy of Forged Asymmetric Gear

The main goal of this study is to produce an asymmetric spur gear by using the precision forging process. Thus the dimensional accuracy of the forged gear is highly important. The purpose of the pre-determined tooth profile modifications of the asymmetric spur gear forging die is to produce the final gear dimensions of the prototype gear. The tooth profile of the forged gear was measured by using Kemco 3D Coordinate Measuring Machine (CMM) and the results were compared with those obtained from the elastoplastic die forging FE simulations (see Figures 8.19 and 8.20).

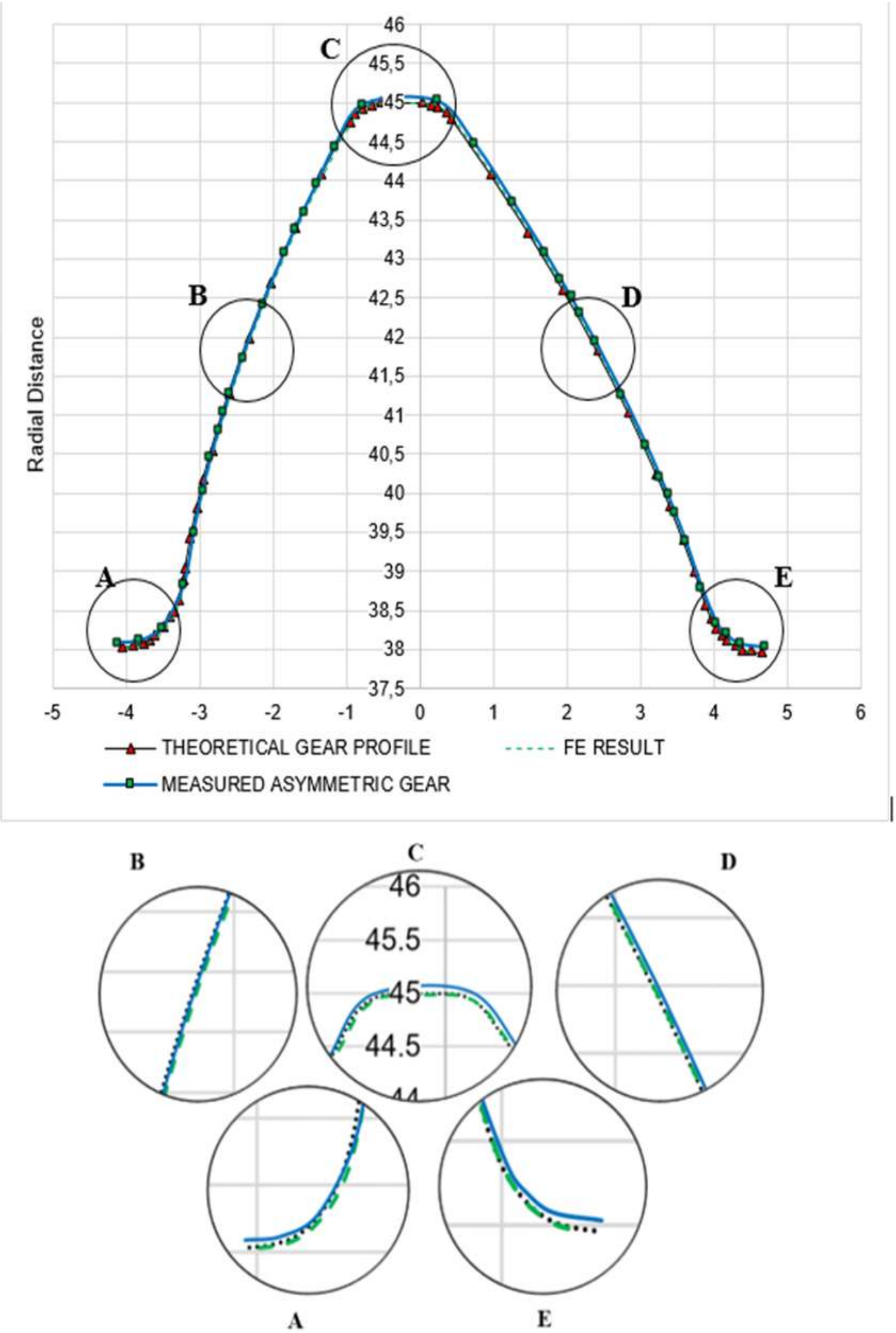

Figure 8.19 Comparison of the theoretical and forged gear tooth profiles

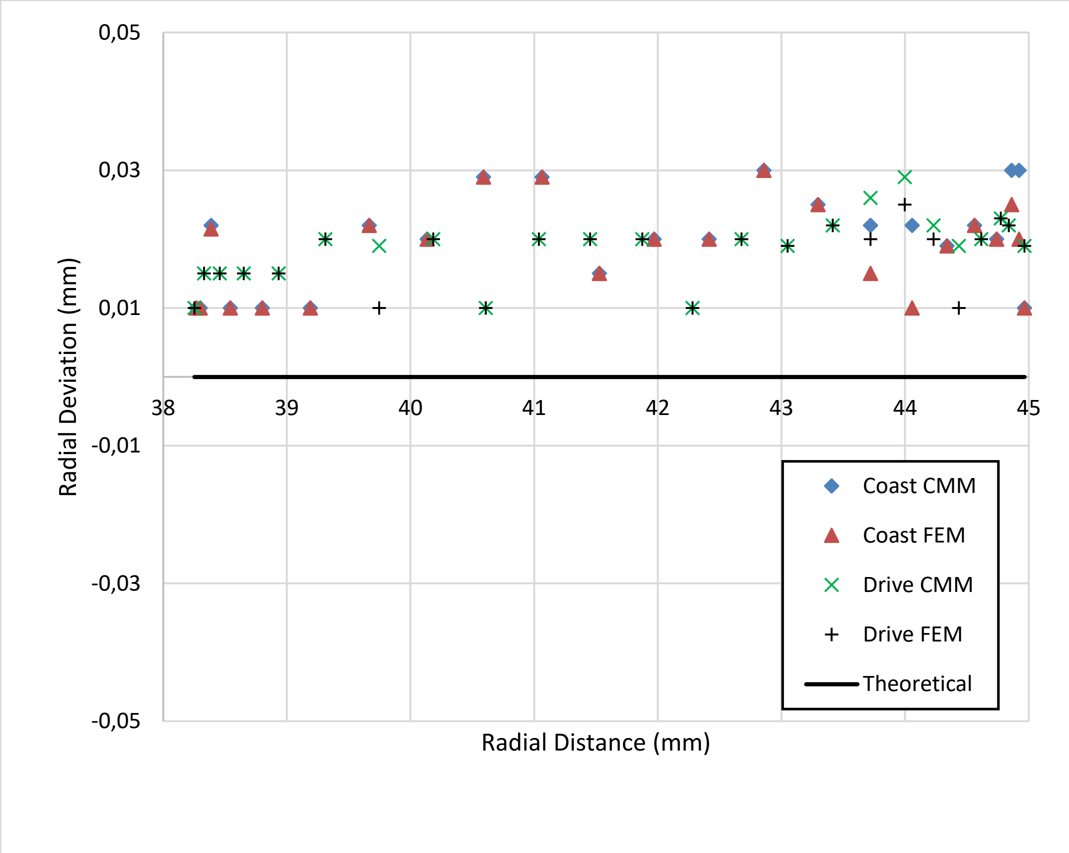

Figure 8.20 Differences between the theoretical and forged gear tooth profiles

The results show that the maximum deviation from the tooth profile is changing between 0.01 and 0.03 mm throughout the tooth length. All of the deviations are positive (i.e. forged gear is bigger than the theoretical), this is purposely given for the final finishing allowance. The deviation of the pitch diameter is 0.015 mm. While the theoretical thickness of the tooth at the pitch diameter is 4.66 mm the tooth thickness at the pitch diameter is approximately 4.69 mm. (Table 8.5).

Table 8.5 Measured errors of the forged asymmetric spur gear

Parameter	Theoretical size (mm)	Measured by CMM (mm)	CMM Deviation from theoretical (mm)
Da	45	45.06	0.06
Do	42	42.015	0.015
Df	38.25	38.275	0.015
p	9.45	9.42	0.02
h_t	6.75	6.785	0.035

8.4 Gear Tooth Quality

The main purpose of the production is to use the product in daily life to facilitate the customer's life. For this reason, the product must meet some standard requirements. In order to evaluate the product, some standards had been determined. Therefore, the product is evaluated according to these standards and if it meets the standards, it can be said that the product is suitable for daily life.

In this section, the asymmetric forged gear was evaluated according to some standards requirements. The criteria of evaluations are;

- Tooth total profile deviation (F_f)
- Tooth profile form deviation (f_f)
- Tooth profile angle deviation ($f_{H\alpha}$)
- Individual pitch deviation (f_p)
- Normal base pitch deviation (f_{pe})
- Pitch error (f_u)
- Total pitch deviations (F_p)

The evaluation will be done in two groups. One is the tooth profile deviations and pitch deviations. Measurement was done from the profile control radius (C_f) to the tip form radius (F_a). The length Lα is the profile evaluation length and gα is the active profile length. Thus Nf is the start point of the active profile.

8.4.1 Gear Tooth Profile Deviations

In this section, tooth total profile, tooth form and tooth profile angle deviations were evaluated. The results can be seen in Table 8.6 and from the Figure 8.21 to Figure 8.26.

Table 8.6 Tooth profile deviation values

Deviations	Coast Side (μm)	Drive Side (μm)
Tooth Total Profile Deviation (F_f)	20	19
Tooth Profile Form Deviation (f_f)	14	12
Tooth Profile Angle Deviation ($f_{H\alpha}$)	20	19

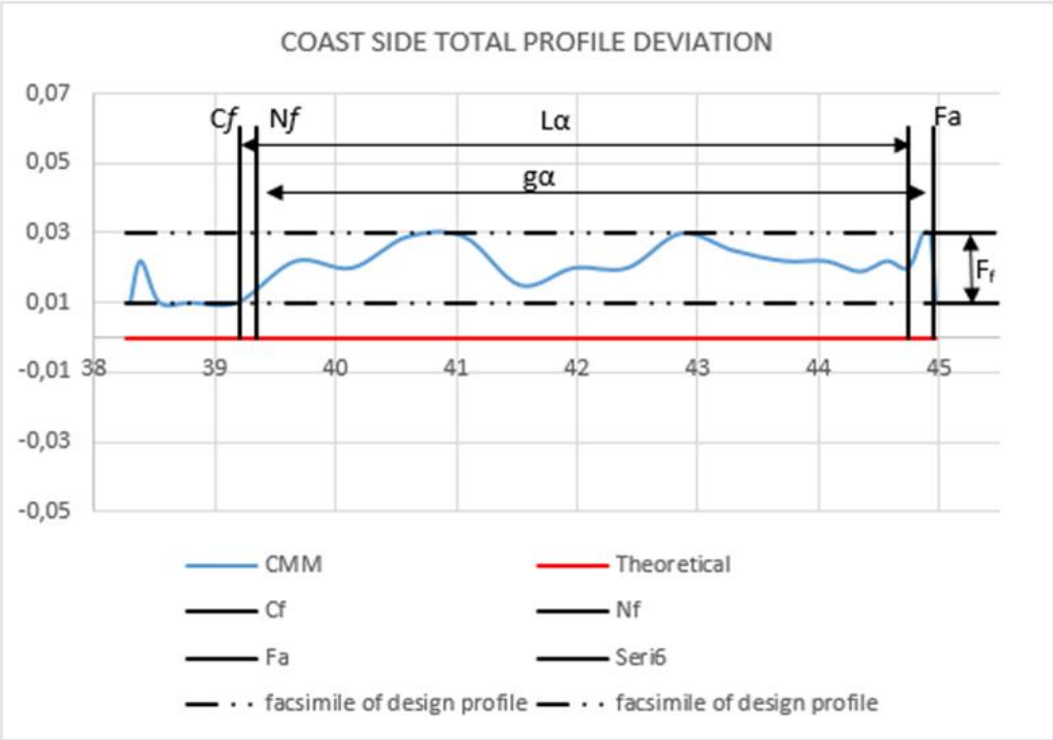

Figure 8.21 Tooth total profile deviation of coast side

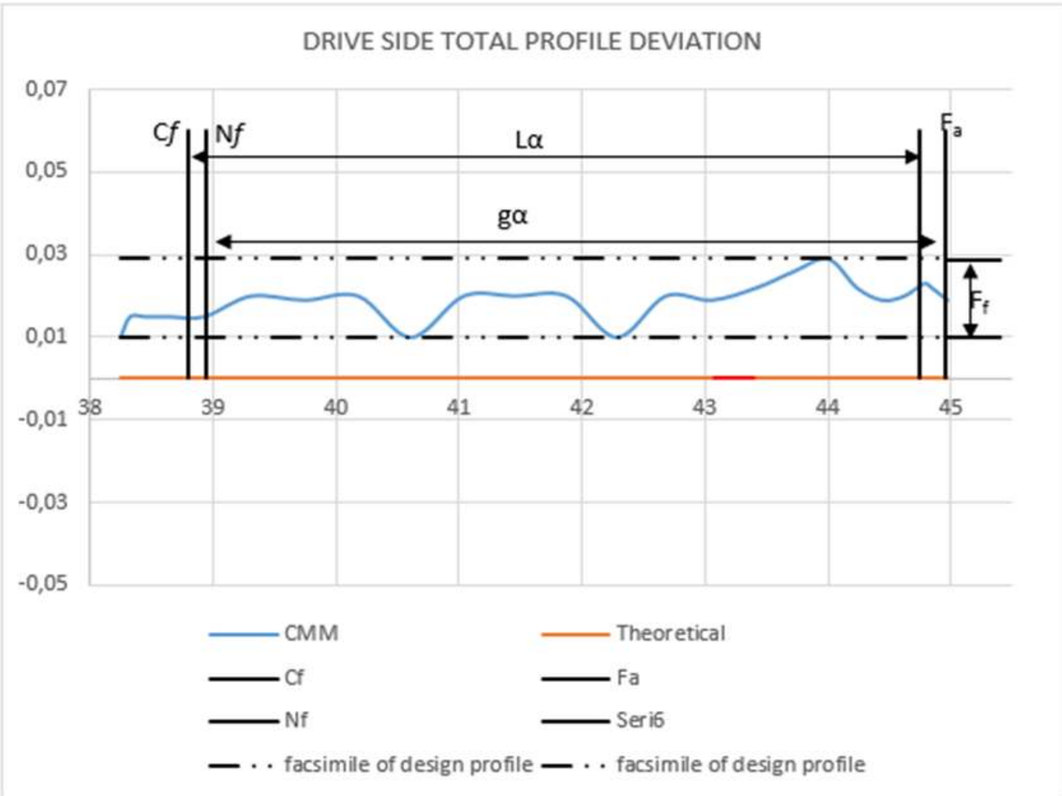

Figure 8.22 Tooth total profile deviation of drive side

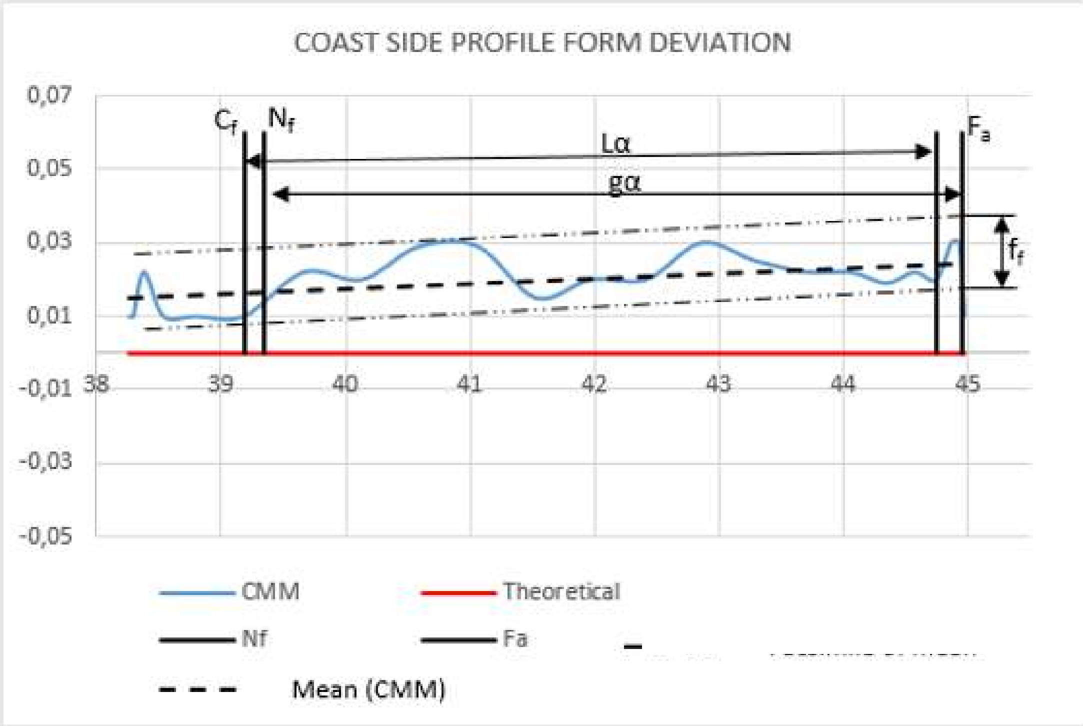

Figure 8.23 Tooth profile form deviation of coast side

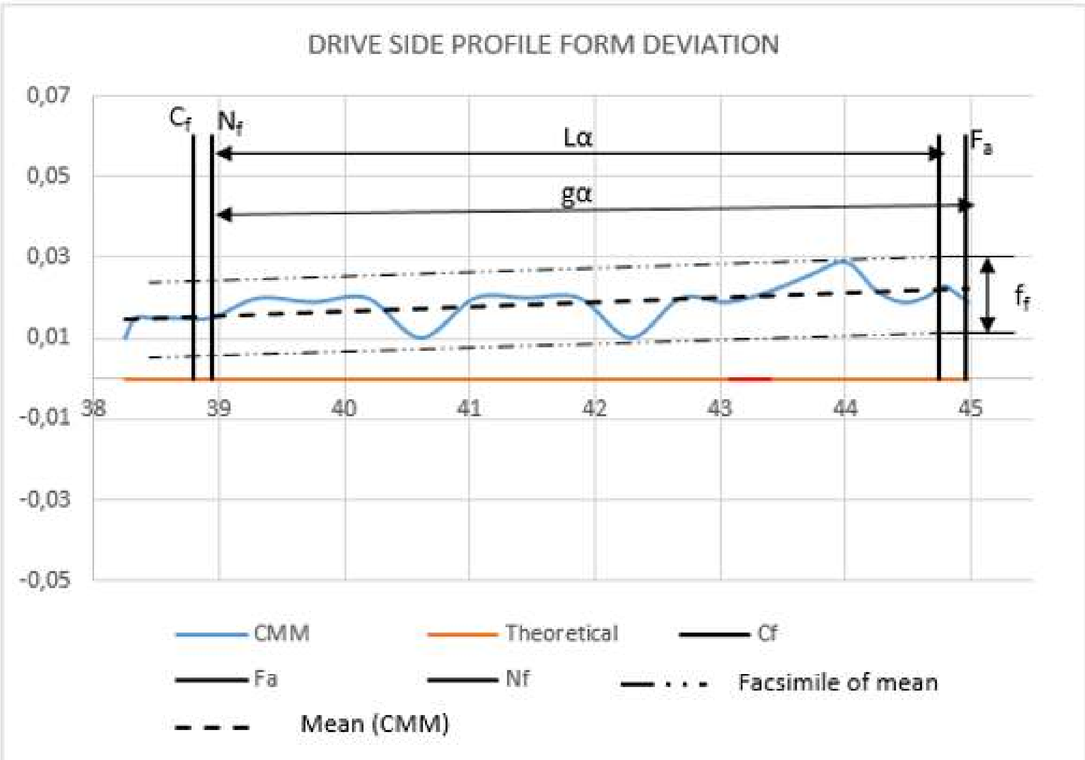

Figure 8.24 Tooth profile form deviation of drive side

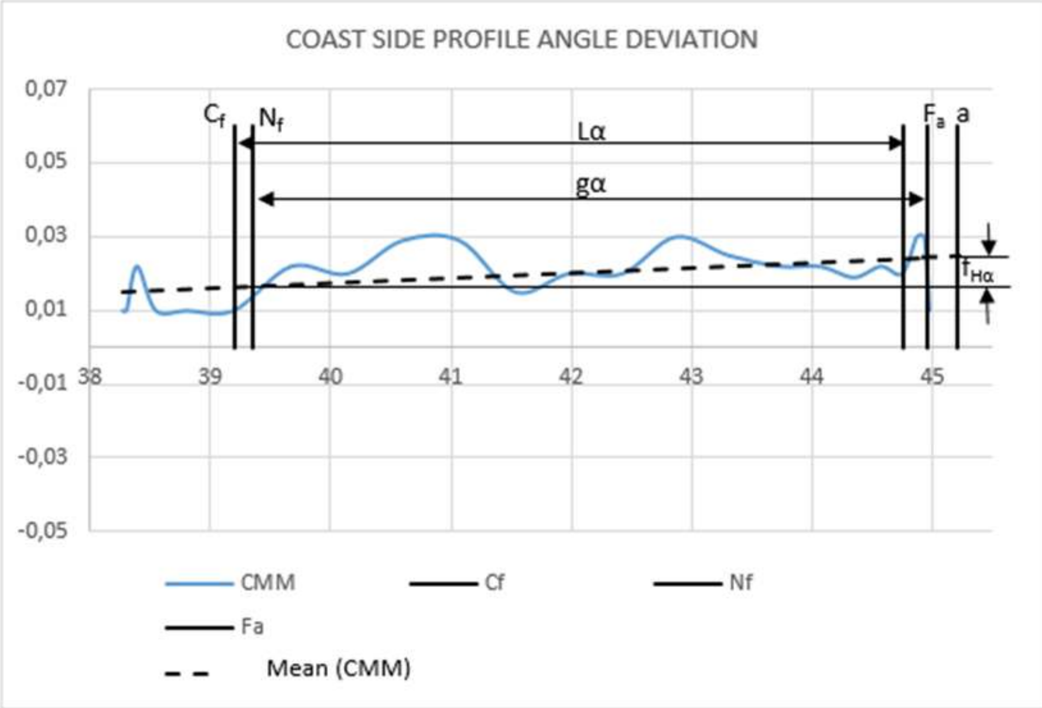

Figure 8.25 Tooth profile angle deviation of coast side

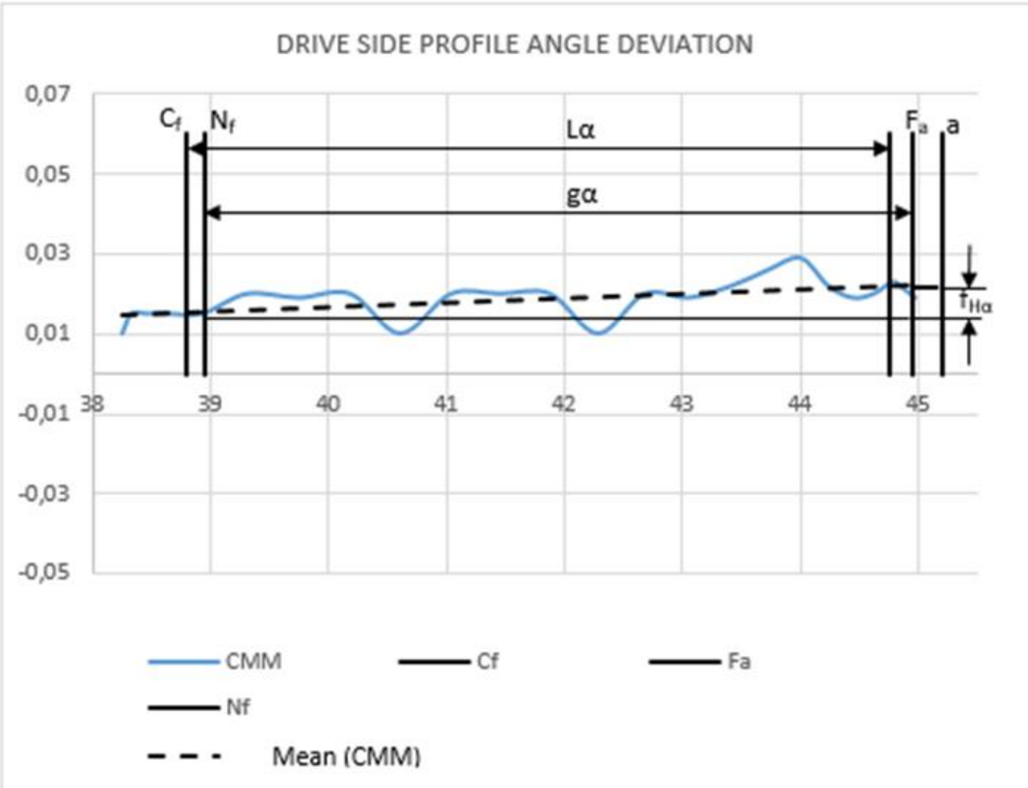

Figure 8.26 Tooth profile angle deviation of drive side

8.4.2 Pitch Deviations

In this section, theoretical, and measured values were given. Deviations between the theoretical and measured values that can be seen in Table 8.7 were evaluated.

Table 8.7 Pitch deviations of the asymmetric forged gear

Deviation Type	Measured Values (mm)	Theoretical Values (mm)	Deviation amount (μm)
Individual pitch deviation (f_p)	9.4405	9.4245	16
Normal base pitch deviation (f_{pe})	8.5842	8.5652	19
Pitch error (f_u)	42,015	42	15
Total pitch deviations (F_p)	37.76	37.698	62

The results of the measurement show that forged asymmetric gear has a gear tooth quality of grade 8 according to DIN 3962 standards (See Figure 8.27). This is a medium quality range and it can be used for general gearboxes (lifting and agricultural machinery) without further finishing. For automobile and turboprop gearbox applications, further finishing processes (i.e. grinding) must be required.

STANDARD	CLASS												
AGMA 390.03 (USA)	15	14	13	12	11	10	9	8	7	6	5	4	3
DIN 3962 (GERMANIA)	1	2	3	4	5	6	7	8	9	10	11	12	
ISO 1328 (ITALIA)	**1**	**2**	**3**	**4**	**5**	**6**	**7**	**8**	**9**	**10**	**11**	**12**	
BS 4 (REGNO UNITO)					A^1	A^2	B	C	D				
3SEIS (FRANCIA)				A	B	C	D	E					
JIS B 1702 (GIAPPONE)				0	1	2	3	4	5	6	7	8	
KS B 1405 (COREA)				0	1	2	3	4	5	6	7	8	

Figure 8.27 Gear quality numbers for AGMA, JIS, ISO and DIN 3962.

CHAPTER 9

CONCLUSIONS, AND RECOMMENDATIONS FOR FUTURE STUDIES

9.1 Introduction

The precision forging of asymmetric spur gear was studied in this thesis. The design criteria for the asymmetric spur gear die design are presented. For this purpose, upper bound analyses (UBEA) and finite elements (FE) simulations of the gear forging process were carried out to determine the forging load and die stresses. The gear tooth profile modifications of the die required for the dimensional accuracy of the forged gear were evaluated. The UBEA and FEA results were compared with the experimental studies.

The following may be concluded from the results of the study.

- The pre-determination of forging load is required for both the die design and the press capacity selection. For the prediction of the forging load for asymmetric spur gear, the presented UBEA and the FE models can be used. The results of the UBEA and FEA are in good agreement with the experimental ones. The software developed for the forging load calculation based on the presented UBEA is a practical tool, the forging load and contact pressures can be calculated in a very short time comparing to the FEM.

- In asymmetric spur gear forging, the variation of the forging load according to the punch position (stroke) can be examined in three different regions. The first zone is the initial zone where the deformation occurs until the billet touches the die surfaces and where the forging load corresponding to the 1 mm movement of the punch is low. The second zone is the zone where the forging load increases relatively linearly with respect to the punch movement, where the tooth profile is filled with radial material flow. In the third zone, the forging load increases rapidly and turns into an asymptotic curve in the last section. In this part, while the part of the gear die that touches the upper punch is completely filled, there are still gaps in the area that sits on the lower punch, and thus the friction load increases and hydrostatic pressure zones occur in the material.

- Although, the maximum forging load calculated by upper bound energy analysis is in agreement with the experimental results (error<10%) the difference with respect to the punch position is higher. In the presented UBEA, the bulging of the preform during forging is neglected to keep the analysis in 2D. The bulging of the preform was observed in the FE and experimental metal flow analyses. The difference between the load stroke diagrams of UBEA and experimental study can be reduced by considering the bulging effect, i.e. 3D UBEA. However, for the maximum forging load predicted by 2D UBEA is slightly higher (< %10) than the experimental one, it is suitable for staying in the safe zone in determining the die design and press capacity.

- The maximum forging load for hot forging is about half of the warm forging, although the forging temperatures are 1200ºC and 800ºC, respectively. Therefore, the forging load and temperature are not linearly changing whereas the trends of the load-stroke curves are similar.

- The results of the rigid-die-elastoplastic-preform and elastoplastic-die-elastoplastic-preform FE models showed that the maximum stroke lengths and forging loads are different for the two models. The forging load that was obtained from rigid-die-elastoplastic-preform FE simulation is higher than the elastoplastic-die model one. The reason is the elastic expansion of the die allows the flow of the material with lower forces. However, the length of the punch stroke of the elastoplastic-die model is higher than the rigid-die one. This is due to the expansion of the die under load for the elastoplastic material property. The experimental results are very close to the elastoplastic-die-elastoplastic-preform FE model. Therefore, elastoplastic-die-elastoplastic-preform FE model is more realistic.

- A single-cylinder die is not enough to withstand the very high stresses due to very high forging loads required in precision gear forging. The strength of the inner die is generally increased by fitting it to one or more outer rings with some amount of interference. In this way, the compressive preload is created on the outer surface of the inner die and this can significantly reduce the tangential tensile stress applied by the forging load to the inner die. A die interference fit by an outer ring can be for the asymmetric spur gear forging and the amount of interference and the dimensions of the die components can be calculated by using the developed software.

- The dimensions of asymmetric spur gear die geometry are affected by the forging loads and temperature and manufacturing deviations. An amount of finishing allowance is also required to produce the final surface quality. Therefore, the effects of these parameters have to be preliminary determined and the die geometry must be corrected accordingly. The presented method for gear tooth modifications and the developed die geometry analysis software can be used for the generation of the corrected tooth path.

- The working temperature is very effective in asymmetric spur gear forging in terms of encountered effective stress, contact pressure, and forging load. The heat is transferred from the preform to the die and environment during forging operation. Although some amount of heat is generated during deformation, the temperature drops by the time pass. The rate of temperature drop is higher for hot forging due to a higher temperature gradient. Cooling of the preform is faster after the punches touch to it. Although the total forging time is less than a second both for hot and warm forging cases, a considerable amount of cooling takes place.

- The study shows that precision forging is a feasible method for the manufacturing of asymmetric spur gears and the method eliminates the limitations of the tooth profile of gear cutting or generation methods. However, the design of the forging die is critical in the success of the process. The design criteria presented in the study can be used successfully.

9.2 Recommendations for Future Work

For the future work about the precision forging process of asymmetric gear, the followings can be recommended.

- Performance analysis of the forged asymmetric gear can be done and can be compared with the performance analysis of the asymmetric one that manufactured by cutting processes.

- Die life of the precision forging of the asymmetric gear can be investigated. Additionally, the economy of the process can be analyzed.

- Precision forging of the asymmetric gear can be performed for different asymmetric gears that have a different module, pressure angles in order to investigate how the module and pressure angle affect the forging load and dimensional accuracy.

- Hot- and warm-precision forging of the asymmetric gear can be done and analyzed for steel as the workpiece material.

REFERENCES

[1] Kapelevich, A. L. (2019). *Asymmetric gearing*. Boca Raton: CRC Press Taylor & Francis Group.

[2] Kapelevich, A. L. (2013). *Direct gear design*. Boca Raton: CRC Press Taylor & Francis Group.

[3] Eyercioglu, O.; Walton, D.; Dean, T. A. (1997). Comparative Bending Fatigue Strength of Precision Forged Spur Gears. *Proceedings of IMechE Part-C Journal of Mechanical Engineering Science* **21(4)** 293-299.

[4] Eyercioglu, O., Dean, T. A., Walton, D. (1994). Dimensional Accuracy of Hot Precision Forged Spur Gears In: Fawcett, J.N. (Ed.). *Proceedings of the International Gearing Conference*. Newcastle Upon Tyne, 285–290.

[5] Eyercioglu, O., Dean, T. A., Walton, D. (1996). Precision Forging of Gears. *7th Int. Machine Design and Production Conference*.

[6] Balambica, V., Deepak, V., Kumar, S. (2019). Design and Efficiency of An Asymmetric Gear. *International Journal of Mechanical and Production Engineering Research and Development*, **9(3),** 223–230.

[7] Kapelevich, A. L., Shekhtman, Y. V. (2019). Optimization of Asymmetric Tooth Root Generated with Protuberance Hob. *Forschung im Ingenieurwesen/Engineering Research*. **83(3),** 627–634.

[8] Mo, S., Ma, S., Jin, G. (2019). Research on Composite Bending Stress of Asymmetric Gear in Consideration of Friction. *Proceedings of the Institution of Mechanical Engineers, Part C: Journal of Mechanical Engineering Science*. **233(8),** 2939–2955.

[9] Shuai, M., Shuai, M., Guang, J. G., Xiang, Y. Z., (2019). Research on Dynamic Load-Sharing Characteristics of Two-Stage Asymmetric Star Gear System. *IEEE Access*, **7**, 126799–126811

[10] Thomas, B., Sankaranarayanasamy, K., Ramachandra, S., Suresh Kumar, S. P. (2019). Power Loss Prediction in Asymmetric Spur Gear Considering Gear Tooth Dynamic Load. *IOP Conference Series: Materials Science and Engineering*, **624(1).**

[11] Prabhu Sekar, R. (2019). Performance Enhancement of Spur Gear Formed Through Asymmetric Tooth. *Proceedings of the Institution of Mechanical Engineers, Part J: Journal of Engineering Tribology*, **233(9)**, 1361–1378.

[12] Abhang, L. B., Dekhane, A. G. (2018). Use of Polylactic Acid (PLA) Material for Asymmetric Spur Gear Manufactured by 3-D Printing. *Springer International Publishing*.

[13] Thomas, B., Sankaranarayanasamy, K., Ramachandra, S., Suresh Kumar, S. P. (2018). Search Method Applied for Gear Tooth Bending Stress Prediction in Normal Contact Ratio Asymmetric Spur Gears. *Proceedings of the Institution of Mechanical Engineers, Part C: Journal of Mechanical Engineering Science.* **232(24),** 4647–4663.

[14] Vaghela, P., Prajapati, J. (2018). Optimization of Tooth Root Profile Using Bezier Curve with G2 Continuity to Reduce Bending Stress of Asymmetric Spur Gear Tooth. *MATEC Web of Conferences.* **237**, 2–7.

[15] Demet, S. M., Ersoyoğlu, A. S. (2018). Fatigue Fracture Behaviour of Asymmetric Spur Gear Tooth under Cyclic Loading. *Procedia Structural Integrity.* **13**, 2030–2035.

[16] Yilmaz, T. G., Doğan, O., Yüce, C., Karpat, F. (2017). Improvement of Loading Capacity of Internal Spur Gear with Using Asymmetric Trochoid Profile. *ASME International Mechanical Engineering Congress and Exposition, Proceedings (IMECE).* **11(2009),** 1–8.

[17] Chen, Y. J., Yang, H. C., Pai, P. F. (2016). Design and Kinematics Evaluation of a Gear Pair with Asymmetric Parabolic Teeth. *Mechanism and Machine Theory*, **101**, 140–157.

[18] Marimuthu, P., Muthuveerappan, G. (2016). Design of Asymmetric Normal Contact Ratio Spur Gear Drive through Direct Design to Enhance the Load Carrying Capacity. *Mechanism and Machine Theory.* **95**, 22–34.

[19] Masuyama, T., Miyazaki, N. (2016). Evaluation of Load Capacity of Gears with an Asymmetric Tooth Profile. *International Journal of Mechanical and Materials Engineering.* **11(1).**

[20] Marimuthu, P., Muthuveerappan, G. (2016). Investigation of Load Carrying Capacity of Asymmetric High Contact Ratio Spur Gear Based on Load Sharing Using Direct Gear Design Approach. *Mechanism and Machine Theory*. **96**. 52–74.

[21] Dharashivkar, N. S., Sondur, V. B., Joshi, K. D. (2016). 3D Photoelastic and Finite Element Analysis of Asymmetric Involute Spur Gear. *International Conference on Electrical, Electronics, and Optimization Techniques, ICEEOT* 2016, 1838–1842.

[22] Cazan, S., Plesu, G. (2016). A Mathematical Approach Regarding a Better Geometry of the Root Fillet of Symmetric and Asymmetric Gears with the Main Scope of Increasing the Fatigue Strength of Gear Teeth and Avoiding the Occurrence of Cracks. *IOP Conference Series: Materials Science and Engineering*. **145(4).**

[23] He Deng, X., Hua, L., Hui Han, X. (2015). Characteristic of Involute Slope Modification of Asymmetric Spur Gear. *Journal of Central South University*, **22(5),** 1676–1684.

[24] Prabhu Sekar, R., Muthuveerappan, G. (2015). Estimation of Tooth Form Factor for Normal Contact Ratio Asymmetric Spur Gear Tooth. *Mechanism and Machine Theory*. **90**, 187–218.

[25] Kargin, P. A. (2015). Prospects for Involute Transmissions with Asymmetric Tooth Profiles. *Russian Engineering Research.* **35(1),** 3–7.

[26] Deng X., Hua, L., Han, X. (2015). Research on the Design and Modification of Asymmetric Spur Gear. *Mathematical Problems in Engineering*, **2015**.

[27] Banica, M., Ravai-Nagy, S. (2015). Manufacturing Precision on the Numeric Simulation of Spur Gear with Asymmetric Teeth. *Applied Mechanics and Materials* **809–810**, 772–777.

[28] Olguner, S., Filiz, İ. H. (2014). A study on the Design of Asymmetric Spur Gears in Gear Pump Applications. *International Gear Conference 2014: 26th–28th August 2014*, Lyon, **l,** 406–417.

[29] Sekar, R. P., Muthuveerappan, G. (2014). Load Sharing Based Maximum Fillet Stress Analysis of Asymmetric Helical Gears Designed Through Direct Design - A Parametric Study. *Mechanism and Machine Theory*. **80**, 84–102.

[30] Marimuthu, P., Muthuveerappan, G. (2014). Optimum Profile Shift Estimation on Direct Design Asymmetric Normal and High Contact Ratio Spur Gears Based on Load Sharing. *Procedia Engineering*. **86**, 709–717.

[31] Kapelevich, A. L. (2014). Pitch Factor Analysis for Symmetric and Asymmetric Tooth Gears. *International Gear Conference 2014*: *26th–28th August 2014*, Lyon, 284–293.

[32] Marimuthu, P., Muthuveerappan, G. (2014). Effect of Drive Side Contact Ratio on Direct Design Asymmetric High Contact Ratio Spur Gear Based on Load Sharing. *Applied Mechanics and Materials.* **592–594**, 2292–2296.

[33] Zhao, N., Zhang, M. Q., Guo, H. (2014). Stress Analysis of Asymmetric Spur Face-Gear Pair Based on Finite Element Method. *Applied Mechanics and Materials* **483**, 309–314.

[34] Marimuthu, P., Muthuveerappan, G. (2014). Influence of Pressure Angle on Load Sharing Based Stresses in Asymmetric Normal Contact Ratio Spur Gear Drives. *Applied Mechanics and Materials*, **465–466**, 1229–1233.

[35] Deng, X. H., Cai, J. (2014). The Contact Stress Analysis on Involute Slope Modification of Asymmetric Spur Gear. *Advanced Materials Research*. **926–930**, 1436–1439.

[36] Karpat, F., Dogan, O., Ekwaro-Osire, S., Yuce, C. (2014). A Novel Method for Calculation Gear Tooth Stiffness for Dynamic Analysis of Spur Gears with

Asymmetric Teeth. *ASME International Mechanical Engineering Congress and Exposition, Proceedings (IMECE)*. **4A**, 1–8.

[37] Ning, L., Li, W. (2012). Research on Meshing Theory of Involute Helical Gear with Asymmetric. *Advanced Materials Research*. **383–390**, 2838–2844.

[38] Liming, L., Guimin, L. (2012). Dynamic Simulation Analysis of Asymmetric Involute Gear Drive System. *Applied Mechanics and Materials*. **215–216**, 974–977.

[39] Sandooja, A., Jadhav, S. (2012). Analysis of Gear Geometry and Durability with Asymmetric Pressure Angle. *SAE International Journal of Commercial Vehicles*. **5(2),** 546–558.

[40] Agrawal, S., Himte, R. L. (2012). Evaluation of Bending Stress at Fillet Region of an Asymmetric Gear with a Hole as Stress Relieving Feature using a Fea Software Ansys. *International Journal of Computer Applications* **51(8),** 28–33.

[41] Alipiev, O. (2011). Geometric Design of Involute Spur Gear Drives with Symmetric and Asymmetric Teeth Using the Realized Potential Method. *Mechanism and Machine Theory*. **46(1),** 10–32.

[42] Kargin, P. A. (2011). Transition Curve of Involute Gear Teeth with Asymmetric Profiles. *Russian Engineering Research.* **31(3),** 200–202.

[43] Li, N., Li, W., Liu, N., Liu, H. (2011). Analytical Method on Contact Stress of Helical Gear with Asymmetric Involutes. *Advanced Materials Research.* **321**, 157–160.

[44] Liu, Y., Fan, J. (2011). Design of Asymmetric Double Circular Arc Gear for Large-Scale High-Pressure Gear Pumps. *Advanced Materials Research*. **181–182**, 361–365.

[45] Pedersen, N. L. (2010). Improving Bending Stress in Spur Gears Using Asymmetric Gears and Shape Optimization. *Mechanism and Machine Theory.* **45(11)**, 1707–1720.

[46] Kargin, P. A. (2009). Application, Synthesis, and Manufacture of Involute Gear Transmissions with Asymmetric Gear Profiles. *Russian Engineering Research*, **29**(11), 1073–1077.

[47] Costopoulos, T., Spitas, V. (2009). Reduction of Gear Fillet Stresses by Using One-Sided Involute Asymmetric Teeth. *Mechanism and Machine* Theory, **44(8),** 1524–1534.

[48] Kumar, P., Kommogi, R. K., Senthilvelan, S. (2009). Injection Molded Asymmetric Spur Gear Development and Preliminary Performance Evaluation. *International Journal of Plastics Technology*, **13(2),** 186–192.

[49] Muni, D. V., Muthuveerappan, G. (2009). A Comprehensive Study on the Asymmetric Internal Spur Gear Drives Through Direct and Conventional Gear Design. *Mechanics Based Design of Structures and Machines*. **37(4),** 431–461.

[50] Spitas, V., Spitas, C., Costopoulos, T. (2009). Reduction of Tooth Fillet Stresses Using Novel One-Sided Involute Asymmetric Gear Design. *Mechanics Based Design of Structures and Machines*, **37(2),** 157–182.

[51] Senthil Kumar, V. D., Muni, V., Muthuveerappan, G. (2008). Optimization of Asymmetric Spur Gear Drives to Improve the Bending Load Capacity. *Mechanism and Machine Theory.* **43(7),** 829–858.

[52] Karpat, F., Ekwaro-Osire, S., Khandaker, M. P. H. (2008). Probabilistic Analysis of MEMS Asymmetric Gear Tooth. *Journal of Mechanical Design, Transactions of the ASME*. **130(4),** 1–6.

[53] Yang, S. C. (2007). Study on an Internal Gear with Asymmetric Involute Teeth. *Mechanism and Machine Theory*, **42(8),** 977–994.

[54] Di Francesco, G., Marini, S. (2007). Asymmetric Teeth: Bending Stress Calculation. *Gear Technology.* **24(2),** 52–55.

[55] Muni, D. V., Kumar, V. S., Muthuveerappan, G. (2007). Optimization of Asymmetric Spur Gear Drives for Maximum Bending Strength Using Direct Gear Design Method. *Mechanics Based Design of Structures and Machines.* **35(2),** 127–145.

[56] Karpat, F., Ekwaro-Osire, S., Khandaker, M. P. H. (2006). Probabilistic Analysis of MEMS Asymmetric Gear Tooth. *American Society of Mechanical Engineers, Design Engineering Division (Publication) DE*, pp. 2–7.

[57] Yang, S. C. (2005). Mathematical Model of a Helical Gear with Asymmetric Involute Teeth and Its Analysis. *International Journal of Advanced Manufacturing Technology*. **26(5–6),** 448–456.

[58] Litvin, F. L., Fuentes, A., Howkins, M. (2001). Design, Generation and TCA of New Type of Asymmetric Face-Gear Drive with Modified Geometry. *Computer Methods in Applied Mechanics and Engineering*. **190(43–44)**, 5837–5865.

[59] Kapelevich, A. (2000). Geometry and Design of Involute Spur Gears with Asymmetric Teeth. *Mechanism and Machine Theory*. **35(1),** 117–130.

[60] Ravai Nagy, S., Lobontiu, M. (2014). Expanding Research in the Field of Asymmetric Gear Design and Manufacturing. *Applied Mechanics and Materials* **657**, 504-508

[61] Ravai Nagy, S., Lobontiu, M. (2010). Manufacture of Gears with Asymmetric Teeth On CNC Machine Tools. *Annals of the Oradea University. Fascicle of Management and Technological Engineering*, Volume **IX (XIX)**.

[62] Qi, Y., Du, Z., Sun, H., Chen, L., Wang, C. (2017). Study on Warm Forging Process of 45 Steel Asymmetric Gear. *IOP Conference Series: Materials Science and Engineering*. **230(1).**

[63] Dang, Y., Deng, X., Wang, B. (2014). Elastic-plastic Numerical Simulation of Cold Rotary Forging for Hypoid Gear and the Springback Error. *Applied Mechanics and Materials*. **633–634**, 826–831.

[64] Samołyk, G. (2013). Investigation of the Cold Orbital Forging Process of an AlMgSi Alloy Bevel Gear. *Journal of Materials Processing Technology*, **213(10),** 1692–1702.

[65] Feng, W., Cao, J. C., Wu, S. T., Li, Y. F. (2013). Prediction of Forming Load for the Helical Gear Precision Forging by BP Neural Network. *Advanced Materials Research*. **823**, 170–174.

[66] Feng, W., Hua, L., Han, X. (2012). Finite Element Analysis and Simulation for Cold Precision Forging of a Helical Gear. *Journal of Central South University*. **19(12),** 3369–3377.

[67] Cai, G. P., Zhao, X. H., Su, H. T. (2012).The Finite Element Simulation Used in Straight Tooth Bevel Gear's Vibration Rotary Forging. *Advanced Materials Research*. **430–432**, 1716–1720.

[68] Deng, X., Hua, L., Han, X., Song, Y. (2011). Numerical and Experimental Investigation of Cold Rotary Forging of a 20CrMnTi Alloy Spur Bevel Gear. *Materials and Design.* **32(3),** 1376–1389.

[69] Khalilpourazary, S., Dadvand, A., Azdast, T., Sadeghi, M. H. (2011). Design and Manufacturing of a Straight Bevel Gear in Hot Precision Forging Process Using Finite Volume Method and CAD/CAE Technology. *International Journal of Advanced Manufacturing Technology*. **56(1–4),** 87–95.

[70] Wei, F., Lin, H. (2011). Multi-objective Optimization of Process Parameters for the Helical Gear Precision Forging by Using Taguchi Method. *Journal of Mechanical Science and Technology.* **25(6),** 1519–1527.

[71] Zhao, J., Yi, J., Luo, S. (2011). Study on the Rules and Effects of Wear on Die Service Life in Steel Synchronizer Gear Ring Forging Process. *Advanced Materials Research.* **291–294**, 668–671.

[72] Li, L. (2011). Numerical Simulation and Technology Research on the Precision Forging for Inner Ring Gear. *Applied Mechanics and Materials*. **88–89**, 29–33.

[73] Yang, C., Zhao, S. (2011). Effect of Floating Die on Tooth Filling of Spur Gear Forging. *Advanced Materials Research*, **295–297**, 1631–1634.

[74] Chang, C. C., Kuo, W. L. (2010). Effects of Temperature and Grain Refinement on the Closed-Die Forging of a Micro Gear. *Proceedings of the*

Institution of Mechanical Engineers, Part B: Journal of Engineering Manufacture. **224(11),** 1767–1773.

[75] Hu, C. L., Liu, Q. K., Zhao, Z., Chen, J., Wu, G. M. (2010). Two Step Forging Process of Spur Gear Based on Rigid Parallel Motion. *Journal of Shanghai Jiaotong University (Science)*. **15(2),** 241–244.

[76] Wang, P., Li, L., Wang, B., Yi, L. (2010). Numerical Simulation and Analysis of Forging Process for Automotive Starter Motor Ring Gear. *Proceedings - 2010 International Conference on System Science, Engineering Design and Manufacturing Informatization, ICSEM 2010*, **2**, 296–298.

[77] Zhang, Q., Cui, H., Wang, Y. (2010). Process Design for Cold Precision Forging of Bevel Gear. *Proceedings - 2010 International Conference on Digital Manufacturing and Automation, ICDMA 2010*, **2**, 114–116.

[78] Ji, D. S., Wang, X. Y., Deng, L., Xia, J. C. (2010). Closed Hot Precision Forging Process of a Bevel Gear with Large Cone Angle. *Advanced Materials Research*. **154–155**, 143–146.

[79] Debin, S., Jie, X., Chunju, W., Bin, G. (2009). Hybrid Forging Processes of Micro-double Gear Using Micro-forming Technology. *International Journal of Advanced Manufacturing Technology*. **44(3–4),** 238–243.

[80] Eyercioglu, O., Kutuk, M. A., Yilmaz, N. F. (2009). Shrink Fit Design for Precision Gear Forging Dies. *Journal of Materials Processing Technology*, **209(4),** 2186–2194.

[81] Liu, J., Cui, Z. (2009) Hot Forging Process Design and Parameters Determination of Magnesium Alloy AZ31B Spur Bevel Gear. *Journal of Materials Processing Technology.* **209(18–19),** 5871–5880.

[82] Kim, S. Y., Kubota, S., Yamanaka, M. (2008). Application of CAE in Cold Forging and Heat Treatment Processes for Manufacturing of Precision Helical Gear Part. *Journal of Materials Processing Technology*, **201(1–3),** 25–31.

[83] Chen, X., Jung, D. (2008). Gear Hot Forging Process Robust Design Based on Finite Element Method. *Journal of Mechanical Science and Technology*, **22(9),** 1772–1778.

[84] Irani, M., Taheri, A. K. (2008). Effect of Forging Temperature on Homogeneity of Microstructure and Hardness of Precision Forged Steel Spur Gear. *Materials Chemistry and Physics.* **112(3),** 1099–1105.

[85] Song, J. H., Im, Y. T. (2007). Process Design for Closed-Die Forging of Bevel Gear by Finite Element Analyses. *Journal of Materials Processing Technology.* **192–193(10),** 1–7.

[86] Yang, T. S., Hwang, N. C., Chang, S. Y. (2007). The Prediction of Maximum Forging Load and Effective Stress for Different Material of Bevel Gear Forging. *Journal of Mechanical Science and Technology.* **21(10),** 1566–1572,.

[87] Sheu, J. J., Yu, C. H. (2007). The Cold Orbital Forging Die and Process Design of a Hollow-Ring Gear Part. *Proceedings of the 35th International MATADOR 2007 Conference*, 110–114.

[88] Skunca, M., Skakun, P., Keran, Z., Sidjanin, L., Math, M. D. (2006). Relations Between Numerical Simulation and Experiment in Closed Die Forging of a Gear. *Journal of Materials Processing Technology.* **177(1–3),** 256–260.

[89] Zhang, Z., Xie, J. (2006). A Numerical Simulation of Super-plastic Die Forging Process for Zr-Based Bulk Metallic Glass Spur Gear. *Materials Science and Engineering A*. **433(1–2),** 323–328.

[90] Yang, T. S., Hsu, Y. C., (2006). Application of Abductive Network and FEM to Predict the Maximum Forging Force and the Final Face Width of Spur Gear. *Materials Science Forum*, **532–533**, 861–864.

[91] Yang, T. S., Hsu, Y. C. (2006). A Finite Element Analysis for the Forging Process of Hollow Spur Gear. *Materials Science Forum*, **505–507(2),** 733–738.

[92] Kang, G. J., Song, W. J., Kim, J., Kang, B. S., Park, H. J. (2005). Numerical Approach to Forging Process of a Gear with Inner Cam Profile Using FEM. *Journal of Materials Processing Technology.* **164–165**, 1212–1217.

[93] Kutuk, M. A., Eyercioglu, O., Yildirim, N., Akpolat, A. (2003). Finite Element Analysis of a Cylindrical Approach for Shrink-fit Precision Gear Forging Dies. *Proceedings of the Institution of Mechanical Engineers, Part C: Journal of Mechanical Engineering Science*. **217(6),** 677–686.

[94] Hsu, H. H. (2002). A Study on Precision Forging of Spur Gear Forms and Spline by the Upper Bound Method. *International Journal of Mechanical Sciences*. **44(8),** 1543–1558.

[95] Chitkara, N. R., Kim, Y. J. (2001). Near-net Shape Forging of a Crown Gear: Some Experimental Results and an Analysis. *International Journal of Machine Tools and Manufacture.* **41(3),** 325–346.

[96] Lee, Y. K., Lee, S. R., Lee, C. H., Yang, D. Y. (2001). Process Modification of Bevel Gear Forging Using Three-dimensional Finite Element Analysis. *Journal of Materials Processing Technology.* **113(1–3),** 59–63.

[97] Kim, Y. J., Chitkara, N. R. (2001). Determination of Preform Shape to Improve Dimensional Accuracy of the Forged Crown Gear Form in a Closed-Die Forging Process. *International Journal of Mechanical Sciences.* **43(3),** 853–870.

[98] Radzevich, S. P. (2012). *Dudley's handbook of practical gear design and manufacture*. Boca Raton: CRC Press Taylor & Francis Group.

[99] Carnegie Mellon University. School of Computer Science Available at Https://www.cs.cmu.edu/~rapidproto/mechanisms/chpt7.html. Accessed 20.07.2020

[100] Nisbett, J. G., Budynas R.G. (2006). *Shigley's mechanical engineering design*. Eighth Edi. McGraw−Hill Primis: USA.

[101] Lynwander P., (1983). *Gear drive systems design and application*. New York: Marcel Dekker, Inc: USA.

[102] Olguner,S. (2014) *A study on the design of asymmetric gears for application in gear pumps*. M.sc thesis, University of Gaziantep.

[103] Kapelevich, A. L. (2016). Direct Gear Design for Asymmetric Tooth Gears. *Mechanisms and Machine Science*. **34**, 381–392.

[104] Novikov, A. S., Paikin, A. G., Dorofeyev, V. L., Ananiev, V. M., Kapelevich, A. L. (2008). Application of Gears with Asymmetric Teeth in Turboprop Engine Gearbox. *2007 Proceedings of the ASME International Design Engineering Technical Conferences and Computers and Information in Engineering Conference, DETC2007.* **7,** no. February, 327–334.

[105] Eyercioglu, O. (1995) *Developments and performance analyses of precision forged spur gears*. PhD Thesis, School of Manufacturing and Mechanical Engineering, The University of Birmingham,.

[106] "Tutorial Simufact Forming Introduction to Simufact Forming.". 1–28, 2013.

[107] "Upper-Bound Analysis (Chapter 8) - Metal Forming." [Online]. Available: https://www.cambridge.org/core/books/metal-forming/upperbound-analysis/57B61315E6262E1C022EAFFEDAA97FB6. [Accessed: 25-Jun-2020].

[108] Choi, J.C., Choi, Y. (1998). A Study on the Forging of External Spur Gears: Upper Bound Analyses and Experiments. *Int J Mach Tool Des Res*; **38**:1193-1208.

[109] Choi, J., Cho, H. Y., Jo, C. Y. (2000). An Upper-Bound Analysis for the Forging of Spur Gears. *J. Mater. Proc. Tech*. **104**, 67-73,.

[110] Hosford W. F., Caddell, R. M. (2007). *Metal forming: mechanics and metallurgy.* Third Edition. Cambridge: Cambridge University Press,

[111] M. Aladağ, (2020). *Design and manufacturing of asymmetric spur gear forging die*. M.sc thesis, Gaziantep University Graduate School of Natural & Applied Sciences, August. 2020

CURRICULUM VITAE

Gülağa Taş, Ph.D

Gaziantep University, Engineering Department, Mechanical Engineering

Email: h.agt.1974@gmail.com

PERSONAL PROFILE

Nationality	: Turkish (TC)
Date and Place of Birth	: 06 February 1974, Kahramanmaraş / Elbistan

PROFESSIONAL PROFILE

- Computer Aided Design and Manufacturing (CAD/CAM)
- Additive Manufacturing
- Python programming
- Finite Element Analysis

EDUCATION

- Doctor of Philosophy in Mechanical Engineering, Gaziantep University, Engineering Faculty, Mechanical Engineering. (2020)
  Support area: Finite element analysis, forging die design, die design.
  Thesis: Precision Forging of Asymmetric Spur Gear.
- Bachelor of Science in Mechanical Engineering, Aksaray University, Engineering Faculty, Mechanical Engineering Department. (2012).
  Graduation project: Solar Energy
- Bachelor of Science in Biology, Kazım Karabekir Faculty of Education, Atatürk University. (1995).

- High School, Mersin Gazi Lisesi. (1991)

ACADEMIC/TEACHING EXPERIENCE

Biology teacher at the Ministry of Education since 1995.

PUBLICATONS

Refereed Journal Publications

- O. Eyercioglu, **G. Tas**, and M. Aladag, “Evaluation of Tooth Profile Changes of Symmetric and Asymmetric Spur Gear Forging Dies Due To Shrink Fit,” Sigma J. Eng. Nat. Sci., vol. 38, no. 1, pp. 71–81, 2020.
- O. Eyercioglu, **G. Tas**, and M. Aladag, “Asimetrik düz dişli dövme işleminin üst sınır enerji metodu ile analizi”, Gazi Üniversitesi Mühendislik Mimarlık Fakültesi Dergisi, 2020.

Refereed Conference Proceedings

- Eyercioglu, O.; Yilmaz, N., F., **Tas, G**., Aladag, M**.**; “Stress Evaluation of Asymmetric And Symmetric Spur Gear Forging Dies Using Finite Element Method”, 6th International GAP Engineering Conference GAP2018, 2018.
- Aladag, M.; Eyercioglu, O.; and **Tas, G**. “The Effects of Punch Speed on The Forging Load of Hot Precision Bevel Gear Forging” The International Conference of Materials and Engineering Technologies TICMET’19, 2019.
- Eyercioglu, O.; **Tas, G.**; Aladag, M. “Comparison of Warm and Hot Precision Forging Process af Asymmetric Spur Gear” 2nd International Turkish World Engineering and Science Congress, November 7-10Antalya, Turkey, 2019.
- Eyercioglu, O.; **Tas, G.,** “Improving Die Filling Utilizing Bi-Directional Forging Process” International Conference on Advanced Technology & Sciences (ICAT’16) September 01-03, 2016 Konya, Turkey.